



MAGISTERARBEIT

Titel der Magisterarbeit

Dynamics of the Local Group in different theories of gravity

angestrebter akademischer Grad

Magister der Naturwissenschaften (Mag. rer. nat.)

Verfasser: **Christoph Saulder**
Matrikel-Nummer: **a0400944**
Studienrichtung: **Astronomie A 066 861**
Betreuer: **Christian Theis**

Wien, im März 2010

Erklärung

Hiermit erkläre ich an Eides statt, dass ich die vorliegende Arbeit selbstständig und ohne fremde Hilfe verfasst, andere als die angegebenen Quellen und Hilfsmittel nicht benutzt und die aus anderen Quellen entnommen Stellen als solche gekennzeichnet habe.

Wien, am 14. März 2010



Christoph Saulder

Zusammenfassung

In meiner Diplomarbeit untersuche ich die Bewegung und Verteilung der Galaxien der Lokalen Gruppe um ihre Geschichte und ihren Ursprung zu verstehen. Unsere Galaxiengruppe besteht aus zwei großen Galaxien, der Milchstraße und M31 (Andromedagalaxie), sowie etwa 40 weiteren Galaxien. Der Startpunkt meiner Untersuchung ist die beobachtete Verteilung der Galaxien in der Lokalen Gruppe, welche von unseren Erwartungen abweicht. Das Problem ist, dass die meisten Galaxien in unserer Galaxiengruppe in einer relativ dünnen Ebene, welche nicht mit der Scheibenebene einer der beiden dominante Spiralgalaxien übereinstimmt, angeordnet sind. Diese ebene Verteilung stimmt nicht mit unseren Erwartungen von kosmologischen Simulationen überein. Eine mögliche Erklärung für die beobachtete Verteilung ist eine mögliche Wechselwirkung zwischen der Milchstraße und M31 vor ungefähr 10 bis 12 Gigajahren. Demnach wäre Gas von den äußeren Teilen der Galaxien in deren Bahnebene gestreut worden. Ich versuche herauszufinden, für welche Mitglieder der Lokalen Gruppe diese Modell realistisch ist und die Ergebnisse von Sawa und Fujimoto (Sawa and Fujimoto, 2005) zu reproduzieren sind. Dafür wurden stellardynamische numerische Simulationen unter der Verwendung meines Newton'schen Hubble Expansions Integrators (*NewHEXI*) durchgeführt. Diese Programm ist in der Lage, N-Körper-Berechnungen mit Newton'scher Gravitation (und Dunkle Materie Halos), Hubble-Expansion und dynamischer Reibung durchzuführen. Die Orbits der Zwerggalaxien um ihre Zentralgalaxie sind empfindlich bezüglich des Potentials der Zentralgalaxie sowie der dynamischen Reibung. Somit ist die Dynamik der Lokalen Gruppe ein perfektes Labor um das Dunkle Materie Paradigma sowie auch eine alternative Theorie, welche MODifizierte Newton'sche Dynamik (MOND) genannt wird, zu testen. In dieser Theorie wird das Gravitationsgesetz für kleine Beschleunigungen, welche in den äußeren Teilen von galaktischen Scheiben und auch in Galaxiengruppen auftreten, modifiziert. Dazu wurden Simulation für die Lokale Gruppe unter Verwendung eines selbstentwickelten DEep-MONDD-Integrators (*DeMonI*) durchgeführt. Dieses Programm kann stellardynamische N-Körper-Systeme unter Verwendung von deep-MOND-Gravitation und Hubble-Expansion berechnen. In einem vorausgehenden Versuch Modelle in MOND zu berechnen, habe ich das Programm *N-MODY* (Londrillo and Nipoti, 2009) verwendet, aber es hat sich als nicht praktikabel für meine Anwendungen erwiesen und ich fand, dass der Code einige allgemeine Probleme hat. Die Anfangsbedingungen werden mittels eines genetischen Algorithmus optimiert. Ich habe 11 verschiedene Modelle berechnet, um unterschiedliche Aspekte der Dynamik der Lokale Gruppe zu untersuchen. Die grundlegende Struktur unserer Galaxiengruppe kann in allen Modellen reproduziert werden, aber eine detaillierte Untersuchung zeigt viele Probleme. Angesichts der Werte der Fitness-Funktion des genetischen Algorithmus kann MOND die Verteilung der Galaxien in der Lokalen Gruppe besser reproduzieren als die Newton'sche Gravitation mit Dunkler Materie. Trotz der Tatsache, dass MOND in der Lage ist, die räumliche Verteilung der Galaxien in unserer Galaxiengruppe sehr gut zu reproduzieren, ist sie sehr schlecht

dabei die Radialgeschwindigkeiten zu reproduzieren, weil sich die meisten Galaxien einfach zu schnell bewegen in den Simulationen mit MOND. Darüber hinaus bewegt sich die Andromeda Galaxie in einige Modellen mit MOND nicht auf die Milchstraße zu, was im deutlichen Kontrast zu den Beobachtungen steht. Die Newton'schen Modelle haben jedoch auch einige Probleme beim reproduzieren der Radialgeschwindigkeiten, aber sie sind weniger schwerwiegend wie in MOND. Alle Newton'schen Modelle zeigen sehr ähnliche anfängliche Verteilungen zur Zeit der Nahebegegnung von der Milchstraße und der Andromeda Galaxie, doch die Galaxienverteilung kann am Ende sehr unterschiedliche aussehen in jedem einzelnen Modell. In MOND sind die anfänglichen Verteilungen so vielfältig wie die Ergebnisse nach der Integration. Weiters befindet sich die Andromedagalaxie immer auf ihren zweiten Orbit in den Modellen mit MOND, im Gegensatz zu den Newton'schen Modellen, wo M31 gerade ihr erstes Apogalaktikum passiert hat. Ein weiterer interessanter Aspekt ist, dass die Ebene der Galaxien nicht mit der Bahnebene der Milchstraße und M31 übereinstimmt, und zu dieser geneigt ist. Im Allgemeinen kann man sagen, dass die Ergebnisse sehr vielfältig sind und viele Möglichkeiten für Interpretationen offen sowie einige noch zu lösende Probleme zurück lassen. Es werden auch Vorschläge für weiterführende Untersuchungen gemacht.

Abstract

In my thesis I study the movement and distribution of the Local Group galaxies to understand their history and origin. Our home galaxy group consists of two large galaxies, the Milky Way and M31 (Andromeda Galaxy), and about 40 known galaxies. The starting point of my investigation is the observed distribution of the galaxies in the Local Group, which differs from our expectations. The problem is that most galaxies in our galaxy group are arranged in a quite thin plane which does not correspond to the disc-plane of one of the two dominant spiral galaxies. This planar distribution does not correspond with our expectations from cosmological simulations. A possible explanation for the observed distribution is an interaction of the Milky Way and M31 about 10 to 12 Gigayears ago. At this time gas from outer parts of the galaxies has been scattered in the orbital plane of these two galaxies. I try to find out for which members of the Local Group this model is realistic and to reproduce the results of Sawa and Fujimoto (Sawa and Fujimoto, 2005). In order to do this, stellar dynamical numerical simulations using my Newtonian Hubble Expansion Integrator (*NewHEXI*) have been run. This programme is capable of performing n-body calculations with Newtonian gravitation (and Dark Matter halos), Hubble expansion and dynamical friction. The orbits of dwarf galaxies around the host galaxies are sensitive to the shape of the host's potential and to dynamical friction. So the dynamics of the Local Group are a perfect laboratory to test the Dark Matter paradigm and also an alternative theory, which is called MODified Newtonian Dynamics (MOND). In this theory the law of gravitation is modified for small accelerations which occur in the outer parts of galactic discs and also in a galaxy group. Therefore simulations for the Local Group have been run using a self-developed DEep-MOND-Integrator (*DeMonI*). This programme is able to calculate stellar dynamic n-body systems using deep-MOND gravity and Hubble expansion. In a previous attempts to calculate models in MOND I used the programme *N-MODY* (Londrillo and Nipoti, 2009), but it has not proved practical for my application and I found that the code has some problems in general. The initial conditions of my models are optimised using a genetic algorithm. I ran 11 different models to investigate various aspects of the dynamics of the Local Group. The basic structure of our galaxy group can be reproduced in all models, but a detailed analysis shows many problems. Due to the values of the genetic algorithm's fitness function MOND can fit the distribution of galaxies in the Local Group better than Newtonian gravity with Dark Matter. Despite MOND is able to reproduce the spatial distribution of galaxies in our galaxy group very well, it does extremely poorly for the radial velocities, because most galaxies simply are moving too fast in the MONDian simulations. Furthermore the Andromeda Galaxy is not approaching the Milky Way in some of the MONDian models, which is in striking contrast to observations. The Newtonian models also have some problems in fitting the radial velocities, but they are less significant than in MOND. All Newtonian models show quite similar initial distributions at the time of the close encounter of the Milky Way and the Andromeda Galaxy, though the final distribution of galaxies may look quite different

in every single model. In MOND the initial distributions are as multifarious as the results after the integration. In addition to that, the Andromeda Galaxy is always on its second orbit in the MONDian models, in contrast to the Newtonian models, where M31 has just passed its first apogalacticum. Another interesting aspect is that the plane of galaxies does not correspond to the orbital plane of the Milky Way and M31 but it is inclined toward it. In general one can say that the results are very multifarious and open a lot of possibilities for interpretations as well as there remain several problems to be solved. Also some suggestions for further investigations are presented.

Contents

Erklärung	I
Zusammenfassung	III
Abstract	V
Contents	VII
1 The Local Group	1
1.1 General features	1
1.2 Members	3
1.2.1 Milky Way	3
1.2.2 Andromeda Galaxy (M31)	4
1.2.3 Triangulum Nebula (M33)	6
1.2.4 The Magellanic Clouds	7
1.2.5 Other dwarf galaxies	11
1.3 A plane of galaxies	13
1.4 Origin of dwarf galaxies	14
2 Basic physics	15
2.1 Gravitation	15
2.2 Dark Matter halos	18
2.3 Dynamical friction	20
2.4 Cosmology and the Hubble expansion	22
3 MODified Newtonian Dynamics	25
3.1 Galaxies rotate too fast	25
3.2 The MOND paradigm	26
3.3 TENSOR-VECTOR-SCALAR gravity	29
3.4 Problems	30
3.4.1 Bullet Cluster	30
3.4.2 Galaxy clusters	30
3.4.3 Timing of the Local Group	30
3.4.4 Lyman- α	31
4 N-MODY	33
4.1 Introduction	33
4.2 How does it work?	34
4.3 Errors	36

4.3.1	Overview	36
4.3.2	Few-body problems	36
4.3.3	Merger	39
4.3.4	Disk-galaxies	40
4.3.5	Flattening of Plummer-Spheres	47
5	Simulations	61
5.1	Motivation	61
5.2	Testing the programmes	62
5.2.1	Overview	62
5.2.2	Dynamical friction	62
5.2.3	Hubble Expansion	66
5.2.4	Gravitation	68
5.3	A very simple Model.	72
5.3.1	Equal masses	72
5.3.2	A realistic mass ratio for the dark matter case	73
5.3.3	Masses in the MONDian case	74
5.4	The main models	80
6	Results	87
6.1	Convergence of the genetic algorithm	87
6.2	Results of all models	89
6.2.1	NM	89
6.2.2	NN	98
6.2.3	N4M	103
6.2.4	N2M	107
6.2.5	NBH	110
6.2.6	NSH	113
6.2.7	MM	116
6.2.8	MN	120
6.2.9	M4M	123
6.2.10	M2M	126
6.2.11	MH	129
6.3	Conclusions	133
	Acknowledgments	135
	Bibliography	137
	Appendices	141
A	Programmes	142
A.1	Overview	142
A.2	Mkinput	143
A.3	Mkmodel	144
A.4	NewHEXI	145
A.5	DeMonI	147
A.6	Cutter	148
A.7	RealDist	149

A.8 GeneAl	150
A.9 Output Best	152
A.10 Other programmes and third-party programmes	153
B From the collisionless Boltzmann-equation to the Plummer-model	155
Curriculum Vitae	157

Chapter 1

The Local Group

1.1 General features

The Local Group contains more than 40 known galaxies including our home galaxy the Milky Way. The galaxies of this group are spread over more than a Megaparsec. Our galaxy group's dynamics are dominated by its two clearly most massive galaxies: the Milky Way and M31. The total mass of the Local group is estimated to be a few $10^{12}M_{\odot}$ (Li and White, 2008; van der Marel and Guhathakurta, 2008; Chernin et al., 2009). The galaxies in our group are not distributed homogeneously, there are several subgroups. Many dwarf galaxies are located around the two dominant members, but there are also some loose subgroups without a massive galaxy in the centre. The neighbouring galaxy groups of the Local Group are the M83-group, the Sculptor-group, the Maffei-group, the Canes-I-group and the small Antlia group, which is also the nearest neighbour of the Local Group (van den Bergh, 1999). Furthermore, our galaxy group is approaching the Virgo-Cluster with (200 ± 50) km/s (de Freitas Pacheco, 1986) and it belongs to one of the outer filaments of the Virgo-Supercluster. All of them, and also our home group belong to the Virgo-Super-cluster. A great advantage of studying the Local Group is that one has observational data of unique quality and quantity compared to other systems of similar extension. Despite our vast knowledge of the Local Group there remain many interesting and challenging puzzles to be solved and some of them give us a singular possibility to investigate the very foundations of physics. The Local Group and its history can be used as a laboratory for many problems in astrophysics like Dark Matter, structure formation, distance measurement and much more.

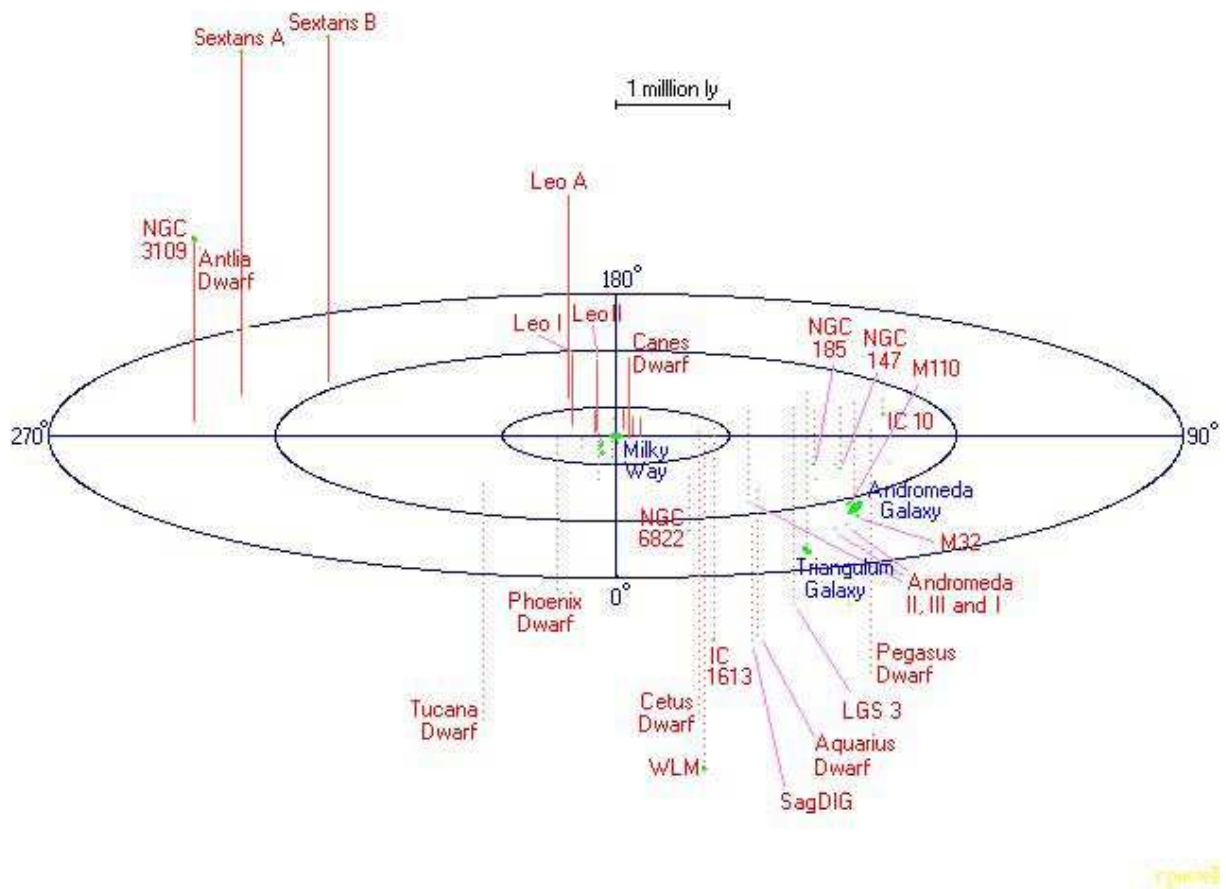


Figure 1.1: Three-dimensional map of the Local Group (by Richard Powell)

1.2 Members

1.2.1 Milky Way

The Milky Way is our home galaxy and the second largest galaxy in the Local Group. Our home galaxy is a barred spiral of the Hubble-type SBbc. The Milky Way possesses a so called Molecular Ring consisting of many large Molecular Clouds situated in its inner parts and a supermassive Black Hole called Sagittarius A* in its very centre. There are 180 ± 20 globular clusters (van den Bergh, 2003) in our galaxy. The age of our Galaxy is very difficult to determine, but the oldest star which has been discovered up to now, is in the age of about 13.2 Gyr (Frebel et al., 2007). Other studies have shown that the halo is estimated to be (13.5 ± 0.7) Gyr old while the disk exists for about (8.8 ± 1.7) Gyr (del Peloso et al., 2005). Our position inside the Milky Way (see figure 1.2) helps us to get excellent data for local phenomena but the same fact makes it harder to get a good estimate on the general properties of our home galaxy. The table 1.1 contains information about the characteristic parameter of the Milky Way galaxy like its total mass M_{tot} under the assumption of the existence of dark matter, its disc mass M_{disc} , its bulge mass M_{bulge} and the mass of its central supermassive black hole M_{BH} . Other parameters are the total luminosity L_{tot} which corresponds to an absolute magnitude m_{abs} . The table also contains information about the scale length of the Galaxy's disc l_{disc} as well as about the scale height of its thin disc h_{thin} , which consists mainly of younger stars and also about the scale height of the thick disc h_{thick} , which represents the dynamic of the older stars. The radius of the stellar halo r_{hs} and the radius of the dark matter halo r_{hd} can also be found in this table. In addition to that it contains parameters like the distance of our sun from the centre of the Galaxy r_{\odot} and the rotation speed at this distance $v_{\text{rot}, \odot}$. Some parameters of the Milky Way are rather inaccurate like the radius of the Dark Matter halo and consequently the total mass of our Galaxy.



Figure 1.2: The Milky Way plane seen from Earth (by Digital Sky LLC).

M_{tot}	$1 - 2 \cdot 10^{12} M_{\odot}$ (Baiesi Pillastrini, 2009)
M_{disc}	$(2.5 \pm 1) \cdot 10^{10} M_{\odot}$ (Binney and Tremaine, 2008)
M_{bulge}	$(5 \pm 2) \cdot 10^9 M_{\odot}$ (Binney and Tremaine, 2008)
M_{BH}	$(3.9 \pm 0.3) \cdot 10^6 M_{\odot}$ (Binney and Tremaine, 2008)
L_{tot}	$(3 \pm 1) \cdot 10^9 L_{\odot}$ (Binney and Tremaine, 2008)
m_{abs}	-20.9^{m} (Pritchett and van den Bergh, 1999)
l_{disc}	$(2.5 \pm 0.5) \text{ kpc}$ (Binney and Tremaine, 2008)
h_{thin}	300 pc (Binney and Tremaine, 2008)
h_{thick}	1 kpc (Binney and Tremaine, 2008)
r_{hs}	50 kpc (Binney and Tremaine, 2008)
r_{hd}	a few 100 kpc (estimated)
r_{\odot}	$(8.0 \pm 0.5) \text{ kpc}$ (Binney and Tremaine, 2008)
$v_{\text{rot}, \odot}$	220 km/s (IAU value)

Table 1.1: Parameters of the Milky Way.

1.2.2 Andromeda Galaxy (M31)

The most massive member of the local group is the Andromeda Galaxy; it is also the most distant object which can still be seen by naked eye from Earth. It is assumed that the dark halo of M31 is extended up to more than 220 kpc (Sarajedini, 2007). In contrast to early estimates (about 100 km/s (Loeb et al., 2005)), the tangential velocity v_{\perp} of the Andromeda Galaxy is quite small (less than 56 km/s (Bekki, 2008)). M31 has a binary nucleus (van den Bergh, 2000), one of them contains a supermassive Black Hole, a warped disc outside 25kpc and extended stellar streams, which indicate a very turbulent history (Corbelli et al., 2009). Furthermore, there are estimated to be 450 ± 100 globular clusters (van den Bergh, 2000). The table 1.2 contains information about the main parameters of M31. The abbreviations are similar the previous table although there are also additional parameters included like the distance of the Andromeda galaxy from our sun d , the radial velocity of the galaxy with respect to our own v_{rad} and the baryonic mass M_{baryon} .

M_{tot}	$(1.2 - 3.4) \cdot 10^{12} M_{\odot}$ (Bekki, 2008; Baiesi Pillastrini, 2009; Loeb et al., 2005)
M_{baryon}	$(7.5 - 14) \cdot 10^{10} M_{\odot}$ (Shi, 2009; Corbelli et al., 2009)
M_{BH}	$3.3 \cdot 10^7 M_{\odot}$ (van den Bergh, 2000)
d	760 kpc (van den Bergh, 2003)
m_{abs}	-21.2^{m} (Pritchett and van den Bergh, 1999)
v_{rad}	-301 km/s SIMBAD Astronomical Database
v_{\perp}	$< 56 \text{ km/s}$ (Bekki, 2008)
v_{rot}	$(270 \pm 10) \text{ km/s}$ (Rubin and Ford, 1970)

Table 1.2: Parameters of the Andromeda Galaxy.



Figure 1.3: The Andromeda Galaxy (by John Lanoue).

1.2.3 Triangulum Nebula (M33)

The third spiral in the Local Group is M33, which is also called the Triangulum Nebula, because it can be found in the constellation Triangulum. This galaxy, which is classified as Hubble-type Sc, is clearly less massive than the other two spirals. M33 belongs to the Andromeda subgroup and it may be gravitationally bound to M31 of which the Triangulum nebula is separated by approximately 200 kpc (van den Bergh, 2003). A stream of neutral hydrogen, which connects M33 with its host galaxy, has been detected (Bekki, 2008). This stream supplies the Andromeda Galaxy with new gas from the outskirt areas of M33 (Putman et al., 2009). The extended HI disc of the Triangulum Nebula, which reaches out 22 kpc (Putman et al., 2009), is warped due to tidal interaction with M31. M33 has passed the pericenter of its orbit around M31 the last time less than 3 Gyr ago at a distance of less than 100 kpc (Putman et al., 2009). The inner disc (about 9 kpc radius (Cioni, 2009)) shows a continuous relatively high star formation (Magrini et al., 2007). This star formation is triggered by infalling gas of about $1 M_{\odot}/yr$ (Magrini et al., 2007). Furthermore, there is a continuous cluster formation in M33 for the last 10 Gyr (Chandar et al., 1999a; Chandar et al., 1999b). M33 is bluer and more metalpoor than the Milky Way (McConnachie et al., 2006) but there is also a very old (>10 Gyr) stellar component (Sarajedini and Yang, 2010). The Triangulum Nebula has hardly any buldge or stellar halo (McConnachie et al., 2006). In table 1.3 one can find the basic parameters of M33.

M_{tot}	$(4 - 20) \cdot 10^{10} M_{\odot}$ (Bekki, 2008; Giraud, 2000; ?)
M_{disc}	$3_{-0.9}^{+1.5} \cdot 10^9 M_{\odot}$ (Giraud, 2000)
M_{baryon}	$(5 - 10) \cdot 10^9 M_{\odot}$ (Giraud, 2000) and estimates for consistency
L_{tot}	$6.5 \cdot 10^9 L_{\odot}$ (Magrini et al., 2007)
d	795 kpc (van den Bergh, 2003)
m_{abs}	-18.9^{m} (Pritchett and van den Bergh, 1999)
v_{rot}	130 km/s (Magrini et al., 2007)

Table 1.3: Parameters of the Triangulum Nebula.

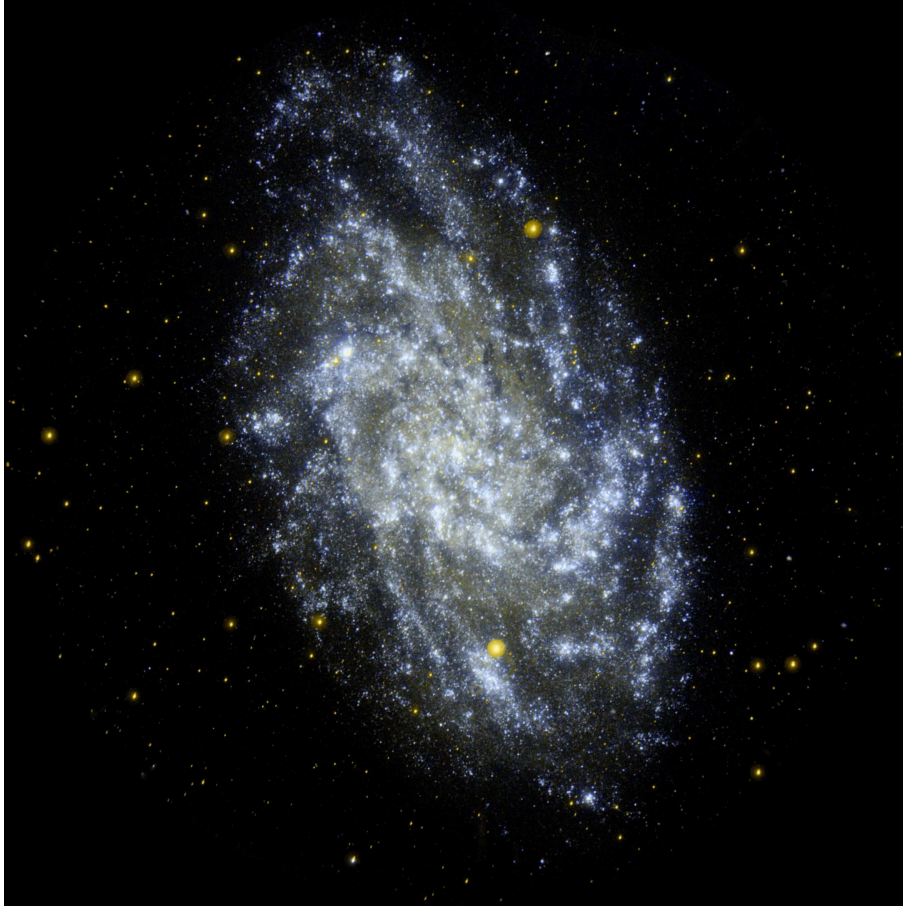


Figure 1.4: The Triangulum Nebula (by Hewholooks).

1.2.4 The Magellanic Clouds

The two Magellanic Clouds are irregular dwarf galaxies, which belong to the Milky Way subgroup. The Large Magellanic Cloud (LMC) is the fourth massive member of the Local Group and its smaller neighbour, the Small Magellanic Cloud (SMC), is clearly less massive. For a long time one has thought that the Magellanic Clouds are gravitational bound to the Milky Way but recent measurements of their tangential velocities have raised doubts. Their velocities are close to their escape velocities from the Milky Way and this phenomenon is known as the "angular momentum problem" of the Magellanic Clouds. It is speculated that the two galaxies only have had one perigalactic passage in their entire history (Mastropietro, 2009). Due to the high velocity of the two dwarf galaxies, tidal stripping is unlikely to have created the Magellanic Stream. Ram pressure stripping of the Magellanic Clouds seems to be a more realistic model for creation of the Magellanic Stream (Mastropietro, 2009). There have been at least two close encounters of both Magellanic Clouds with each other, one about 4 Gyr ago and another one about 100-200 Myr ago. The last encounter has very likely created the Magellanic Bridge (Cioni, 2009). The LMC shows a continuous star formation with two exceptional events at approximately 4 and 12 Gyr ago, when star clusters have been formed (Sabbi et al., 2009). Furthermore, the LMC posses a bar (Novati et al., 2006) as one can see in figure 1.5. The bar is likely younger than 6 Gyr, which is in agreement with observations that show bursts of star formation at 4 - 6 Gyr and 1 - 2 Gyr ago ???. The SMC has a long star formation history for about

12 Gyr (Sabbi et al., 2009). There have been periods of enhanced star formation activity 6 Gyr ago, 3-4 Gyr ago and now for about 500 Myr (Sabbi et al., 2009). Nowadays the enhanced star formation in the SMC is not global, but with several local centres (see figure 1.6). An interesting feature of the SMC is that, the only globular cluster in this galaxy is only about 2 - 3 Gyr old (Sabbi et al., 2009). In contrast to old stellar component, which shows no rotation, the HI shows rotation in the SMC (Gonidakis et al., 2009). It shall be notated that, compareably little Dark Matter is needed to explain this rotation (Gonidakis et al., 2009). The main parameters of the Magellanic Clouds can be found in tables 1.4 and 1.5.

M_{tot}	$(0.9 - 2.6) 10^{10} M_{\odot}$ (van der Marel et al., 2002; Alves, 2004; Mastropietro, 2009)
M_{baryon}	$(2 - 5) \cdot 10^9 M_{\odot}$ (Mastropietro, 2009; van der Marel et al., 2002) and estimates for consistency
d	50 kpc (van den Bergh, 2003)
m_{abs}	-18.5^{m} (Pritchett and van den Bergh, 1999)
v_{rel}	378 km/s (Mastropietro, 2009)

Table 1.4: Parameters of the Large Magellanic Cloud.

M_{tot}	$(3 - 6.5) 10^9 M_{\odot}$ (Kallivayalil et al., 2009; Bekki and Stanimirović, 2009)
M_{baryon}	$1.6 \cdot 10^9 M_{\odot}$ (personal estimate based on various sources)
d	59 kpc (van den Bergh, 2003)
m_{abs}	-17.1^{m} (Pritchett and van den Bergh, 1999)
v_{rel}	302 km/s (Mastropietro, 2009)

Table 1.5: Parameters of the Small Magellanic Cloud.



Figure 1.5: The Large Magellanic Cloud (by NASA).

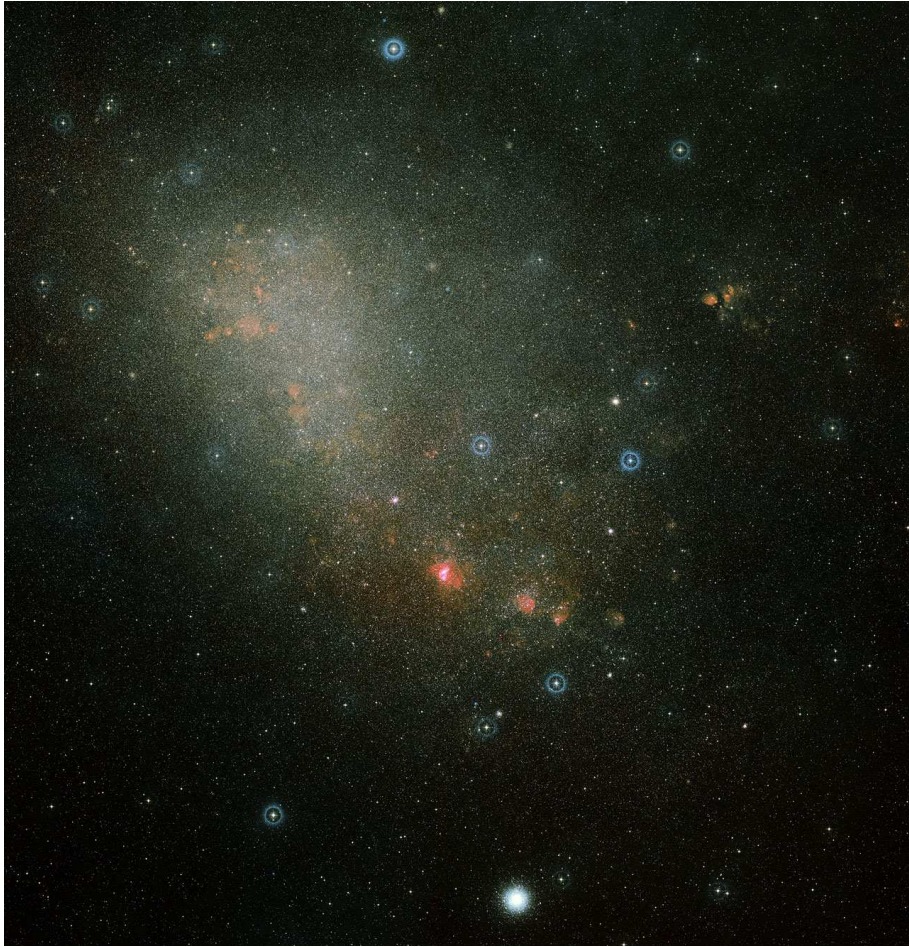


Figure 1.6: The Small Magellanic Cloud (by ESA/Hubble and Digitized Sky Survey 2).

1.2.5 Other dwarf galaxies

There are about 40 other known galaxies within the Local Group. They are arranged in 4 subgroups, which are the Local Group Cloud (LGC), the NGC 3109 subgroup (N3109-SG), the Andromeda subgroup (M31-SG) and the Milky Way subgroup (MW-SG). A list of all members of the Local Group with their positions on the sky, their distances and their radial velocities can be found in table 5.6 and some additional data about the Local Group dwarfs can be found in table 1.6. Almost all dwarf galaxies in our galaxy group are older than 10 Gyr ???. In addition to that, most of the dwarf spheroidals have not experienced star formation activity in the recent past, while the irregular galaxies show very active star formation (e.g. IC10). Several members of the Local Group have undergone phases of high star formation rates, like IC1613 7 Gyr ago or And II between 6 to 9 Gyr ago (van den Bergh, 2000). The nearest known galaxy, the Sagittarius dwarf galaxy, is located on the opposite side of the Milky Way at a distance of about 24 kpc from our sun. It is on a tight orbit around the Milky Way between a perigalacticum of ~ 13 kpc and an apogalacticum of ~ 41 kpc and one revolution takes approximately 550 - 750 Myr (van den Bergh, 2000). The Sagittarius dwarf galaxy has already lost more than half of its mass (van den Bergh, 2000) and it will eventually merge with the Milky Way. Another outstanding galaxy is M32. This galaxy is the most compact known elliptical dwarf galaxy. It is a companion of M31, and it is assumed that M32 has a unique history and might have suffered a transformation due to the strong tidal field of its host galaxy. Because of its uniqueness some authors even doubt that M32 is a member of the Local Group but a more distant normal elliptical galaxy (Young et al., 2008). Most of the small galaxies in the Local Group are classified as dwarf spheroidals (dSph), and are concentrated around the Milky Way and the Andromeda galaxy.

name	type	subgroup	$M_{\text{tot}} [10^6 M_{\odot}]$	$R_c [pc]$
WLM	Irr IV-V	LGC	150	710
NGC55	Irr IV	LGC	15600	875
IC10	dIrr	M31-SG	1580	475
NGC147	dSph / dE5	M31-SG	110	170
And III	dSph	M31-SG	-	180
NGC185	dSph / dE3p	M31-SG	130	155
NGC205	E5p / dSph-N	M31-SG	740	260
M32	E2	M31-SG	2120	635
And I	dSph	M31-SG	-	375
Sculptor	dSph	MW-SG	6.4	110
LGS3	dIrr / dSph	M31-SG	13	160
IC1613	Irr V	M31-SG / LGC	795	585
And II	dSph	M31-SG	-	205
Phoenix	dIrr / dSph	MW-SG / LGC	33	310
Fornax	dSph	MW-SG	68	460
UGCA92	dIrr	M31-SG	-	85
Carina	dSph	MW-SG	13	210
Leo A	dIrr	MW-SG / N3109-SG	11	185
Sextans B	dIrr	N3109-SG	885	445
NGC3109	Irr IV-V	N3109-SG	6550	630
Antlia	dIrr / dSph	N3109-SG	12	230
Leo I	dSph	MW-SG	22	215
Sextans A	dIrr	N3109-SG	395	700
Sextans	dSph	MW-SG	19	335
Leo II	dSph	MW-SG	9.7	160
GR8	dIrr	isolated	7.6	110
Ursa Minor	dSph	MW-SG	23	200
Draco	dSph	MW-SG	22	180
Sagittarius	dSph-N	MW-SG	-	550
SagDIG	dIrr	LGC	9.6	125
NGC6822	Irr IV-V	LGC	1640	260
Aquarius	dIrr / dSph	LGC	5.4	95
IC5152	dIrr	LGC	400	390
Tucana	dSph	LGC	-	130
UGCA438	dIrr	LGC	-	150
Pegasus	dIrr / dSph	LGC	58	280
Cetus	dSph	M31-SG / LGC	-	-
And V	dSph	M31-SG	-	-
Cassiopeia	dSph	M31-SG	-	-
Pegasus II	dSph	M31-SG	-	-

Table 1.6: List of the Local Group dwarf galaxies based on the work of different authors (Mateo, 1998; van den Bergh, 2003)

1.3 A plane of galaxies

Maybe the most astonishing feature of the Local Group is that the distribution of galaxies, which is quite different from what we expect from cosmological simulations using Λ -CDM cosmology (see section 2.4). In fact there are two problems: the so called missing satellites problem and the problem of the very anisotropic distribution of galaxies in our galaxy group. The first problem is a hot discussed topic, because one would expect several hundred dwarf galaxies due to cosmological CDM simulations (Moore et al., 1999; Diemand et al., 2008) in the Local Group. But up to now there have only a little more than 40 galaxies been discovered. A possible solution for this problem is that a dark matter sub halo needs a minimum mass to gather enough baryonic matter to form a visible galaxy (Libeskind et al., 2005). My work will not be focused on the first problem but on the second, which at least is equally interesting und maybe even more challenging. The first hints for a ring like structure (seen from Earth) of the Local Group galaxies have already been discussed in the 70s of the last century (Kunkel, 1979). Later analyses have confirmed the existence of a surprisingly planar distribution of the galaxies within our galaxy group. Using the data of 41 galaxies of our galaxy group (see table 5.5), Sawa and Fujimoto have calculated an orientation of this plane. They have found out that the normal vector of this plane is pointing towards the galactic coordinates 206° longitude and -11° latitude (Sawa and Fujimoto, 2005). Furthermore they have claimed most galaxies of the Local Group are located within this 50 to 100 kpc thick plane. Using the same data they did and also some new ones (see table 5.6), I have repeated the calculations using the least-mean-square method for fitting. These results for various parameters can be found in table 1.7. SF represents the results of Sawa and Fujimoto, given in their paper using the coordinates of 41 galaxies from table 5.5. 41G uses the values of 41 Local Group galaxies given in table 5.5. 41GR uses the same coordinates as 41G, but also an additional condition: the Milky Way and the Andromeda Galaxy are restricted to be exactly on the plane. In 45G, the coordinates of 45 galaxies from table 5.6 are used. 45GR uses the same values as 45G with the same restriction as 41GR.

model parameters	direction of the plane's normal vector in galactic coordinates (l ;b)	standard error in kpc
SF	$206^\circ; -11^\circ$	50-100
41G	$200^\circ; -20^\circ$	46
41G after a 2σ -clipping	$203^\circ; -27^\circ$	31
41GR	$200^\circ; -20^\circ$	48
41GR after a 2σ -clipping	$199^\circ; -39^\circ$	36
45G	$199^\circ; -20^\circ$	46
45G after a 2σ -clipping	$204^\circ; -25^\circ$	29
45GR	$220^\circ; -21^\circ$	46
45GR after a 2σ -clipping	$219^\circ; -19^\circ$	36

Table 1.7: Orientation of the Local Group plane.

1.4 Origin of dwarf galaxies

The question of the origin of the dwarf galaxies in the Local Group sounds simple but it is much more difficult than one would expect. It has already been mentioned that the observed distribution of dwarf galaxies in the Local Group differs from our expectations from standard Λ -CDM cosmology. A possible scenario to explain the observed planar distribution of galaxies is that the dwarf galaxies entered the Local Group as one or maybe two groups (Li and Helmi, 2008; ?). This model does not seem to be very likely, because the observed distribution of dwarf galaxies in the Local Group is too flat (Metz et al., 2009). It is also possible that the planar structure is caused by a triaxial halo (Hartwick, 2000) of the Local Group, or by some effects from neighbouring galaxy groups (Raychaudhury and Lynden-Bell, 1989). Especially in case of MOND, where the accelerations from the neighbouring groups (assuming a mass of $10^{13} M_{\odot}$, a distance of 2 Mpc and 10% baryonic matter) are about a factor 6 greater than in Newtonian gravity, this effects will be worth a consideration. Another model is based on a possible harassment of the still extended discs of the Milky Way and M31 during an early encounter about ten or more Gigayears ago. The gas was compressed in the area, where the extended gas discs of both galaxies were touching each other and formed many dwarf galaxies. At this point it should be mentioned that the discs have an inclination of about 60° towards each other. Later these dwarf galaxies fell into the massive galaxies potential and were scattered along the orbital plane of the Milky Way and the Andromeda galaxy (Sawa and Fujimoto, 2005). Similar effects have already been observed in other galaxy groups (Deeg et al., 1998).

In their simulalations Sawa and Fujimoto, they have treated 4 galaxies as massive using the masses in table 1.8 for their model. Data from previous studies (Sawa et al., 1999; Fujimoto et al., 1999) have been used for the orbits of the Magellanic Clouds. Furthermore, they have considered extended halos for the Milky Way and Andromeda Galaxy and dynamical friction caused by these halos as well as Hubble expansion. Afterwards, they have done a parameter study for every other dwarf galaxies of the Local Group individually. They have found that 23 of 36 dwarf galaxies can be fitted by assuming a close encounter of the Milky Way and the Andromeda galaxy. Due to the calculations of Sawa and Fujimoto, this encounter happened at a distance between both large spiral galaxies of approximately 140 to 150kpc and took place during the first and only perigalactic passage of M31 about 10.4 to 12 Gyr ago. This model can explain most of the observed distribution of galaxies in the Local Group and furthermore the high angular momentum of the Magellanic Clouds, which are supposed to have been formed in this event too (Sawa and Fujimoto, 2005). But this model also has some problems like that the formation site is larger than expected or that the influence of third most massive galaxy, M33, is not included. Further problems for this model, but also all other scenarios, are the largely unknown tangential velocities of most galaxies in our galaxy group and inaccuracies in the masses of the Local Group galaxies.

name of the galaxy	mass
Milky Way	$3 \cdot 10^{12} M_{\odot}$
M31	$4 \cdot 10^{12} M_{\odot}$
LMC	$2 \cdot 10^{10} M_{\odot}$
SMC	$2 \cdot 10^9 M_{\odot}$

Table 1.8: Masses used by Sawa and Fujimoto (Sawa and Fujimoto, 2005) in their simulations.

Chapter 2

Basic physics

2.1 Gravitation

Gravitation is a force that affects all known particles. Furthermore it is the weakest of the four fundamental forces and there are only positive charges, which are called masses. Sir Isaac Newton was the first scientist to formulate a general description of gravity by unifying the law of falling bodies of Galilei with the orbits of planets of Kepler. In modern notation one can write it like equation (2.1) where Φ is the gravitational potential G the gravitation constant, ρ the matter density and \vec{R} a position vector.

$$\Delta\Phi(\vec{R}) = 4\pi G\rho(\vec{R}) \quad (2.1)$$

One gets the gravitational field with equation (2.2), where \vec{F} represents the force field and M is the mass of the body which is affected by this field.

$$\vec{F}(\vec{R}) = -M\vec{\nabla}\Phi(\vec{R}) \quad (2.2)$$

In case of spherical symmetry one can derive Newton's shell theorems:

1. A spherically symmetric mass distribution affects external objects gravitationally like point mass, with the same total mass as the distribution.
2. Within a spherically symmetric shell, no gravitational force is exerted by the shell on any object inside it, independent of the object's location within the shell.
3. Inside a solid sphere of constant density the gravitational force increases linearly from zero at the centre of mass out to the surface.

These theorems are very helpful when analysing or calculating systems with Newtonian gravity because they can simplify many problems. In case of n point masses one will get the field which is given in equation (2.3). m_i represents the mass of the i^{th} particle and \vec{r}_i for the position vector.

$$\vec{F}(\vec{R}) = -G \sum_{i=1}^n \frac{Mm_i}{|\vec{r}_i - \vec{R}|^3} (\vec{r}_i - \vec{R}) \quad (2.3)$$

This equation is the usual formulation of the gravitational N-body problem which often occurs in stellar dynamics. Knowing that $\vec{F}(\vec{R}) = M(d^2\vec{R}/dt^2)$ one gets an ordinary differential equation which can be solved numerically. This can either be done directly or

with some tricks or approximations like multipole expansions. It is done regularly for stellar dynamical applications. A common alternative for simulating a gravitationally interacting system is solving the Poisson equation (see equation (2.1)). The gravity problem can also be solved analytically in some special cases like for restricted two body and three body systems or for the full two body problem. In case of the two body problem one gets Kepler's laws of planetary motion:

1. A planet's orbit is given by an ellipse with the sun located at a focus. This law is only valid in the restricted two body problem where the mass of the sun is significantly greater than the mass of the planet.
2. The vector pointing from the sun to a planet sweeps out equal areas during equal intervals of time. If one replaces the sun by the centre of mass of the system this law will be valid in general.
3. The orbital period of a planet T and the semi-major axis of its orbit a are related by formula (2.4), where M is the mass of the star, m is the mass of the planet and G the gravitation constant.

$$T^2 = \frac{4\pi^2}{G(M+m)}a^3 \quad (2.4)$$

This relation is valid in general for a two body problem. One can derive by neglecting the influence of the planets on each other following well known formulation of Kepler's third law: $T_1^2/a_1^3 = T_2^2/a_2^3$.

Other simple solutions which are regularly used exist for the restricted two body problem. One can calculate the circular velocity v_{circ} for a test body by setting the gravitational force equal to its centripetal force and one gets

$$v_{\text{circ}} = \sqrt{\frac{GM}{R}} \quad (2.5)$$

where M is the mass to a body that is orbited at distance R . One can get the escape velocity v_{esc} of a test body by setting the kinetic energy and the potential energy (one can simply derive it by using solving equation (2.1) for a point mass) equal (see equation (2.6)).

$$v_{\text{esc}} = \sqrt{\frac{2GM}{R}} \quad (2.6)$$

Although it is sufficient for most applications, the Newtonian formulation of gravity has its limits. A more general concept of gravity has been introduced by Einstein's general theory or relativity. General Relativity is characterised by following axioms in the book of Wolfgang Rindler:

1. *The space-time of events is Lorentzian; that is, pseudo-Riemannian with Minkowskian signature.*
2. *Free test-particles have timelike geodesic worldlines.*
3. *Light in vacuum follows null geodesics.*
4. *The arc along any timelike worldline corresponds to c times the proper time of an ideal point-clock that traces it out. [...]*

5. *Einstein's field equations will relate the metric with the energy tensor of the sources.*

(Rindler, 2006). This is only a brief outline of General Relativity and its features. Additional information can be found in the book of Rindler or any other good textbook on General Relativity. Therefore the geodesic equation (equation (2.7)) is the equation of motion in General Relativity for bodies that are only affected by gravity. It connects the 4-coordinates x^μ and their derivations with the metric $g_{\mu\nu}$ and its derivation which is hidden in the Christoffel symbol $\Gamma_{\lambda\nu}^\mu = (g^{\mu\rho}/2) \cdot (\partial_\lambda g_{\nu\rho} + \partial_\nu g_{\lambda\rho} - \partial_\rho g_{\lambda\nu})$. The geodesic equation can be modified if non-gravitational forces are present.

$$\ddot{x}^\mu + \Gamma_{\lambda\nu}^\mu \dot{x}^\lambda \dot{x}^\nu = 0 \quad (2.7)$$

Einstein's field equations (see equation (2.8)) basically connect geometry with the energy content of space. On the left-hand side there is the metric $g_{\mu\nu}$ and its first and second derivations contracted many times in the Ricci-tensor $R_{\mu\nu} = R_{\mu\lambda\nu}^\lambda$ which consists of the contracted Riemann-tensor $R_{\mu\nu\lambda}^\rho = \partial_\nu \Gamma_{\mu\lambda}^\rho - \partial_\lambda \Gamma_{\nu\mu}^\rho + \Gamma_{\mu\lambda}^\xi \Gamma_{\xi\nu}^\rho - \Gamma_{\mu\nu}^\xi \Gamma_{\xi\lambda}^\rho$ and the Ricci-scalar $R = g^{\mu\nu} R_{\mu\nu}$. The cosmological constant Λ is needed for cosmological applications and it is assumed that it represents the influence of the Dark Energy content of the universe. On the right-hand side one finds the stress-energy tensor $T_{\mu\nu}$ representing the energy and matter content of space-time. The terms with the Ricci-tensor and Ricci-scalar are often summarized to the Einstein-tensor $G_{\mu\nu}$ (see equation (2.9)).

$$R_{\mu\nu} - \frac{R}{2} g_{\mu\nu} + \Lambda g_{\mu\nu} = \frac{8\pi G}{c^4} T_{\mu\nu} \quad (2.8)$$

$$G_{\mu\nu} = R_{\mu\nu} - \frac{R}{2} g_{\mu\nu} \quad (2.9)$$

In General Relativity gravity is not seen as a classic force anymore but an effect due to the curvature of space-time. In general one cannot solve these 11 (there are only 11 equations due to symmetry in the indices) non-linear partial second order differential equations, but there exist solutions for some very special cases and approximations.

Beside Newtonian gravity and General Relativity there are many alternative theories of gravity. An example is the Modified Newtonian Dynamics (MOND) and its general relativistic extension the Tensor-Vector-Scalar theory of gravity (TeVeS). I will review both theories in detail in another chapter of my thesis. A further alternative theory would be Scalar-Tensor-Vector Gravity (STVG) (Moffat, 2006) which is also known as Modified Gravity (MOG).

2.2 Dark Matter halos

We know that the motion of galaxies in clusters cannot be explained by visible matter only since the first detailed studies of galaxy clusters (Zwicky, 1933). We also have the same problem within galaxies. Stars move much faster than one would expect from the mass of the observed matter. Therefore Dark Matter has been introduced to solve this problem. Despite some problems the model of Dark Matter had been a very successful tool during the last decades. Nowadays it is assumed that Dark Matter consists of weakly interaction massive particles (WIMPs) and there are many possible candidates from extension of the standard model of particle physics (e.g.: neutralino from SUSY). The weakest point of the Dark Matter paradigm is that up to now no Dark Matter particles have been detected and consequently the theory still lacks an experimental confirmation. Because dark matter does not interact with electromagnetism one cannot detect it by conventional observational methods directly in the galaxy. One can only try to calculate the distribution of it from the motion of visible matter due to the dark matter's gravitational effects. At least 20% of the total energy content of the universe consists of Dark Matter in the standard model of cosmology (Peacock, 1999). Galaxies are assumed to be embedded into a Dark Matter halo which has a much larger extension than the area filled with visible baryonic matter. Since one can only observe baryonic matter the exact extensions of Dark Matter halos are unknown and can only be estimated. The total mass also depends on the real radius of the halo and therefore one can only get lower bounds for it from observations of rotation curves of galaxies. Another problem presents the inner parts of the Dark Matter halos, where the density of the baryonic matter becomes higher and in the very cores of galaxies the local structure (like bars) can change the profile of the dark matter distribution. Due to all these problems there exist many different profiles for Dark Matter halos in the literature. Each of it has advantages and problems. I will start with the simplest model: the isothermal sphere. In equations (2.10) one can see the properties of a singular isothermal sphere with a mass M_0 inside a radius r_0 .

$$\begin{aligned}\rho(r) &= \frac{M_0}{4\pi r_0} \frac{1}{r^2} \\ M(r) &= M_0 \frac{r}{r_0} \\ v_{\text{circ}} &= \sqrt{\frac{GM_0}{r_0}} \\ \Phi(r) &= \frac{GM_0}{r_0} \ln(r) + \text{const}\end{aligned}\tag{2.10}$$

The circular velocity is constant inside a singular isothermal sphere and it would be able to explain the flat rotation curves of the outer areas of galaxies and the potential is logarithmic. One problem of this profile is that the density rises to infinite in the centre and causes a central cusp, in contrast to the observed flatter core-like structure (Li and Helmi, 2009). Another disadvantage of this profile is that the mass grows with increasing radius to infinity. Because of this one usually introduces a finite cut-off radius at which the halo ends. A big advantage of the singular isothermal sphere is that it provides very simple formulas. Another model is the Burkert-Halo (see equation (2.11)). It has been derived by fitting observational data of dark matter dominated dwarf spiral galaxies

(Burkert, 1996). This profile has a flat core but the enclosed mass is divergent.

$$\rho(r) = \frac{\rho_0 r_0^3}{(r + r_0)(r^2 + r_0^2)}$$

$$M(r) = 2\pi\rho_0 r_0^3 \left\{ \ln \left[\left(1 + \frac{r}{r_0}\right) \sqrt{1 + \left(\frac{r}{r_0}\right)^2} \right] - \operatorname{atan} \left(\frac{r}{r_0}\right) \right\} \quad (2.11)$$

Other important profiles are the Navarro-Frenk-White profile (NFW) (see equation (2.12) and for a modified version by see equation (2.13)) and the Einasto profile (see equation (2.14)) (Navarro et al., 2010).

$$\rho(r) = \frac{\rho_s}{(r/r_s)(1 + r/r_s)^2}$$

$$M(r) = 4\pi\rho_s r_s^3 \left[\ln \left(\frac{r_s + r}{r_s}\right) - \frac{r}{r_s + r} \right] \quad (2.12)$$

$$\rho(r) = \frac{\rho_M}{(r/r_M)^{1.5} (1 + (r/r_M)^{1.5})} \quad (2.13)$$

$$\ln \left[\frac{\rho(r)}{\rho_{-2}} \right] = -\frac{2}{\alpha} \left[\left(\frac{r}{r_{-2}}\right)^\alpha - 1 \right] \quad (2.14)$$

The two parametric NFW-profiles also have the problem of divergent masses for a radius growing to infinity and therefore require a cut-off radius like the isothermal sphere and it also shares the cusp-problem with the isothermal sphere. An advantage of the NFW-profile is that it can fit galaxy clusters very well. The Einasto profile with its three parameters has shown the best results in fitting halos up to now (Navarro et al., 2010). But one can also reject the idea of Dark Matter and therefore the necessity of dark halos. In this case one has to change the theory of gravity, which leads to MOND or similar theories.

2.3 Dynamical friction

Dynamical friction is a quite interesting and also important phenomenon in stellar dynamics. Let us consider a body (e.g. a dwarf galaxy) with the mass m moving through a homogenous medium (e.g. Dark Matter halo) consisting of particles with individual masses much less than m . The body is moving with a velocity \vec{v} through this medium and the body's gravity attracts particles from the medium. Because the body moves on, the particles gather behind it and increase the density of the medium in area behind the body. The denser medium behind the body has a greater matter mass than the medium in front of the body and therefore a gravitational force \vec{a} acts on the body from the denser medium. So the body slows down. If it is orbiting another large mass (e.g. galaxy) the declining velocities causes the body to get closer to the large mass. I have displayed the process schematically in figure 2.1. The general formula for dynamical friction is given

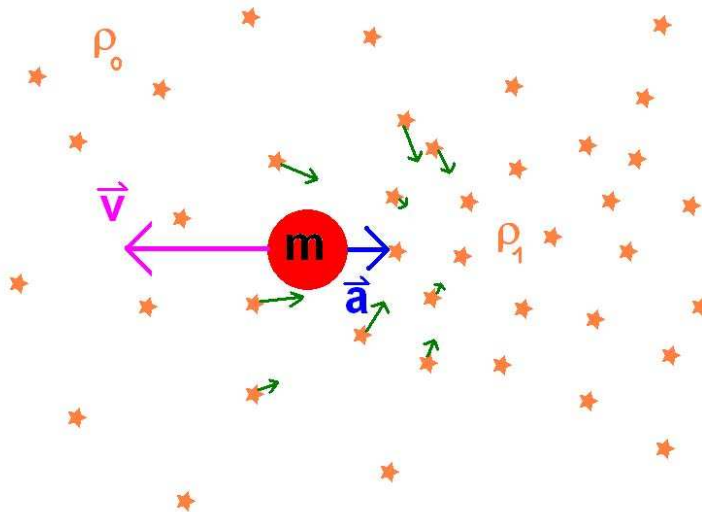


Figure 2.1: Schematic of dynamical friction.

in equation (2.15) (Chandrasekhar, 1943), where $\ln(\Lambda)$ is the Coulomb logarithm (note: Λ is the ratio between the maximum impact parameter and the 90° deflection radius, further information can be found in the textbook of Binney and Tremaine (Binney and Tremaine, 2008)), G the gravitation constant and \vec{v} the velocity (note: $v = |\vec{v}|$). In case of an Gaussian velocity-distribution $f(v)$ for the particles in the medium and a mass m of the object moving through the medium which is much larger then the mass μ of the particles of the medium it becomes equation (2.16). In this equation ρ represents the density of the medium and σ is the 1-dimensional velocity dispersion of the particles in the medium.

$$\frac{d\vec{v}}{dt} = -16\pi^2 \ln(\Lambda) G^2 \mu (m + \mu) \frac{\vec{v}}{v^3} \int_0^v f(w) w^2 dw \quad (2.15)$$

$$\frac{d\vec{v}}{dt} = -4\pi \ln(\Lambda) G^2 \rho m \frac{\vec{v}}{v^3} \left[\operatorname{erf} \left(\frac{v}{\sqrt{2}\sigma} \right) - \frac{\sqrt{2}v}{\sqrt{\pi}\sigma} e^{-\frac{v^2}{2\sigma^2}} \right] \quad (2.16)$$

The Chandrasekhar formula for dynamical friction in case of a singular isothermal halo (see equations (2.10)) takes the shape of equation (2.17).

$$\vec{a} = -\frac{Mm \ln\left(1 + \frac{Mr}{mr_H}\right)}{r_H r^2 v^3} \left[\operatorname{erf}\left(\frac{v\sqrt{r_H}}{\sqrt{M}}\right) - \frac{2v\sqrt{r_H}}{\sqrt{\pi M}} e^{-\frac{v\sqrt{r_H}}{\sqrt{M}}} \right] \vec{v} \quad (2.17)$$

The variable M is the total mass of the halo, r_H stands for the cut-off and scaling radius of the halo and r for the distance to the halo's centre of mass. All other variables still have the same meaning as in the previous formulas. But this does not take into account that one of the conditions used for the derivation of this formula is not fulfilled in the case of singular isothermal halos. Because of the violation of the homogeneity condition the force caused by dynamical friction has to be modified in its direction. For this we introduce an angle β which is defined by equation (2.18).

$$\beta = 0.75 \sqrt{1 - \left(\frac{\vec{v} \cdot \vec{r}}{vr}\right)^2} \quad (2.18)$$

With this angle a new direction \vec{d}_{DF} (see equation (2.19)) for the dynamical friction can be defined, where h is given by equation (2.20).

$$\vec{d}_{\text{DF}} = \cos(\beta)\vec{v} + \sin(\beta)\frac{\vec{h}}{h} \quad (2.19)$$

$$\vec{h} = -\frac{\vec{r}}{r} + \frac{\vec{v} \cdot \vec{r}}{rv^2}\vec{v} \quad (2.20)$$

Finally the new formula for dynamical friction (Petsch, 2007) is equation (2.21) and it is taking account the density gradient in an isothermal halo profile. The variable s is an additional scaling factor for the efficiency of the dynamical friction.

$$\vec{a} = -\frac{Mm \ln\left(1 + \frac{Mr}{mr_H}\right)}{r_H r^2 v^2} \left[\operatorname{erf}\left(\frac{v\sqrt{r_H}}{\sqrt{M}}\right) - \frac{2v\sqrt{r_H}}{\sqrt{\pi M}} e^{-\frac{v\sqrt{r_H}}{\sqrt{M}}} \right] \vec{d}_{\text{DF}} s \quad (2.21)$$

Furthermore one can estimate a merging time for dynamical friction (see equation (2.22)) in case of an isothermal halo (Sánchez-Salcedo et al., 2006), where v_{circ} is the circular velocity.

$$\tau_{df} \sim r^2 v_{\text{circ}} m^{-1} \quad (2.22)$$

2.4 Cosmology and the Hubble expansion

In modern Cosmology the universe is assumed to be homogeneous and isotropic. Of course this is not valid on small scales, but on very large scales ($> 200\text{Mpc}$) it is a good approximation and confirmed by observation (Peacock, 1999). In this case one can solve Einstein's field equations (see equation (2.8)) and the solution is called Friedmann-Lemaître-Robertson-Walker metric (see equation (2.23)).

$$c^2 d\tau^2 = c^2 dt^2 - R^2(t) [dr^2 + S_k^2(r) d\phi^2] \quad (2.23)$$

Of course c stands for speed of light, $R(t)$ is the cosmological radius and $S_k(r)$ a parameter which depends on the curvature k of space-time (see equation 2.24).

$$S_k(r) = \begin{cases} \sin(r) & (\text{if } k = 1) \\ \sinh(r) & (\text{if } k = -1) \\ r & (\text{if } k = 0) \end{cases} \quad (2.24)$$

Usually a dimensionless scale factor $a(t)$ (definition in equation (2.25)), which rises from zero (Big Bang) to one (today), is preferred. In this equation R_0 is the present day cosmological radius. Using the dimensionless scale factor the Friedmann-Lemaître-Robertson-Walker metric takes a form (see equation (2.26)) that is often used, where A is a constant which is proportional to $1/R_0$. The curvature parameter k is 0 for a flat universe (Euclidian geometry), -1 for a open universe (hyperbolic geometry) and 1 for a closed universe (spherical geometry).

$$a(t) = \frac{R(t)}{R_0} \quad (2.25)$$

$$c^2 d\tau^2 = c^2 dt^2 - a^2(t) \left[\frac{dr^2}{1 - k(Ar)^2} + r^2 d\phi^2 \right] \quad (2.26)$$

We can use this metric to derive the Friedmann equations (see equations (2.27)) with the help of Einstein's field equations (see equation (2.8)). One gets the first Friedmann equation from the 00-component of the field equations and the second one from their trace. ρ is the average density of the universe, Λ the cosmological constant, p a pressure and H the Hubble parameter.

$$\begin{aligned} H^2 &= \left(\frac{\dot{a}}{a} \right)^2 = \frac{8\pi G}{3} \rho - \frac{kc^2}{a^2} + \frac{\Lambda c^2}{3} \\ \dot{H} + H^2 &= \frac{\ddot{a}}{a} = -\frac{4\pi G}{3} \left(\rho + \frac{3p}{c^2} \right) + \frac{\Lambda c^2}{3} \end{aligned} \quad (2.27)$$

One can define a critical density ρ_c of the universe (see equation (2.28)), which should be equal to average mass density if the universe is flat. If the average density of the universe is higher than the critical density the universe is closed and if it lower than the critical density the universe is open.

$$\rho_c = \frac{3H^2}{8\pi G} \quad (2.28)$$

With this density one is able to define a dimensionless density parameter Ω (see equation (2.29)).

$$\Omega = \frac{\rho}{\rho_c} \quad (2.29)$$

We know from observations that the universe does consist of different types of energy which all contribute to the total density. In the early universe radiation was very important and there a is radiation density Ω_γ but since it scales with $\rho \propto a^{-4}$ its value has fallen to almost zero today. Another component which is still important is the matter density Ω_m which is the sum over all cold dark matter Ω_{CDM} and baryonic matter Ω_b in the universe. Pressure less matter scales with $\rho \propto a^{-3}$. Finally the vacuum energy (Dark Energy) Ω_Λ , whose density stays constant over time. Knowing that the Friedmann equation treats all contributions to the density parameter in the same way one can derive equation (2.30).

$$\frac{kc^2}{H^2 R^2} = \Omega_m(a) + \Omega_\gamma(a) + \Omega_\Lambda(a) - 1 \quad (2.30)$$

In case of a flat universe ($k = 0$) the total density parameter Ω stays constant ($= 1$) for all times. The Hubble-parameter for a multi-component universe is given by equation (2.31). H_0 is the present day Hubble parameter and it should be noted at this point that the expansion (in some models also collapse) of the universe is an intrinsic property of the Friedmann-Lemaître-Robertson-Walker metric and does not require additional assumptions.

$$H^2(a) = H_0^2(\Omega_\Lambda + \Omega_m a^{-3} + \Omega_\gamma a^{-4} - (\Omega - 1)a^{-2}) \quad (2.31)$$

One can find some up-to-date values for the most important cosmological parameters of the universe in table (2.1). The universe is obviously Dark Energy dominated and accelerating its expansion due to its negative pressure (also interpreted as cosmological constant). The matter in the universe is mainly cold dark matter. Furthermore the sum over all components of the total energy density parameters is extremely close to one (within the accuracy of measurement) and therefore it is assumed that is exactly equal one and the universe has a flat geometry. The cosmological standard model is supported by three important and independent observational facts: the abundance of elements due to the Big Bang Nucleosynthesis, the cosmic microwave background radiation and the expansion of the universe.

Ω_Λ	$0.726 \pm 0.015,$
Ω_{CDM}	0.228 ± 0.013
Ω_b	0.0456 ± 0.0015
H_0	$(70.5 \pm 1.3)\text{km s}^{-1}\text{Mpc}^{-1}$
t_0	(13.72 ± 0.12) Gyr
σ_8	0.812 ± 0.026

Table 2.1: recent values for the most important cosmological parameters of the universe based on WMAP-data (Komatsu et al., 2009).

Because it is required for my simulations, I have to find a way how to include the Hubble-Expansion as a background force into an integrator which uses Newtonian (non-relativistic) physics. The result should reproduce the simple present day Hubble relation for small separations (see equation (2.32))

$$v = H_0 x \quad (2.32)$$

The exact geometry of the universe is not very important for my later applications on small scales (from the cosmological point of view) (Sawa and Fujimoto, 2005). I choose for reasons of simplicity a matter dominated ($\Omega_m = 1$) universe, which is a sufficient

approximation for a bound system. In case of this kind of universe we can derive equation (2.33) which describes the Hubble expansion quite well, because $\vec{v} = H(t)\vec{x}$ and $H = (2/3)t^{-1}$ in a first approach for small separations.

$$\vec{v} = \frac{2}{3}t^{-1}\vec{x} \quad (2.33)$$

So we are looking for a differential equation like equation (2.34) which has a solution with the behaviour of equation (2.35).

$$\ddot{x} = c(t)x \quad (2.34)$$

$$\dot{x} = \frac{2}{3}\frac{x}{t} \quad (2.35)$$

With an educated guess and a comparison of coefficient we find equation (2.36) for our searched differential equation and it has a growing solution with fulfils our conditions.

$$\ddot{x} = \frac{\frac{2}{3}}{\frac{1}{2} + \frac{\sqrt{5}}{2}}t^{-2}x \quad (2.36)$$

This result was used in my programmes *NewHEXl* and *DeMonI* to simulate the Hubble expansion. I know that it is only a simple approximation and that it is not entirely physically correct, especially because the Hubble expansion is an effect caused by general relativity and my result works with Newtonian physics. Nevertheless it is an efficient and as physically correct as possible way to include a Hubble expansion into a Newtonian integrator.

Chapter 3

MODified Newtonian Dynamics

3.1 Galaxies rotate too fast

It is a well-known fact that all galaxies rotate faster than one would expect from visible matter (see figure 3.1). In 1959, it was shown that the galaxy M33 rotates different than one would expect from Newtonian gravitation and the visible matter (Volders, 1959). Furthermore, already in the 1930s, Zwicky proposed the existence of additional "Dark Matter" to explain the high relative velocities of galaxies in clusters (Zwicky, 1933). In 1983, Milgrom suggested to change the law of gravitation instead of adding some hidden mass and so the theory of MODified Newtonian Dynamics(MOND) was born (Milgrom, 1983). Both theories, Dark Matter and MOND, are very successful in fitting rotation curves of galaxies based on observational data.

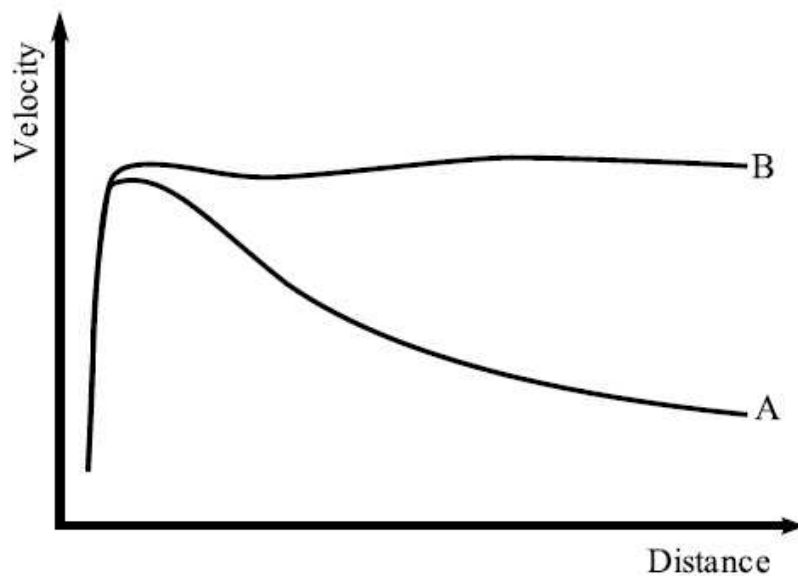


Figure 3.1: Rotation curve of a typical spiral galaxy: (A) predicted and (B) observed (from Wikipedia).

3.2 The MOND paradigm

We know from the observed shape of the rotation curves of disk galaxies that the inner part is in good agreement with our expectations from Newtonian gravity, but in the outer areas of these galaxies the disc spins faster. A detailed analysis of this case shows that the rotation speed of a galaxy stays approximately constant. Therefore if the possibility of additional hidden mass at large radii is excluded, the gravitational force has to become stronger at those larger distances where the accelerations get smaller. Based on these considerations equation (3.1) can be postulated.

$$m\mu\left(\frac{a}{a_0}\right)a = \frac{GMm}{r^2} \quad (3.1)$$

The variable m represents the mass of a test body (which obviously cancels out in this formula), M stands for the central mass (of a galaxy), r is the distance of the test body from this central mass and G is the gravitation constant. From the previous considerations it is clear that the function $\mu(x)$ has to be 1 for large accelerations and to get the right result it should be x for small accelerations at the outer areas of galaxies. The function $\mu(x)$ is called interpolation function and there are basically many possibilities how it should look like. The parameter of this function, x , is usually assumed to be a/a_0 , where a is the total acceleration and a_0 a new fundamental constant with the dimension of an acceleration which describes the transition from the Newtonian regime into the MONDian one. The value of this constant has to be measured by fitting the rotation curves of galaxies using the MOND theory. This new fundamental constant has a value of $1.2 \cdot 10^{-10} \text{ms}^{-2}$ (Milgrom, 2009) which is about $cH_0/(2\pi)$ (Milgrom, 2008) where c is the speed of light and H_0 the present-day value of the Hubble constant. $1/(2\pi) \cdot c(\Lambda/3)^2$ is also very close to the value of a_0 (Milgrom, 2008), where Λ represents the value of the cosmological constant. The problem of these coincidences is the lack of any physical motivation, although it might be a hint for a deeper connection between MOND and cosmology. The shape of the interpolation function μ cannot be derived from theory and has to be obtained by fitting to observational data. There are two different functions in use: $\mu(x) = x/\sqrt{1+x^2}$ and $\mu(x) = x/(1+x)$ with $x = a/a_0$. The first function has been found first but the second function has recently gained more popularity due to its greater success in fitting rotation curves. Both functions share the essential limits for large and small values of x . In the case of large values the function converges to unity and one gets the Newtonian formula for gravitation (equation (3.2)).

$$ma = \frac{GMm}{r^2} \quad (3.2)$$

For very small values for the parameter x , which corresponds to small accelerations in the outer regions of galaxies, the interpolation function becomes simply x . This case is called the deep-MOND limit and the equation which describes gravitation becomes equation (3.3).

$$\begin{aligned} \frac{ma^2}{a_0} &= \frac{GMm}{r^2} \\ a &= \frac{\sqrt{GMa_0}}{r} \end{aligned} \quad (3.3)$$

I have visualized the behaviour of the MONDian gravitational law and its two limits (the Newtonian and the deep-MOND) in figure 3.2. Let us calculate a small example using

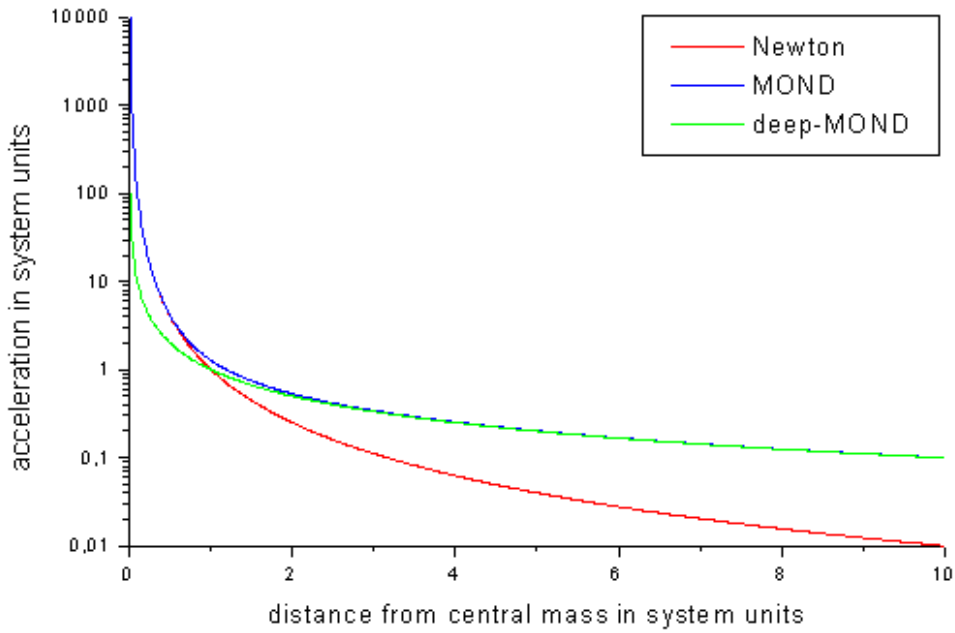


Figure 3.2: Comparison between accelerations in classical Newtonian dynamics, MOND and deep-MOND in case of a radial symmetric system with a point mass in its centre.

deep-MOND. It is known that the centripetal force F_z can be written like in equation (3.4), where v is a velocity.

$$F_z = ma = \frac{mv^2}{r} \quad (3.4)$$

Inserting equation (3.3) into equation (3.4) leads to equation (3.5).

$$v^4 = Ga_0M \quad (3.5)$$

Because deep-MOND is fulfilled in the outer areas of spiral galaxies, where the rotation curves become flat, this result can be interpreted that the fourth power of the rotation velocity v is proportional to the mass M of the galaxy. Assuming a constant mass to luminosity ratio M/L for spiral galaxies, one gets the Tully-Fisher relation (equation (3.6)) directly from the MOND paradigm.

$$L \propto v^4 \quad (3.6)$$

Up to now we have only analysed the case of a central mass but this is too simple and has to be generalised for complex n-body systems. It is obvious that one cannot simply add up the accelerations from all masses because of the non-linearity of the equation. Without the principle of superposition, the motion of a particle depends on the absolute acceleration on it. A general description of non-relativistic gravitation in MOND has been found in 1984 by Bekenstein and Milgrom (Bekenstein and Milgrom, 1984) and is called the modified Poisson equation (equation (3.7) and one can compare it with the normal Poisson equation (equation (2.1)) to see the difference).

$$\nabla \left(\mu \left(\frac{|\nabla\Phi(x)|}{a_0} \right) \nabla\Phi(x) \right) = 4\pi G\rho(x) \quad (3.7)$$

This equation connects the derivations of the potential $\Phi(x)$ with the matter density $\rho(x)$. It should be noted that the gradient of this potential $\nabla\Phi(x)$ is the acceleration and all other variables keep their previous meaning. This formulation of MOND is also known as AQUAL (AQUAdratic Lagrangian) (Bekenstein, 2009), because the modified Poisson equation follows from a Lagrangian density \mathcal{L} which is given in equation (3.8).

$$\mathcal{L} = -\frac{a_0^2}{8\pi G} f\left(\frac{|\nabla\Phi|^2}{a_0^2}\right) - \rho\Phi \quad (3.8)$$

A question that is still open concerning MOND is if it is really a new theory of gravity or a new theory of inertia (Milgrom, 2008). MOND has been very successful in fitting the rotation curves of low surface brightness galaxies as well as high surface brightness galaxies (Sanders, 2001). Mergers in MOND are different because they are less likely to happen, because there is no Dark Matter halo and therefore the cross section is smaller and the collision velocities are higher due the stronger long distant force. On the other hand, the merging process takes longer (features are visible for a longer time) for the same reasons and it is possible to get the same observed merger rate (Nipoti et al., 2007a). Furthermore, modified Newtonian gravity might be a possibility to explain the Pioneer-anomaly (Anderson et al., 2002). But on the other hand, MOND also has several big problems which are summarised in another section.

3.3 TENSOR-VECTOR-SCALAR gravity

For about two decades the MOND-theory had a very big problem: there was no relativistic generalisation of it. But in 2004 Bekenstein published his TENSOR-VECTOR-SCALAR theory of gravity (TeVeS), a relativistic extension of the MOND-theory. *"TeVeS is based on three dynamical gravitational fields: an Einstein metric $g_{\mu\nu}$ with a well defined inverse $g^{\mu\nu}$, a timelike 4-vector field u_μ such that equation (3.9) is valid and a scalar field Φ ; there is also a nondynamical scalar field σ (the acronym TeVeS recalls the theory's Tensor-Vector-Scalar content)."* (Bekenstein, 2004)

$$g^{\mu\nu}u_\mu u_\nu = -1 \quad (3.9)$$

For further calculations we have to define the metric $\tilde{g}^{\mu\nu}$ in equation (3.10).

$$\tilde{g}^{\mu\nu} = e^{2\Phi}g^{\mu\nu} + 2u^\mu u^\nu \sinh(2\Phi) \quad (3.10)$$

Now we can define a field equation for the Einstein tensor $G_{\alpha\beta}$ (see equation (2.9) for the definition) of the metric $g^{\mu\nu}$ as one can see in equation (3.11), where $\tilde{T}_{\alpha\beta}$ represents the physical energy-momentum tensor defined by the metric $\tilde{g}_{\alpha\beta}$.

$$\begin{aligned} G_{\alpha\beta} &= 8\pi G \left(\tilde{T}_{\alpha\beta} + (1 - e^{-4\Phi}) u^\mu \tilde{T}_{\mu(\alpha} u_{\beta)} + \tau_{\alpha\beta} \right) + \Theta_{\alpha\beta} \\ \tau_{\alpha\beta} &= \sigma^2 \left(\Phi_{,\alpha} \Phi_{,\beta} - \frac{1}{2} g^{\mu\nu} \Phi_{,\mu} \Phi_{,\nu} g_{\alpha\beta} - u^\mu \Phi_{,\mu} \left(u_{(\alpha} \Phi_{,\beta)} - \frac{1}{2} u^\nu \Phi_{,\nu} g_{\alpha\beta} \right) \right) - \frac{1}{4} G l^{-2} \sigma^4 F(kG\sigma^2) g_{\alpha\beta} \\ \Theta_{\alpha\beta} &= K \left(g^{\mu\nu} u_{[\mu,\alpha]} u_{[\nu,\beta]} - \frac{1}{4} g^{\sigma\tau} g^{\mu\nu} u_{[\sigma,\mu]} u_{[\tau,\nu]} g_{\alpha\beta} \right) - \lambda u_\alpha u_\beta \end{aligned} \quad (3.11)$$

In addition to the tensor equation the TeVeS-theory also has a vector equation, (equation (3.12)) and a scalar equation (equation (3.13)) too.

$$\begin{aligned} K \left(u_{;\beta}^{[\alpha;\beta]} + u^\alpha u_\gamma u_{;\beta}^{[\gamma;\beta]} \right) + 8\pi G \sigma^2 \left(u^\beta \Phi_{,\beta} g^{\alpha\gamma} \Phi_{,\gamma} + u^\alpha (u^\beta \Phi_{,\beta})^2 \right) = \\ = 8\pi G (1 - e^{-4\Phi}) \left(g^{\alpha\mu} u^\beta \tilde{T}_{\mu\beta} + u^\alpha u^\beta u^\gamma T_{\gamma\beta} \right) \end{aligned} \quad (3.12)$$

$$\left(\mu (kl^2 h^{\mu\nu} \Phi_{,\mu} \Phi_{,\nu}) h^{\alpha\beta} \Phi_{,\alpha} \right)_{;\beta} = kG (g^{\alpha\beta} + (1 - e^{-4\Phi}) u^\alpha u^\beta) \tilde{T}_{\alpha\beta} \quad (3.13)$$

This very complex system of partial differential equations is the basic tool for doing calculations in TeVeS and Bekenstein showed that these equations have limits to General Relativity and non-relativistic MOND. It is also possible to calculate post-Newtonian corrections, gravitational lensing and the cosmological evolution, which are all consistent with observations.

3.4 Problems

Although MOND has been shown to be very successful in fitting rotation curves of galaxies, it also has several unsolved problems.

3.4.1 Bullet Cluster

One of the biggest challenges for this theory is without doubt the so called Bullet Cluster (1E0657-558) (Clowe et al., 2006). This unique cluster has been penetrated by another cluster, which caused the baryonic matter to separate from Dark Matter. The (Dark) Matter distribution in this cluster has been determined by weak lensing observations. The dominant baryonic matter component is hot plasma, which can be observed in X-ray. Due to the penetration of the cluster by another one, hot gas has been displaced from the clusters' potentials, because gas interacts electromagnetically. In MOND one expects gravity (and therefore the lensing effect) to coincide with the distribution of baryonic matter. Since Dark Matter only interacts with gravity (and maybe the weak interaction), one expects that its distribution is hardly afflicted by this high velocity encounter. Thus the Dark Matter model is able to explain the observation quite easily. A similar phenomenon has been discovered in the cluster Cl 0024+17 (Jee et al., 2007). It is argued that these phenomena might be MOND artefacts and possible evidence for MOND transition regions (Milgrom and Sanders, 2008).

3.4.2 Galaxy clusters

Another problem for MOND are galaxy clusters in general. Despite the stronger long range gravity in MOND it is still not strong enough to reproduce the high velocity distributions of galaxies moving in clusters. Although the needed invisible mass can be significantly reduced by MOND, there has to be additional Dark Matter to explain the observations. About a factor of 2-3 discrepancy between the visible and the dark component remains (Sanders, 2003; Aguirre et al., 2001). It is speculated that this might be a hot Dark Matter component like neutrinos (Sanders, 2003). The need of additional invisible matter does not disprove MOND, but it is a blow against the original motivation of the theory to solve the missing mass problem without Dark Matter.

3.4.3 Timing of the Local Group

A similar but somehow opposite challenge for MOND is the timing problem of the Local Group. Assuming that the Milky Way and M31 are still on their first orbit, one can derive masses for both galaxies which are by far too small. The mass of the Milky Way would only be $1.2 \cdot 10^{10} M_{\odot}$ which is about 24% of the estimated baryonic mass of our galaxy (Shi, 2009). In contrast to missing matter, where arguments for some additional hidden matter can be found quite easily, one can hardly argue against already observed visible matter, especially in this magnitude. Possible solutions for this problem within the MOND framework would be a quite high tangential velocity of the Andromeda Galaxy or that both galaxies simply are not on their first orbit anymore.

3.4.4 Lyman- α

A problem of MOND that has been hardly investigated is the Lyman- α -problem. Aguirre et al find that, "*because MOND violates the strong equivalence [sic] principle, the properties of Ly α absorbers depend strongly upon the (unknown) background acceleration field in which they are embedded.*" (Aguirre et al., 2001). Although there are no further discussions of this problem in the literature, it might have been solved by the general relativistic formulation of the MOND paradigm in the form of the TENSOR-VECTOR-SCALAR gravity.

Chapter 4

N-MODY

4.1 Introduction

It is quite a challenge to develop an integrator which treats n-body stellar dynamics in MOND. The full n-body problem in Modified Newtonian Dynamics is much more complex than in simple Newtonian Dynamics, because several concepts, on which we are used to rely, do not work in MOND. Due to the non-linearity of the modified Poisson-equation superposition cannot be used to simplify the force calculation. One needs to solve the full modified Poisson-equation to get the accelerations on the particles and this is what *N-MODY* has to do. The programme has been developed by Pasquale Londrillo and Carlo Nipoti and it is written in *Fortran90*. The code has already been used to investigate several problems (Londrillo and Nipoti, 2009). *N-MODY* has also been used to enlighten the topics of the structure of disc galaxies (Nipoti et al., 2007b), phase mixing (Ciotti et al., 2007) and mergers (Nipoti et al., 2007a) in MOND. There have been also studies about the dynamical friction in MOND (Nipoti et al., 2008). Dynamical friction has been shown to be more effective in MOND by simulations of a rotating bar in galaxy, but the authors have made a wrong generalisation for dwarf galaxies orbiting a host galaxy. In contrast to their statement these galaxies do not suffer from dynamical friction, because in MOND there is no dark matter or any other material in sufficient quantity in the halo. *N-MODY* has brought quite a lot of progress for MOND.

4.2 How does it work?

N-MODY uses a particle-mesh scheme to calculate the particles' accelerations due their mutual modified gravitational interaction. The gravitational forces are calculated on the grid in spherical coordinates by solving the modified Poisson-equation. The particles are moved by a leap-frog scheme which uses the gravitational forces computed on the grid which are linked by a particle-mesh interpolation. There exists a scalar as well as an efficient parallel version of *N-MODY* code.

One starts by creating a set of equal mass particles because *N-MODY* cannot handle neither massless test particles, nor massive particles with different masses. Although the code uses spherical coordinates for the grid, the initial positions and velocities of the particles in the input file have to be given in Cartesian coordinates. This input file has to be written in a special binary format, so one has to write a translation programme if one wants to create a simple example by hand or if one's model is created by another programme, one has to adjust the output to the required format. In any case it is very useful to have a translation programme at hand, because the output-files of *N-MODY* are using the same binary format. In addition to the coordinate file one also needs another input file which contains the basics parameters like the grid size, number of output file, integration time, the scaling parameter and many more. One of the most important parameters in this file is the so called gravity parameter which can be set to three different values. In the case of zero *N-MODY* uses only Newtonian gravity. If the parameter is set to one the programme calculates the mutual gravitational interaction of all particles in the full MONDian framework. The parameter can also have the value two and in this case the integration is done in the deep-MOND limit (see equation 3.3). The first task that the *N-MODY* code has to perform after the initialisation is the calculation of the density grid. "*N-MODY* uses a spherical grid (r, θ, ϕ) with radial coordinate represented by the invertible mapping on the angular ξ coordinate, $0 = \xi < \pi/2$,

$$\begin{aligned} r(\xi) &= L \tan^\alpha(\xi) \\ r'(\xi) &= \frac{\alpha L \tan^{\alpha-1}(\xi)}{\cos^2(\xi)} \end{aligned} \quad (4.1)$$

where the mapping index $\alpha = 1$ or $\alpha = 2$ and the scale length L are user provided parameters. In this representation, any unbounded radial range is mapped onto the finite open interval $[0, \pi/2)$." (Londrillo and Nipoti, 2008). This special mapping and an elegant discretisation avoid singularities on the grid. The mass is assigned to the grid using either linear or quadratic shape functions. Finally the density on the grid is calculated by counting the particles and interpolating between the cells. In the next step this grid based density-field is used to get the particles' acceleration. For this task the modified Poisson-equation (see equation (3.7)) has to be solved and *N-MODY* does it by solving a Newton-like relaxation procedure. In the case of the MOND problem a functional like equation (4.2).

$$f(\Phi(x)) = \nabla \left(\mu \left(\frac{a}{a_0} \right) \nabla \Phi(x) \right) - 4\pi G \rho(x) \quad (4.2)$$

can be used. Starting with an initial guess Φ_0 and some iterations one is able to derive a relaxation operator, which is quite difficult to compute. Using some approximations one can get a simpler operator (see equation (4.3)) with a lower convergence rate, but which is easier to implement.

$$f(\Phi_n) = \delta f_{n-1}(\delta \Phi_{n-1}) + f(\Phi_{n-1}) + \mathcal{O}((\delta \Phi_{n-1})^2) \quad (4.3)$$

Now *N-MODY* only needs to solve a sequence of Poisson equations

$$\nabla^2 \delta\Phi_n = S_n \quad (4.4)$$

where the source term

$$S_n = -\frac{1}{\omega\mu_n} f(\Phi_n) \quad (4.5)$$

contains our functional. Due to the used system this is done in spherical coordinates after expanding the source term and the potential increments $\delta\Phi_n$ in spherical harmonics. From the differences of these potential increments the acceleration increments δa_n are calculated. This process is repeated until the convergence criterion (see equation (4.6)) is reached, where ϵ is the tolerance parameter.

$$\left\| \frac{\delta a}{a} \right\| < \epsilon \quad (4.6)$$

Now one has a grid based acceleration field and need to assign the correct accelerations on the right particles. For this task we first have to transform the Cartesian particle coordinates into spherical ones. Because of the special radial mapping which is used by *N-MODY*, the radial coordinate of every particle has to be transformed such as one can see in equation (4.7).

$$\xi = \arctan \left(\left(\frac{r}{L} \right)^{\frac{1}{\alpha}} \right) \quad (4.7)$$

The acceleration of a particle is evaluated by interpolating using the linear or quadratic shape functions between the grid cells in spherical coordinates and transforming the results into Cartesian coordinates afterwards. In the next step the particles are moved using a standard leap-frog integration scheme. First a half-step position move is performed, then the acceleration is calculated followed by a one-step velocity move and finally it is completed by another half-step position move. At every print-step the particles' positions and additional data are written into files which are labelled *mout*.bin*. One can input the size of a print-step directly because it is calculated by the total calculation time and the number of outputs, which is limited to be 100 (including the initial positions). The output files for the particle data are using exactly the same format as the input file for the initial positions. In other files the grid data (*mond*.bin*), the particles potentials (*pout*.bin*) and the diagnosis on conservations laws (*diag*.dat*) is outputted.

4.3 Errors

4.3.1 Overview

After I got used to *N-MODY*, I have run some simple simulation. During these simulations I have noted some very strange features of the programme. So several tests have been set up to investigate the boundaries of validity of the *N-MODY* code. The results have been surprising, because neither a stable configuration nor a realistic movement of particles in a simple configuration could be found. Varying the basic parameters of the programme and investigating different models have been tried.

4.3.2 Few-body problems

The simplest possible configuration is a two-body system with equal masses. The particle-mesh code, which is used by *N-MODY*, has fundamental problems with systems consisting only out of few bodies. The grid works like a softening length for the gravitational interaction and does not allow to resolve a two-body interaction properly at a scale of a few grid cells and therefore close two-body encounters cannot be calculated. The problem disappears if one significantly increase the number of particles, because then these encounters are not playing an important role anymore. Although knowing about this problem, I've tried to run a couple of simulations with two or a few (up to eight) particles to see if it is working. It has been done to investigate if the programme can be used for my applications despite the known resolution problem. After a few test runs one notices that the results are drastically different from the expectations. The first setup has consisted of two bodies arranged symmetrically around the centre of the coordinate system with a certain tangential velocity. After both particles have moved about 45° on a circular orbit around the centre they have stopped and stayed there wobbling around. Different time steps have been tried for the output to ensure that this strange behaviour has not been caused by a stroboscopic effect. In another test, a ring of eight particles has been set up and every particle has had a small tangential velocity (see figure 4.1). This system has been instable as expected and has flown apart. The surprise is, when one moves exactly the same configuration a few system units off centre and the result is very different (see figure 4.2). The particles form a kind of stream and all of them move away accelerating in approximately the same direction. This violation of symmetry is unexpected but can be explained by the spherical grid. During my detailed analysis of all those models I have had a look on the density grid and it has looked quite different from which one would expect. In case of the two-body problem one would think that there were two peaks of positive mass density on the grid, while everywhere else the density should be zero. But the grid looks different: there is a pattern of positive and negative (!) matter density on the whole concentric sphere on which both particles are placed. This fact is most confusing and has raised first doubts about the correct functionality of the *N-MODY*. But *N-MODY* has not been developed for these special cases and therefore the testing series has been continued with more complex systems, where two-body interactions are neglectable.

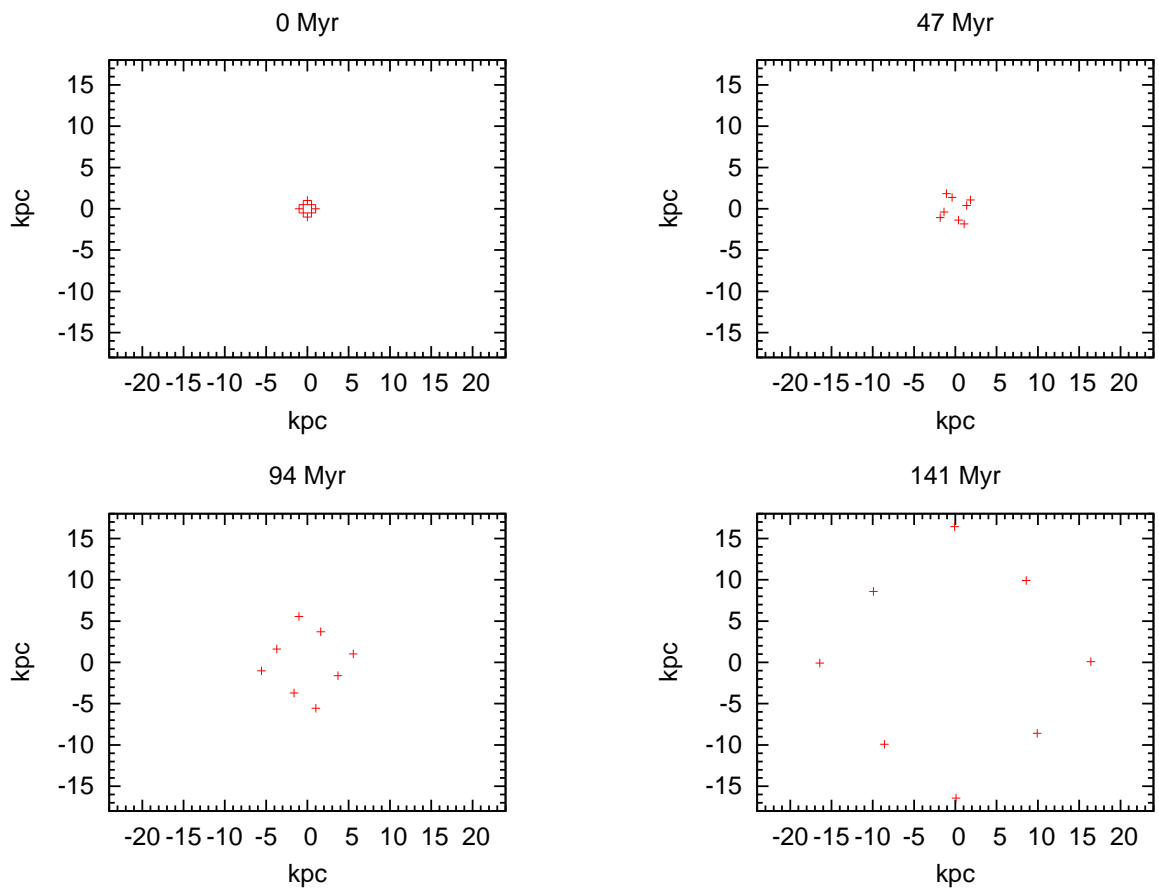


Figure 4.1: The evolution of a centred group of eight particles in N - $MODY$. The symmetry of their distribution is preserved.

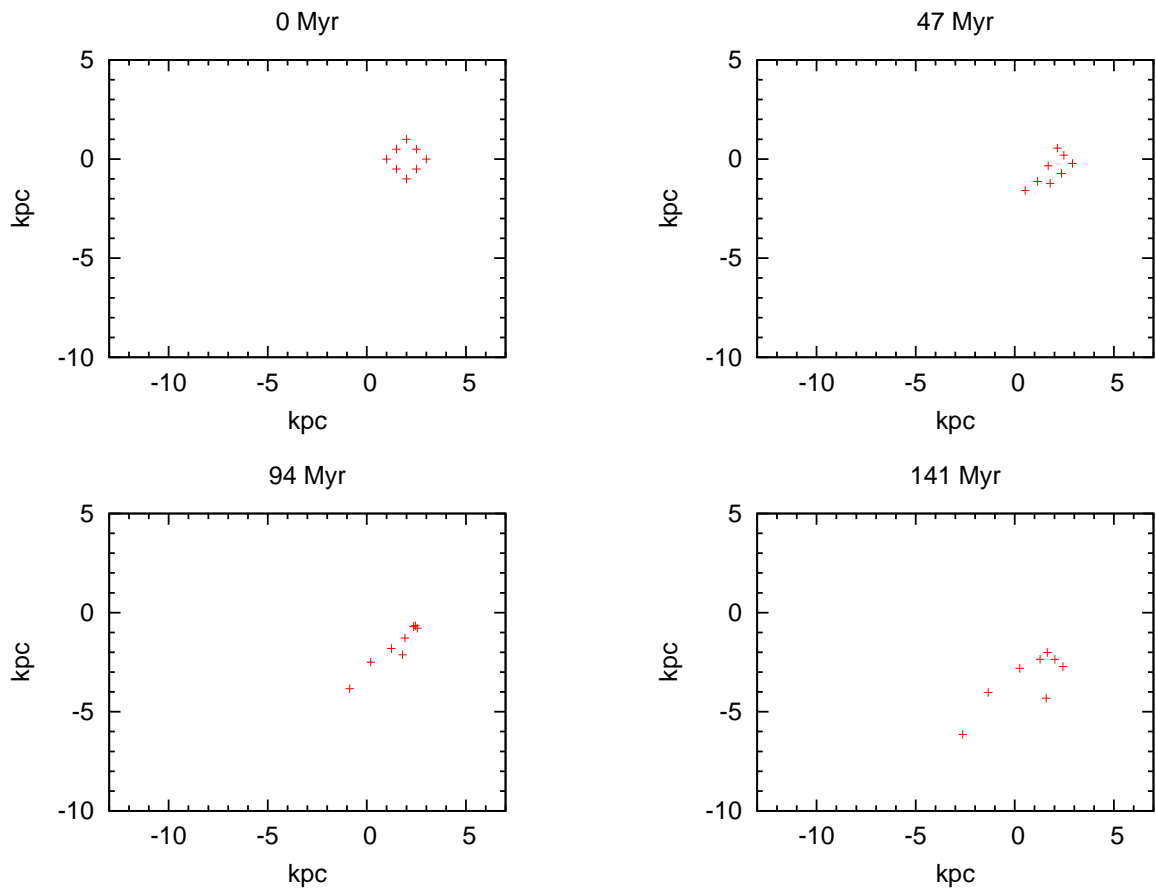


Figure 4.2: The evolution of a group of eight particles in *N-MODY* with its starting positions shifted a little off-centre. The initial symmetry of the particles' distribution breaks down in contrast to figure 4.1).

4.3.3 Merger

Instead of calculating the interaction between two single particles I have decided to have a look at the interaction between two systems consisting out of many particles. Starting with the simplest model one can imagine for this case: one sets up two Plummer-spheres separate by certain initial distance and gives them a small initial velocity for a direct head-on collision. The orbit of those two spheres in *N-MODY* have really been unexpected, because they have not collided. The motion of the centres of mass of both Plummer spheres has been visualized in figure 4.3 and furthermore some selected snapshots of this "merger" have been plotted in figure 4.4. When both Plummer-spheres have got closer, they have started evading themselves. To make the situation even stranger both spheres have shown signs of tidal distortion. Although *N-MODY* has mainly been developed for isolated systems mergers have already been performed with this code. After contacting Nipoti he has informed me that they have used a slightly different version of *N-MODY* for those simulations. Nevertheless the behaviour of this simulation is too wrong for a physically correct code; they shall have collided at least!

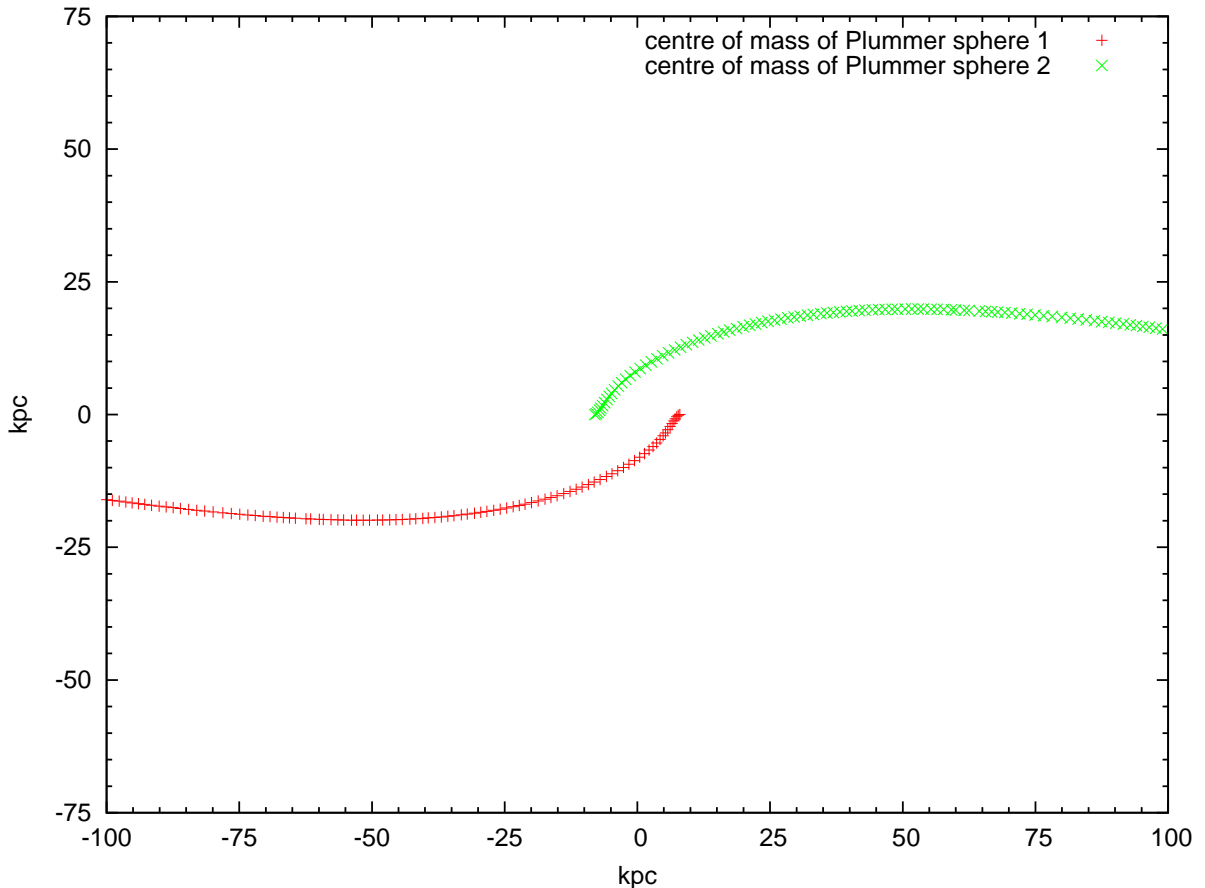


Figure 4.3: Orbits of the centres of mass of the Plummer-spheres in case of a head-on merger with *N-MODY* for 1175 Myrs. One can easily see that the spheres turn aside before the expected merger.

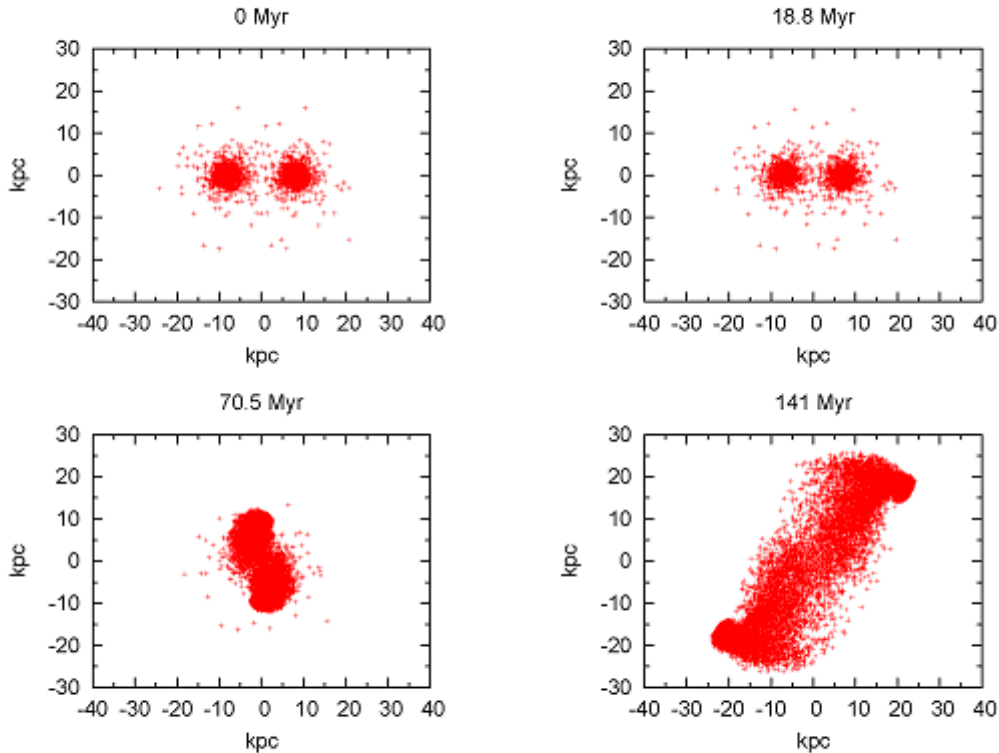


Figure 4.4: Snapshots of a head-on merger with *N-MODY*. First both Plummer-spheres approach a little, but right before the expected collision they turn aside and show tidal features like a close encounter.

4.3.4 Disk-galaxies

It is very difficult to set up a stable disc galaxy in MOND and there are no common tools available for this. My first approach has been quite simple: I have set up a normal disc galaxy with a dark matter halo and have removed the halo afterwards. This method leaves the problem to find a halo corresponding to MOND. To solve it, one can try to find a stable configuration by varying the MONDian acceleration constant a_0 , which corresponds to rescaling the system. The tool *mkkd95* from the *NEMO*-package has been used to create a Kuijken-Dubinski galaxy (Kuijken and Dubinski, 1995) from which the halo has been removed afterward (see figure 4.5). The models have been integrated for several hundred Megayears using *N-MODY* and one sees some surprising effects. One expects some radial instability in the disc plane, especially at the MONDian area between Newtonian core and the outer disc which is in deep-MOND regime. Surprisingly this has been the smallest problem. The outer disc begins to warp and very soon the galaxy looks like a "Pringle" (see figure 4.9). Then the warped disc dissolves itself into a couple of streams orbiting the core and after more than a Gigayear the galaxy resembles an elliptical more than a disc galaxy. The warp which appears very quickly after the beginning of the integration has a quite astonishing property (see figures 4.6 and 4.7, note that these figures are for

Newtonian gravity but the effect is the same with MONDian gravity). On one side it goes down and on the exact opposite side it goes up. At this point I want to especially point out that there is only one totally isolated disc galaxy and no external forces in this simulation. The first thought has been that it might be an effect caused by the initial distribution of particles in the galaxy and therefore a simulation with exactly the same model but rotated by 90° around the z-axis has been run again. But the warp is, seen from the same view port, the same. After seeing this one may think that it might be an effect caused by the grid and so one can run a simulation each with double radial grid resolution, four-times angular grid resolution, eight-times grid resolution and 64-times grid resolution. Also some simulations with an increased number of particles have been done but in all those cases the effect has been still the same. I also have had a look on the density grid again and there I have been able find many grid cells with negative matter density again although in this case the grid cells with positive matter density are dominant. One can disable the MONDian physics in *N-MODY* by setting a variable in the input file to a certain value and then one has a classical Newtonian potential solver. This feature has been used to calculate a whole Kuijken-Dubinski galaxy including the halo. For comparison the same model have been run using the *gyrfalcON* code from the *NEMO*-package and there the model is perfectly stable. But when using *N-MODY* switched to the Newtonian mode one gets a similar warping and dissolution effect for the disc of the galaxy like in MOND mode (see figures 4.5 to 4.9).

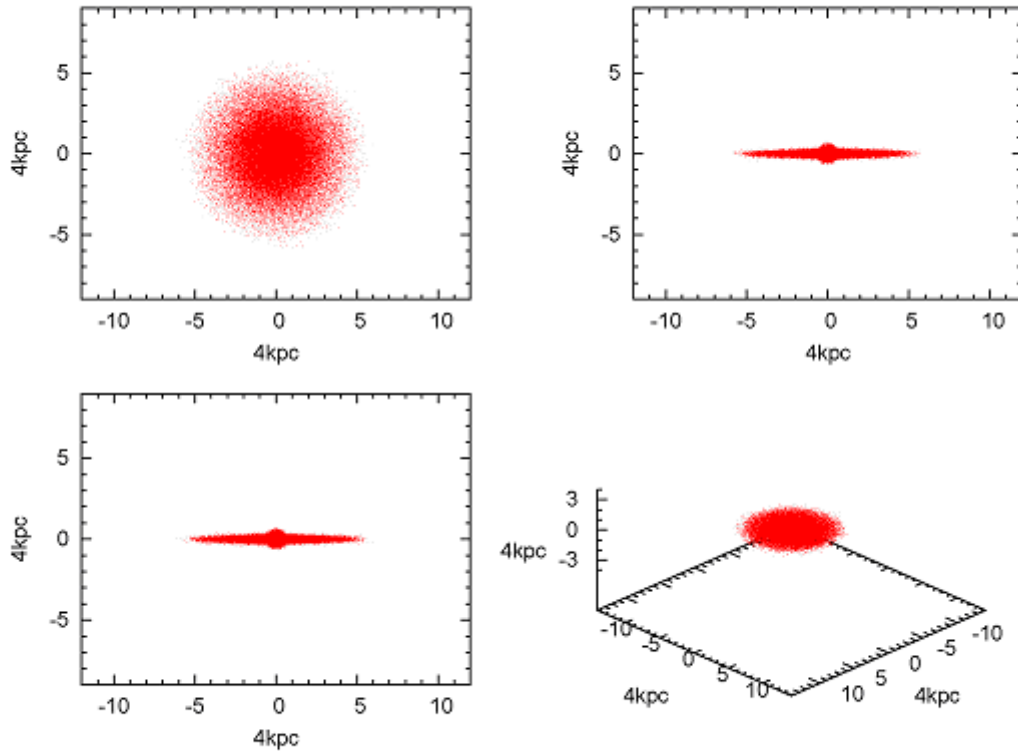


Figure 4.5: Disc and bulge of a KD95-galaxy calculated with *N-MODY* in the Newtonian mode (with an invisible dark matter halo) at 0 Myr. It is perfectly normal disc galaxy. The image in the upper-left corner is the view on the xy-plane, in the upper-right corner one finds the view on the yz-plane, in the lower-left corner there is a view on the xz-plane and in the lower-right corner one can find a 3D view along the first median.

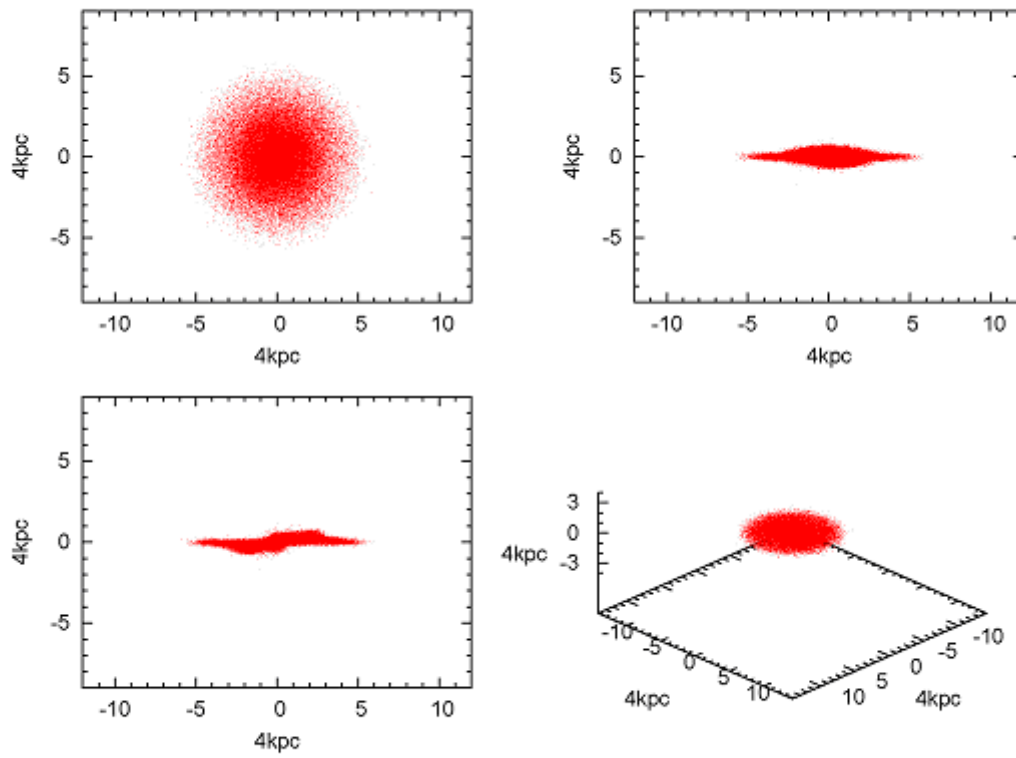


Figure 4.6: Same as figure 4.5, but at time $t = 188$ Myr.

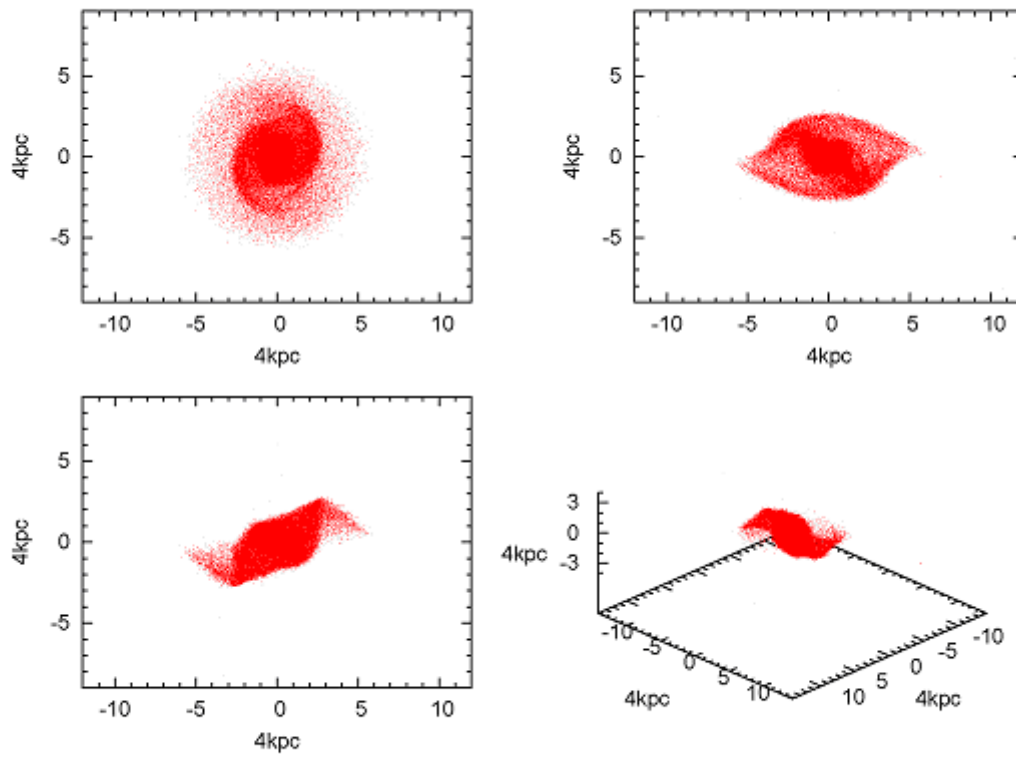


Figure 4.7: Same as figure 4.5, but at time $t = 564$ Myr.

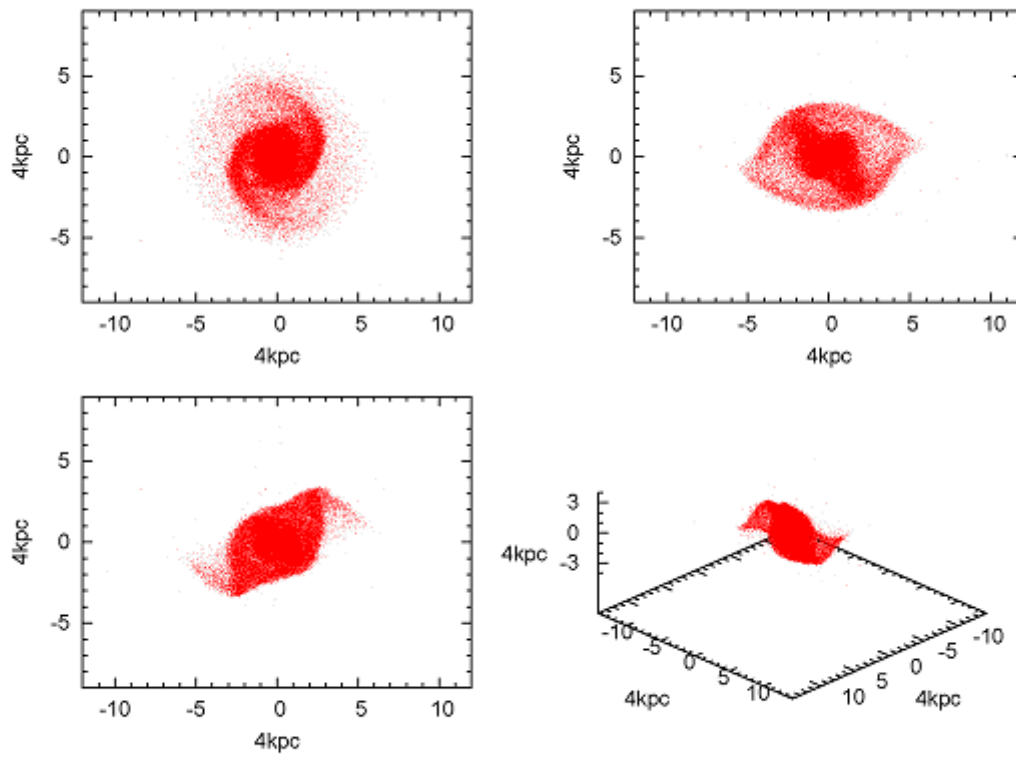


Figure 4.8: Same as figure 4.5, but at time $t = 940$ Myr.

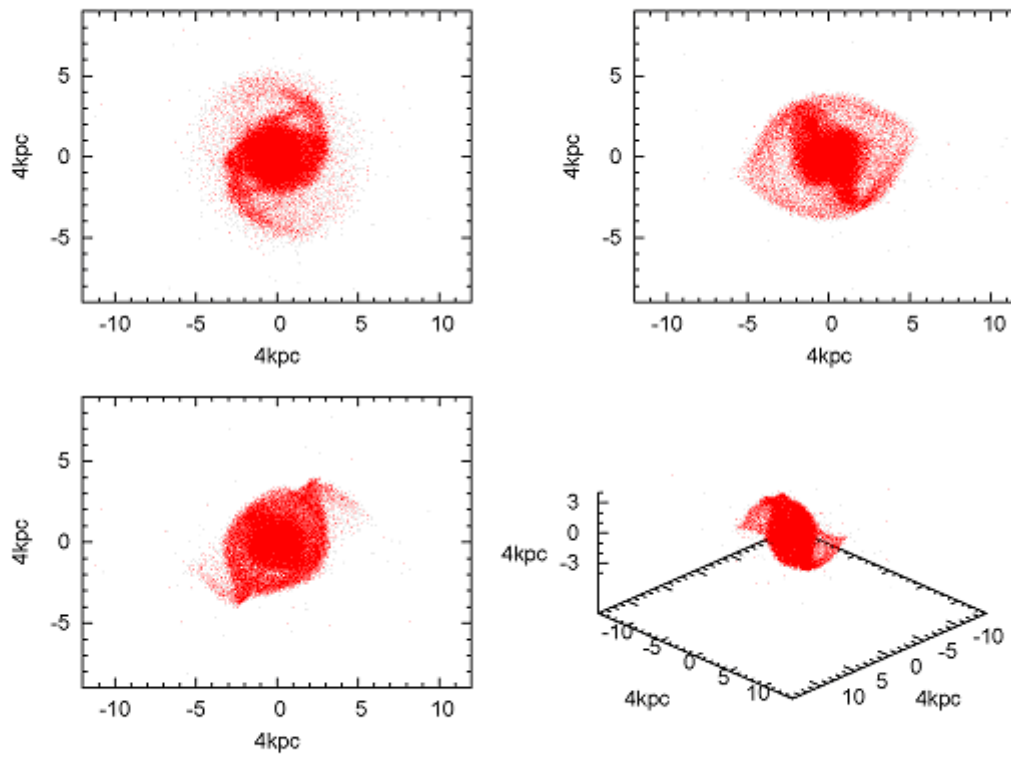


Figure 4.9: Same as figure 4.5, but at time $t = 1504\text{Myr}$.

4.3.5 Flattening of Plummer-Spheres

A code which uses spherical coordinates should work best on a system that has a spherical symmetry. A Plummer sphere has been created using the programme *mkplum* from the *NEMO*-package. This model has been integrated for 1.175 Gigayears and the results have been analysed in detail. One notices that the Plummer-Sphere is not a sphere anymore but an ellipsoid at the end of the simulation. As a consequence of this discovery a whole set of simulations has been run to investigate this phenomenon more closely. Seven simulations with different values for a_0 (see figures 4.18, 4.20, 4.21 and 4.22) have been set up and one simulation in which *N-MODY* is switched to its deep-MOND mode and another simulation with *N-MODY* in the Newtonian mode too and for comparison one additional simulation using the *gyrfalcON*-code. To analyse the flattening a small programme has been written, which calculates the sum of the projected distances on an axis of all particles from the centre for all three axes. The ratio between those three values should be close to one for a spherical system (in case of perfect symmetry: exactly equal one). I have plotted the absolute value of the deviation from one of all those three ratios against the time and one finds some correlations. The anisotropy effect along the z-axis increases with an increasing value of a_0 while the anisotropy in the x-y plane stays much smaller (see figures 4.10, 4.11, 4.12, 4.13, 4.14 and 4.15). To measure the anisotropy one can define a relative anisotropy a_{rel} (see equation 4.8) between two coordinate axes (here called v and w). The variable N denotes the number of particles, the v_i represent the v-coordinates of the particles and the w_i represent the w-coordinates of the particles.

$$a_{\text{rel}} = \left| \frac{\sum_{i=1}^N |v_i|}{\sum_{i=1}^N |w_i|} - 1 \right| \quad (4.8)$$

In the special case of the deep-MOND model there is a real jump in anisotropy after 540.5 Megayears. The reason becomes quickly visible when one has a look on the Lagrange radii or the simulation itself. During the first time steps the Plummer-sphere shows some radial oscillations which are caused by the stronger gravitational force in the deep-MOND regime. After some time the system relaxes and becomes stable. Then suddenly it "explodes" (see figures 4.18, 4.23, 4.24 and 4.25)! This means the radius of the Plummer-sphere increases with one time step by a factor of more than hundred. One can easily see this in the time evolution of the Lagrange radii (see figures 4.16 and 4.17) too. In both simulations using Newtonian physics the anisotropy remains small and in the simulation using *gyrfalcON* instead of *N-MODY* the anisotropy is by far the smallest. The flattening along the z-axis is very likely caused by a radial orbit instability. Because of the stronger gravitational forces due to MOND in the outer parts of the model some orbits get more radial. The greater the value of a_0 the larger the affected area is and one will get more radial orbits. But it fails to explain the explosion of the deep-MOND model or the fact that the Newtonian model in *N-MODY* is more anisotropic than in other codes (see figures 4.18 and 4.19).

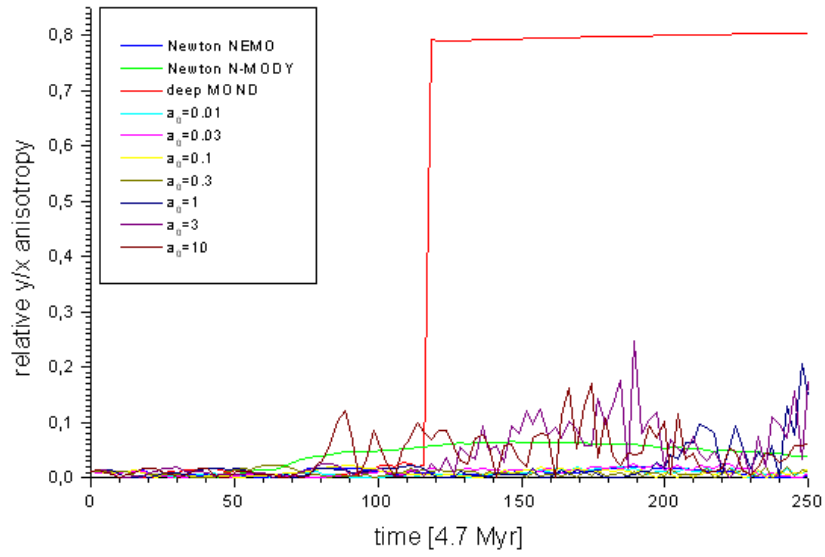


Figure 4.10: Anisotropy between the y - and x -axis of Plummer spheres in N - $MODY$. Note the extreme jump in case of deep-MOND.

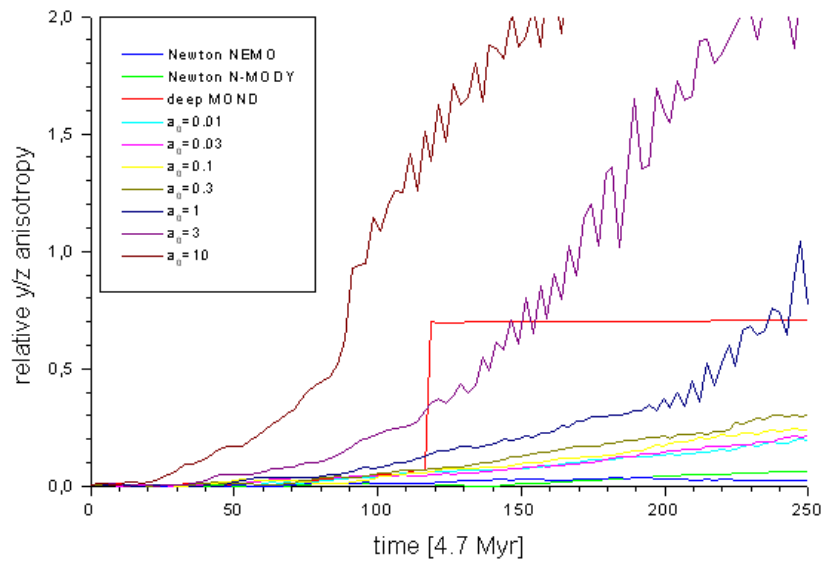


Figure 4.11: Anisotropy between the y - and z -axis of Plummer spheres in N - $MODY$. Note the strong increase for models with a large value of a_0 and the jump in the deep-MOND case.

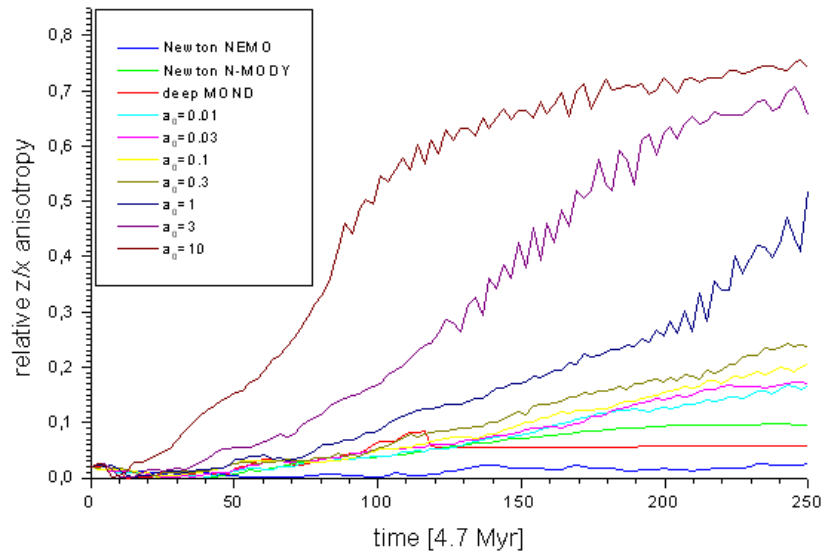


Figure 4.12: Anisotropy between the z - and x -axis of Plummer spheres in N - $MODY$. Note the strong increase for models with a large value of a_0 .

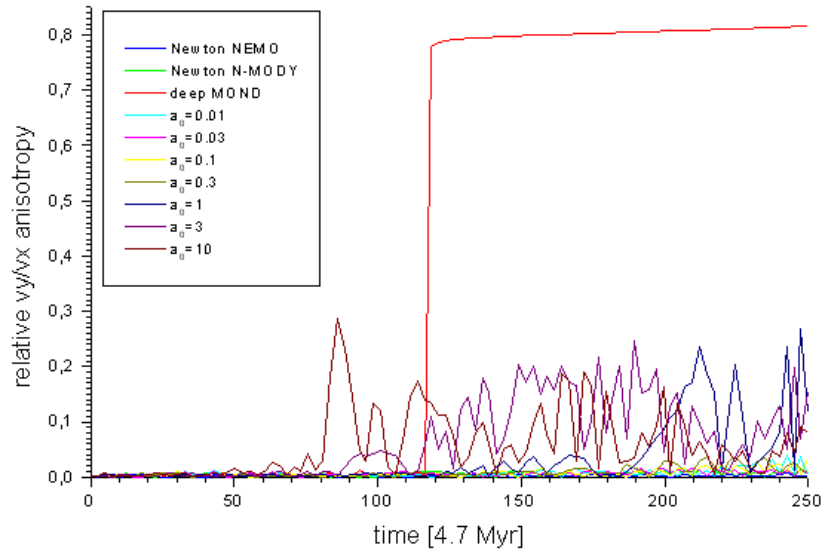


Figure 4.13: Velocity anisotropy between the y - and x -axis of Plummer spheres in N - $MODY$. Note the jump in case of deep-MOND but also the fluctuations for large values of a_0 .

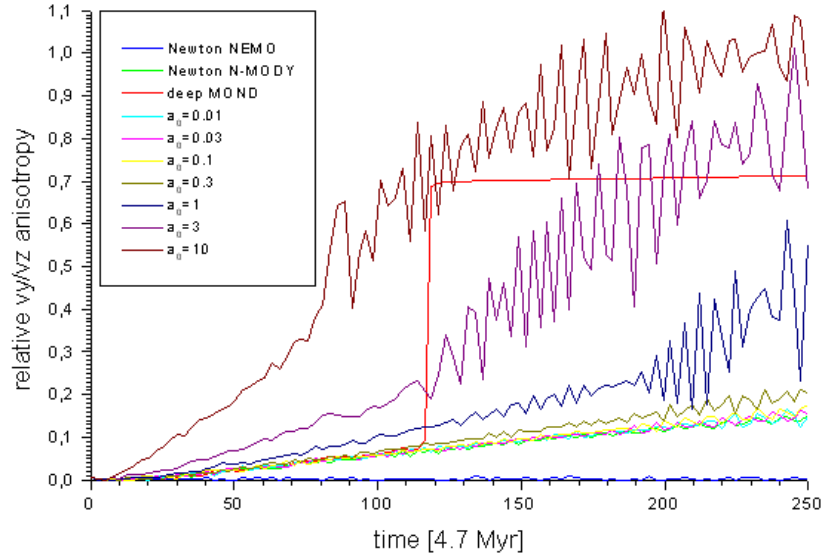


Figure 4.14: Velocity anisotropy between the y- and z-axis of Plummer spheres in *N-MODY*. Note that the increase for all models calculated with *N-MODY* and that its gradient correlates with the value of a_0 .

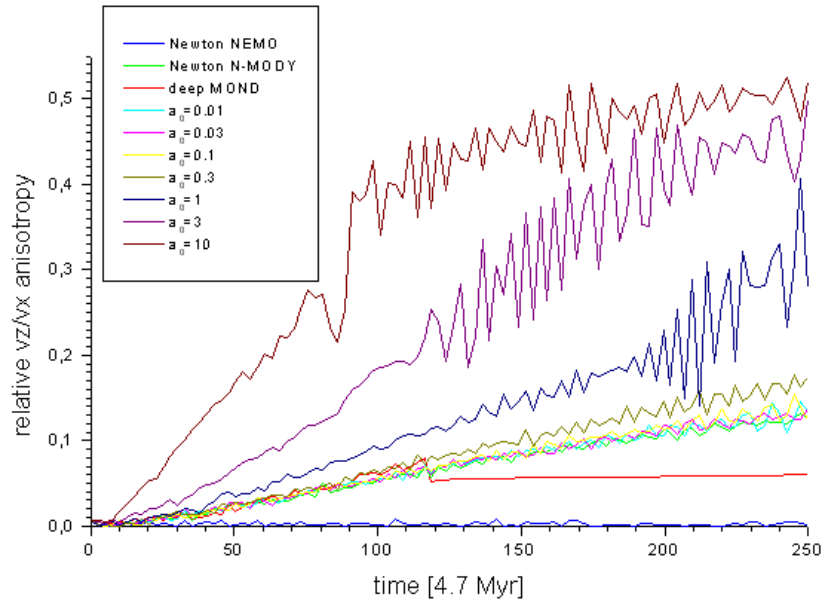


Figure 4.15: Velocity anisotropy between the z- and x-axis of Plummer spheres in *N-MODY*. Note that the increase for all models calculated with *N-MODY* and that its gradient correlates with the value of a_0 .

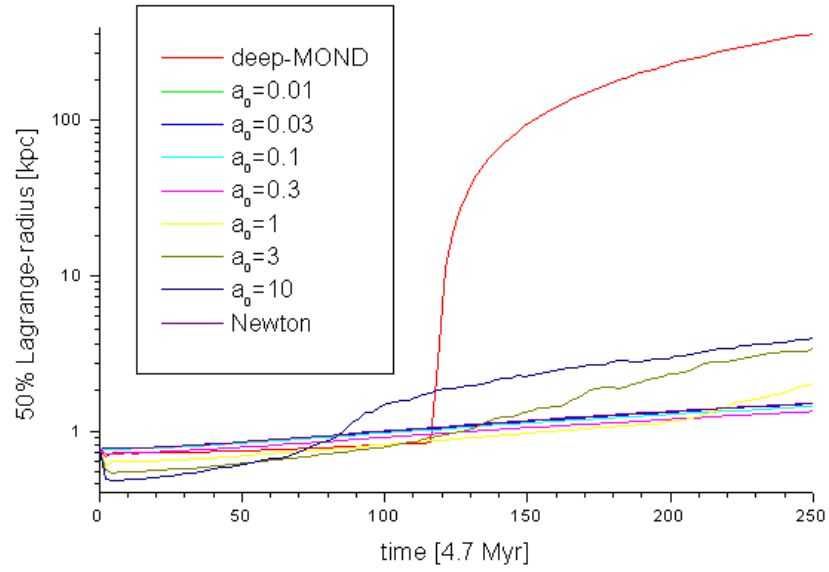


Figure 4.16: Time evolution of 50% Lagrange radii of Plummer-spheres in *N-MODY*. Note the jump in case of deep-MOND and the increase due to the strong flattening for models with large values of a_0 .

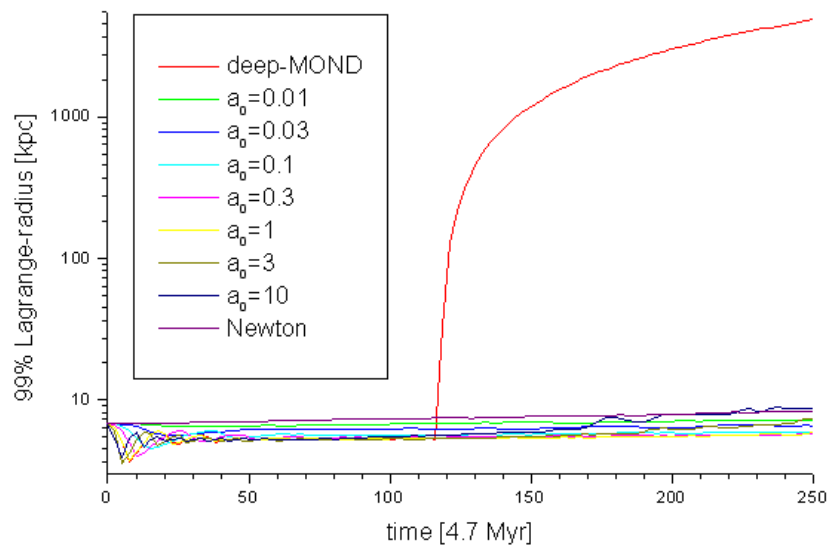


Figure 4.17: Time evolution of 99% Lagrange radii of Plummer-spheres in *N-MODY*. Note the jump in case of deep-MOND.

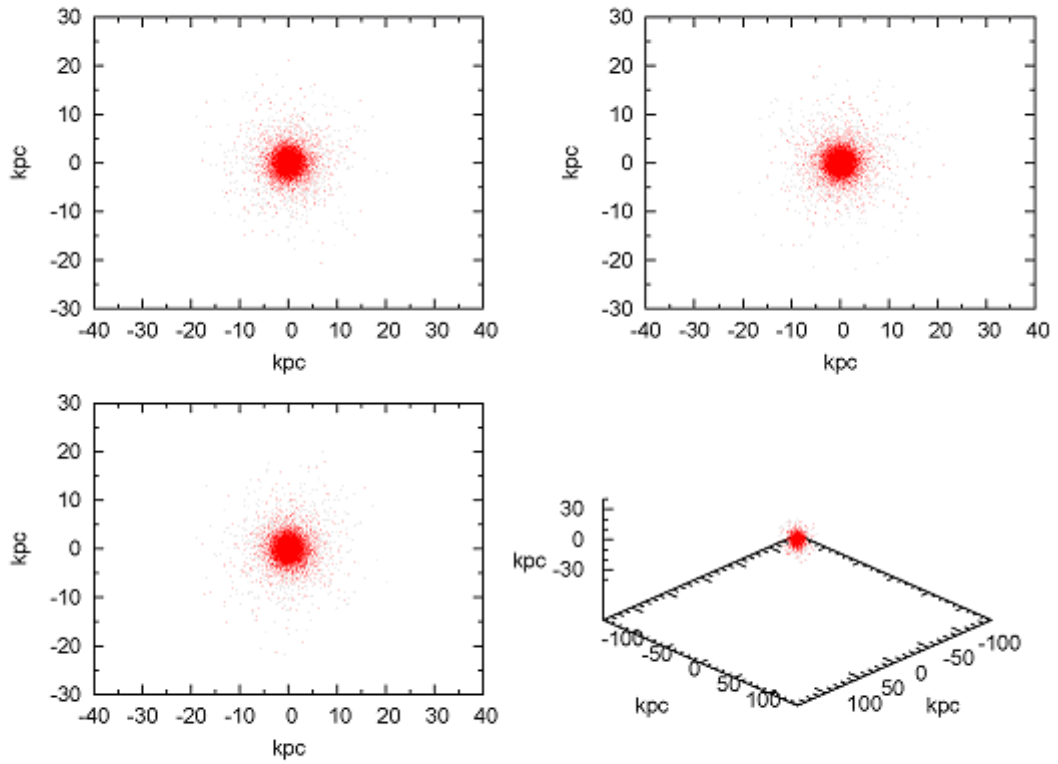


Figure 4.18: The initial model of the Plummer-sphere which is used for all runs. The image in the upper-left corner is the view on the xy -plane, in the upper-right corner one finds the view on the yz -plane, in the lower-left corner there is a view on the xz -plane and in the lower-right corner one can find a 3D view along the first median.

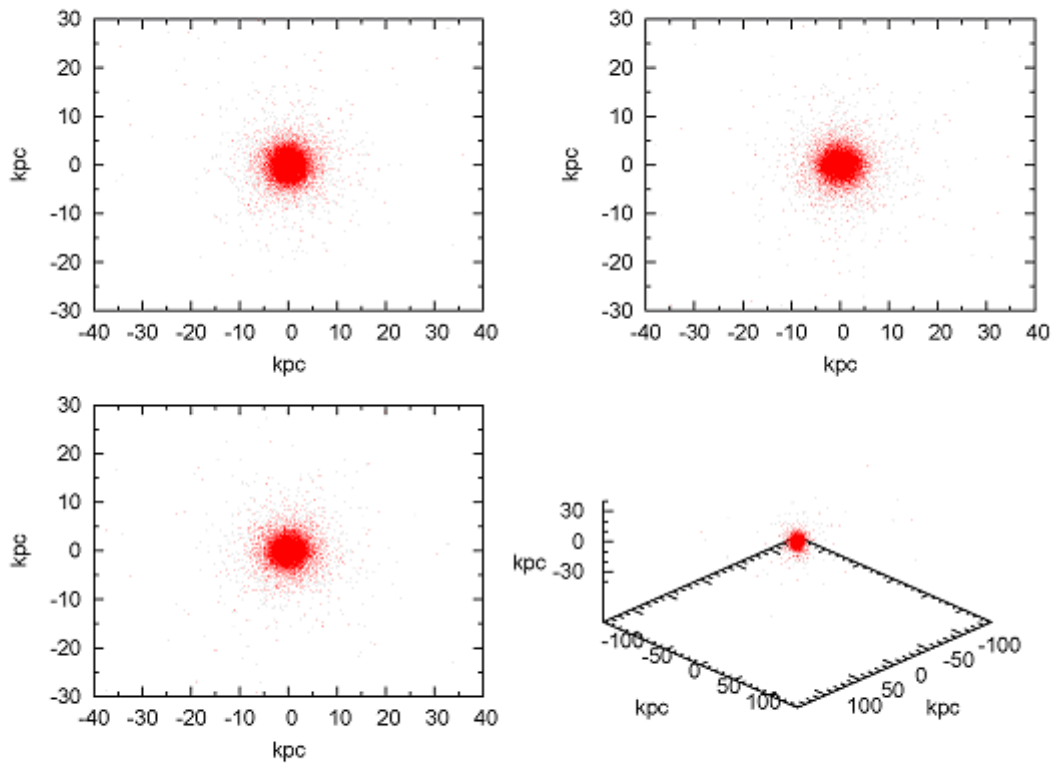


Figure 4.19: The Plummer-sphere calculated in Newtonian gravity in $N\text{-}MODY$ after 1175 Myrs. If one looks closely, one can see a small flattening along the z -axis. The labelling of the images is identical to figure 4.18.

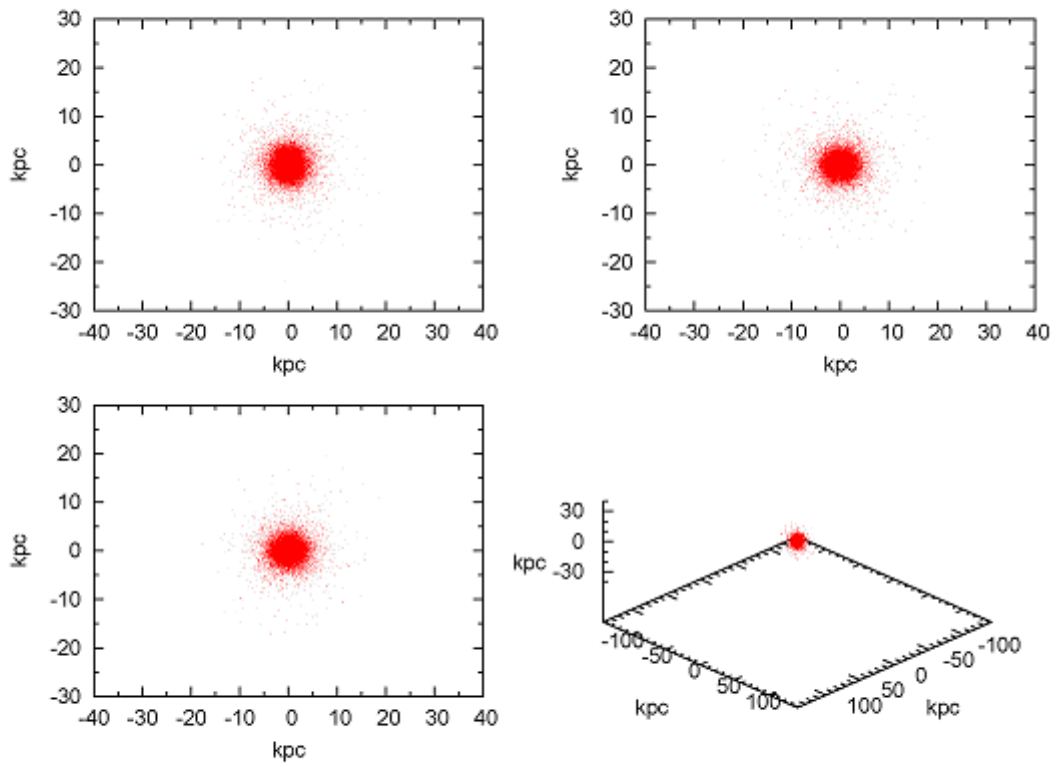


Figure 4.20: The Plummer-sphere calculated with MONDian gravity and an a_0 of $4.17 \cdot 10^{-11} \text{ms}^{-2}$ in *N-MODY* after 1175 Myrs. In this case there is hardly any flattening. The labelling of the images is identical to figure 4.18.

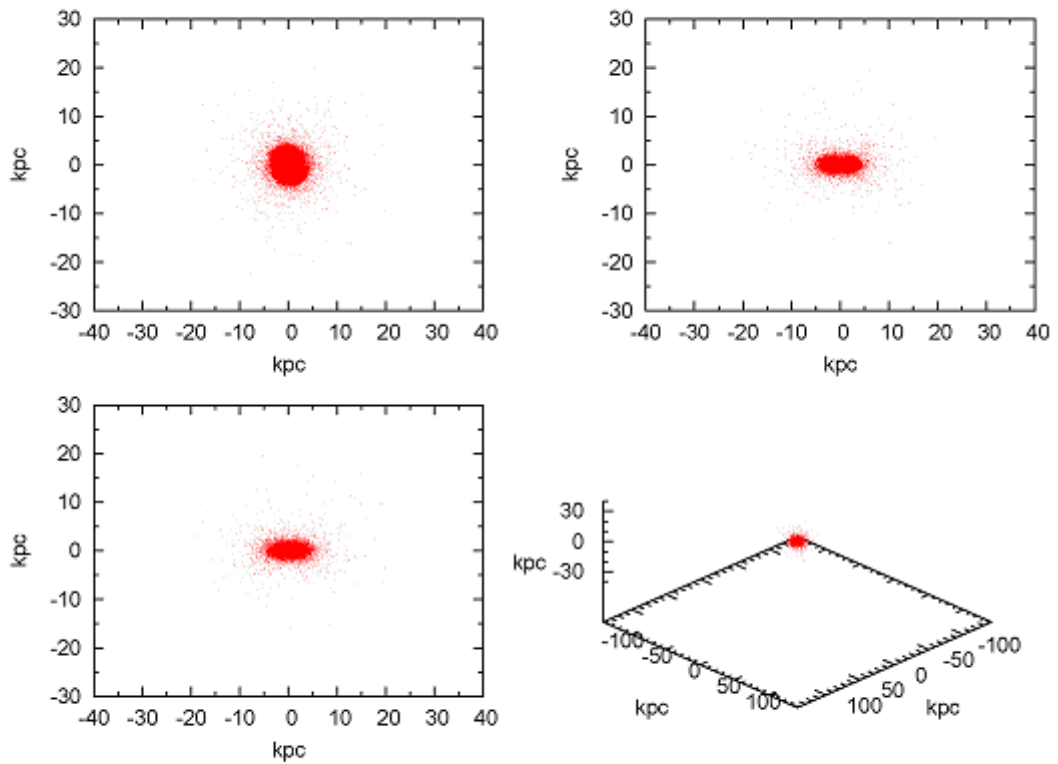


Figure 4.21: The Plummer-sphere calculated with MONDian gravity and an a_0 of $1.39 \cdot 10^{-8} \text{ms}^{-2}$ in *N-MODY* after 587.5 Myrs. One can clearly see a strong flattening effect along the z-axis. The labelling of the images is identical to figure 4.18.

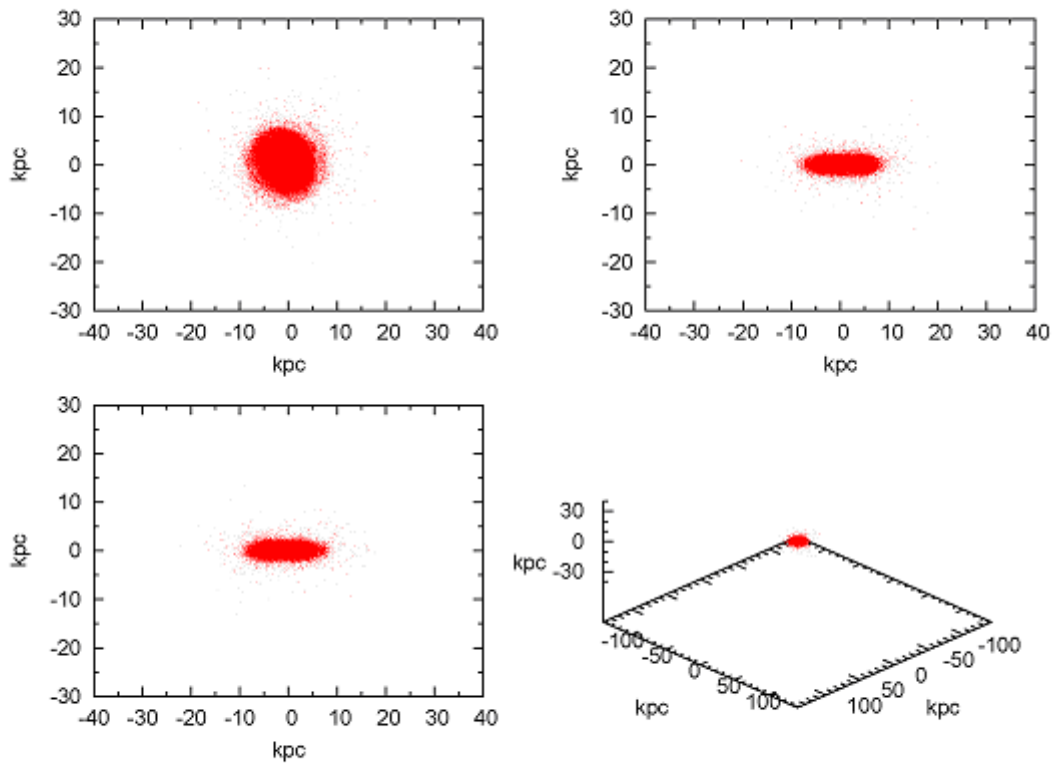


Figure 4.22: The Plummer-sphere calculated with MONDian gravity and an a_0 of $1.39 \cdot 10^{-8} \text{textrm{mms}^{-2}}$ in *N-MODY* after 1175 Myrs. One can clearly see the extreme flattening effect along the z -axis. The labelling of the images is identical to figure 4.18.

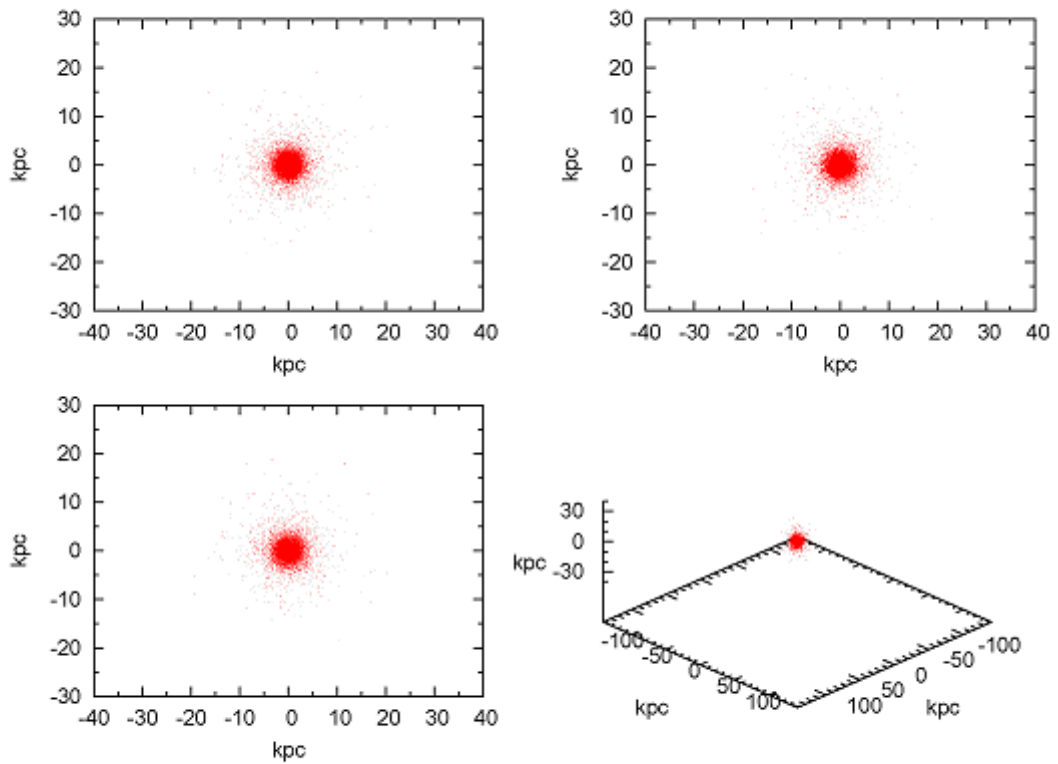


Figure 4.23: The Plummer-sphere calculated with deep-MOND gravity in *N-MODY* after 531.1 Myrs, a couple of Megayears before the "explosion" and everything is looking "normal". The labelling of the images is identical to figure 4.18.

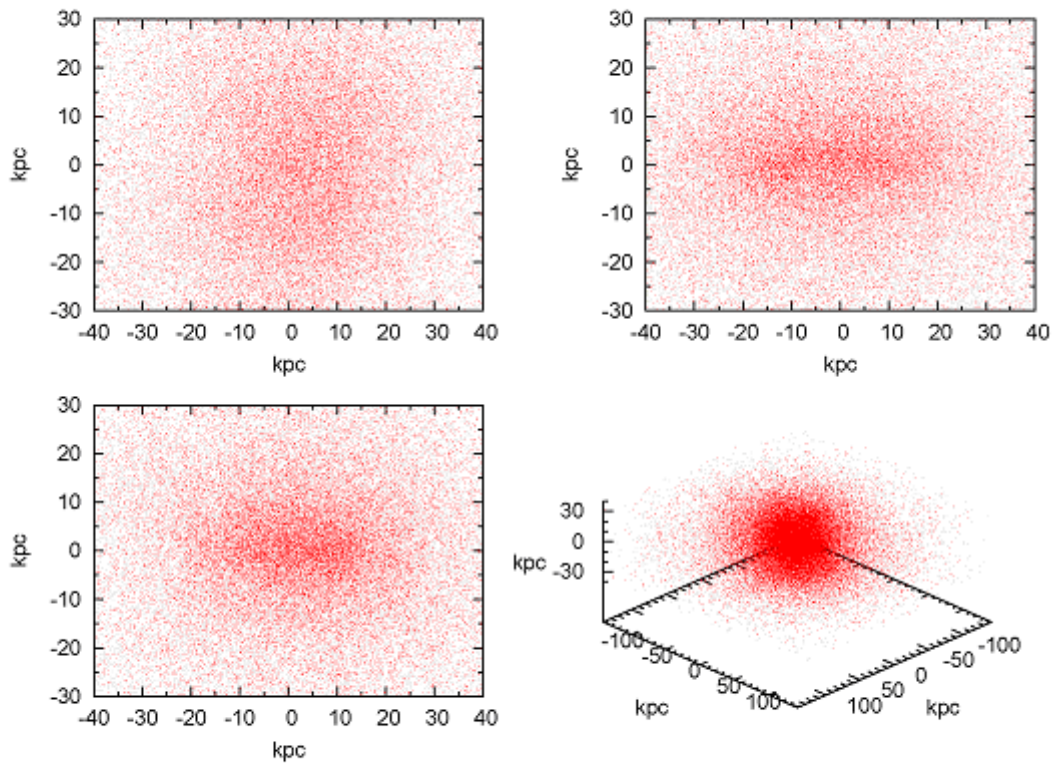


Figure 4.24: The Plummer-sphere calculated with deep-MOND gravity in *N-MODY* after 648.6 Myrs, a couple of Megayears after the "explosion". The whole Plummer-sphere is totally disintegrated. The labelling of the images is identical to figure 4.18.

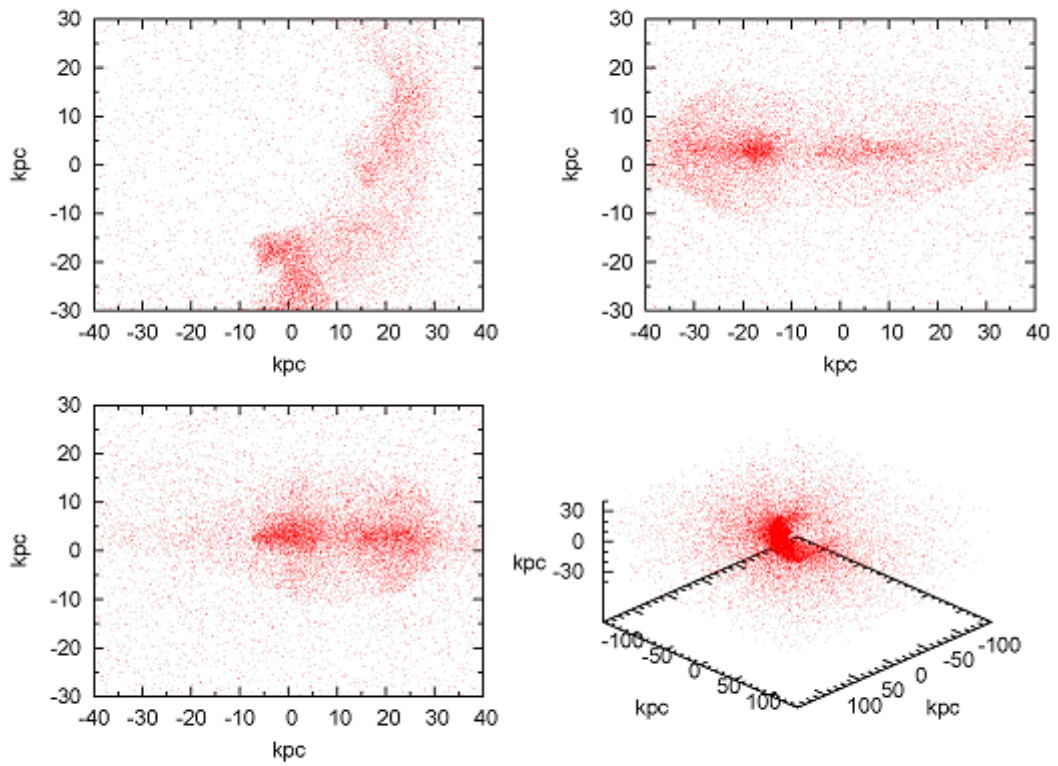


Figure 4.25: The Plummer-sphere calculated with deep-MOND gravity in *N-MODY* after 1175 Myrs. One cannot see any similarities to the original model. The labelling of the images is identical to figure 4.18.

Chapter 5

Simulations

5.1 Motivation

It is a known fact that the distribution of galaxies in the Local Group is much more planar than we would expect in the Λ CMD cosmology. Therefore several theories have been developed to explain the observed distribution. One of those models claims that there was an early interaction between the Proto Milky Way and Proto Andromeda Galaxy shortly after the creation of the Local Group. At this close encounter, gas from the outer parts of their discs had been scattered across the Local Group and formed most of the dwarf galaxies we can observe now. Furthermore it is important to understand the motion of the galaxies in our own galaxy group to make predictions for the future, like a possible merger between the Milky Way and the Andromeda galaxy. The topic is also of special interest because the positions on the sky, the distance and the radial velocity of almost all known galaxies within the Local Group have been measured already but the tangential velocity and its direction is largely unknown. These parameters are of vital importance for the complete understanding of the Local Group. I hope to find some constraints on these parameters, at least for the Andromeda galaxy. Furthermore the dynamics of the Local Group provide a possible window for research on the very basics of our view on gravitation. The orbits of dwarf galaxies around their hosts might be a good possibility to settle the dispute between the MOND and the dark matter paradigm (Klypin and Prada, 2009). Obviously there is a lot to learn about and from the dynamics of the Local Group.

5.2 Testing the programmes

5.2.1 Overview

Before I could start my simulations, I had to assure that my programmes work properly. So I had to ran tests for every feature of every programme. The testing of the very simple programmes like *Mkinput*, *Mkmodel*, *Cutter* and *RealDist* was not very complicated. After the basic debugging I checked if I get the expected output for a several given inputs. The tests got more demanding for the more complex programmes. In the programme *NewHEX* the dynamical friction, the Newtonian gravitation and the artificial Hubble expansion had to be tested carefully. The MONDian gravity and the Hubble expansion had to be tested in the programme *DeMonI* too.

5.2.2 Dynamical friction

I ran a couple of tests to check the correct behaviour of particles affected by dynamical friction. The first one consisted of three test particles orbiting a massive galaxy with halo at different distances. The first test particles were placed inside the halo at a distance of 15 kpc from its centre. The particle runs on an initially circular orbit and the label "test particle" is only correct with respect to the gravitation. This particle is affected by dynamical friction like a particle with a mass of $10^9 M_{\odot}$, but the massive ($10^{11} M_{\odot}$) particle with its halo of a radius of 30 kpc is not gravitational affected by the test particle. Another test particle is set at initial distance of 27 kpc on a similar orbit inside the halo. Furthermore there is a third test particle outside the halo at a distance of 45 kpc from the centre. The simulation with these initial conditions has been done twice, for a start with the dynamical friction turned on and second with it switched off. The results of this test have been visualised in figure 5.1. The red and the cyan lines represent the test body which started at an initial distance of 15 kpc. One can see if the dynamical friction is switched on (red line), it falls into the core of the central galaxy within a little more than 2.3 Gyr. Afterwards it remains moving around in an area near the centre and due to the softening it does not fall in. If the dynamical friction is turned off (cyan line) the orbit is stable. The green and the magenta lines stand for the test body that started at an initial distance of 27 kpc inside the halo. Similar to the previous test body it falls deeper into the halo if the dynamical friction is on (green line) or stays on a stable orbit if it is turned off (magenta line). The infall takes almost 7 Gyr. We know that the dynamical friction timescale in isothermal halos looks like equation 2.22. The circular velocity v_{circ} is constant in an isothermal halo and the mass of the orbiting particle m is also set to constant in this simulation. The initial distance r has been multiplied by 1.8 between the two examples and therefore the timescale increase by a factor of about 3 (in theory it should be 3.24). The last two lines (blue and yellow) stand for the orbit at 45 kpc which is outside the halo and as expected both lines are identical (that's the reason why only the yellow one is visible in the diagram) because none of them is affected by dynamical friction. I had to implement the second test for the dynamical friction a little different, because in this one I used massive particles instead of test particles. I run a simulation with one big halo and a smaller but also massive (and therefore gravitationally interacting) particle (and a small test particle too, because the programme demands at least one test particle to run). I did this for several different initial conditions, always one with dynamical friction switched on and one with it switched off. The central halo is the same like in the previous test. The results are displayed in figure 5.2. The cases

A (red line) and E (magenta line) are particles with a mass of $5 \cdot 10^9 M_{\odot}$ starting at an initial distance of 13.5 kpc on an almost circular orbit (if it would be massless it would be circular). If the dynamical friction is turned on (A) the orbit declines until the particle falls into the halo's core within a little more than 1.5 Gyr. In the other case the orbit is stable as expected. I also ran a body with the same mass at an initial distance of 27 kpc which is represented by the green line (B). The bodies also fall into the core within a little more than 4.7 Gyr. This is a little faster than expected from the approximation formula. As usually the orbit is stable for this configuration F (yellow line) if the dynamical friction is turned off. I ran another test with the same initial distance but with a mass of only $2.5 \cdot 10^9 M_{\odot}$. If the dynamical friction is disabled the orbit of the particle is stable again (H: orange line). In case the dynamical friction is turned on the orbit of the particle slowly declines and it reaches the core of the halo within a little more than 7.8 Gyr (D: cyan line). When comparing this value to the result from case B and using the formula for the dynamical friction timescale we see that the value is a little lower than expected. The cases C (blue line) and G (violet line) are both starting at an initial distance of 45 kpc and because this is outside the halo, both their orbits are stable and unaffected by dynamical friction. Summing up we can say that although the results from simulations do not exactly fit the prediction from the formula, they provide sufficient accuracy to account the test successful. The dynamical friction is working well enough to be used in the main simulations.

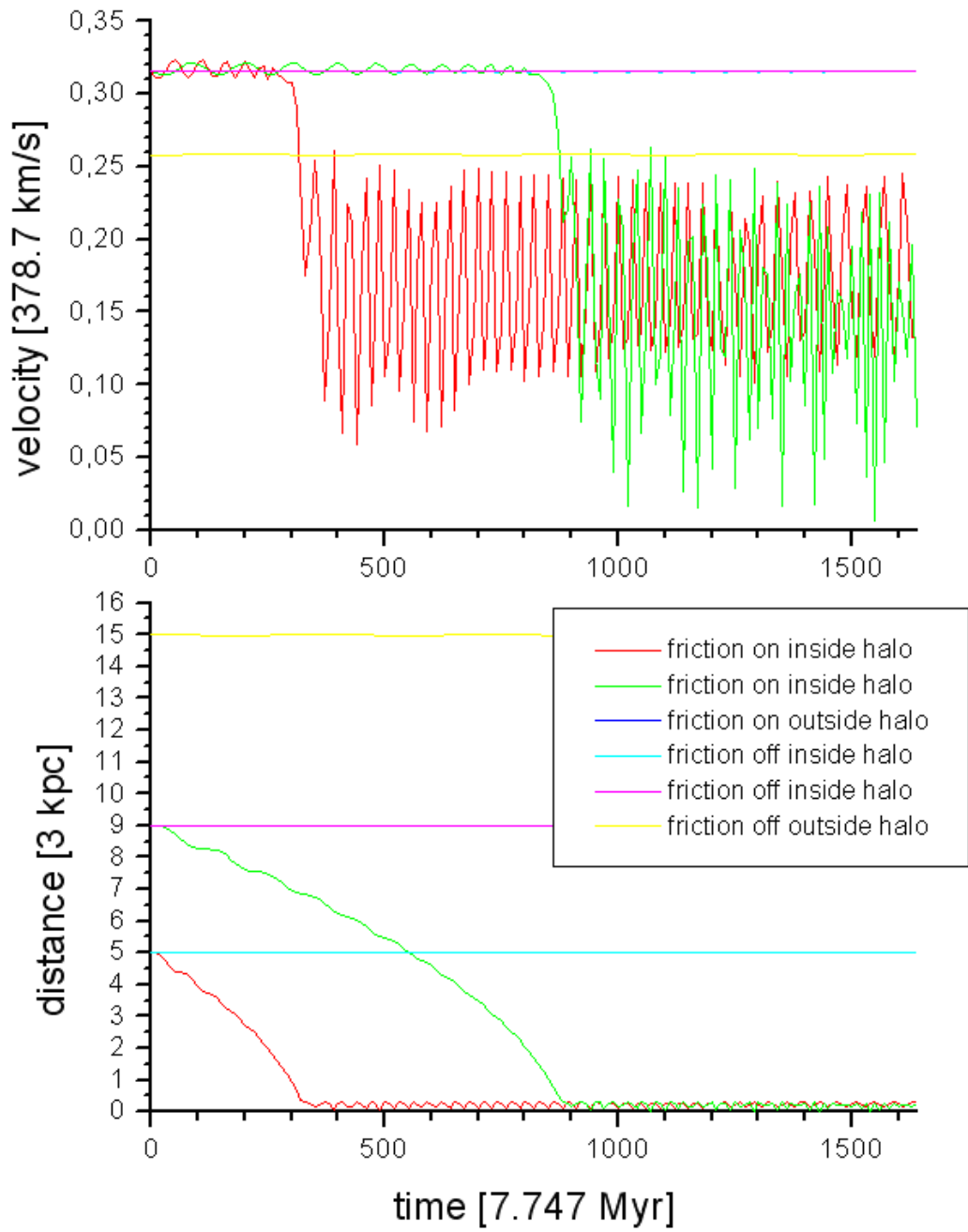


Figure 5.1: Dynamical friction in the case of test bodies. One can clearly see the infall of the particles if the dynamical friction is turned on.

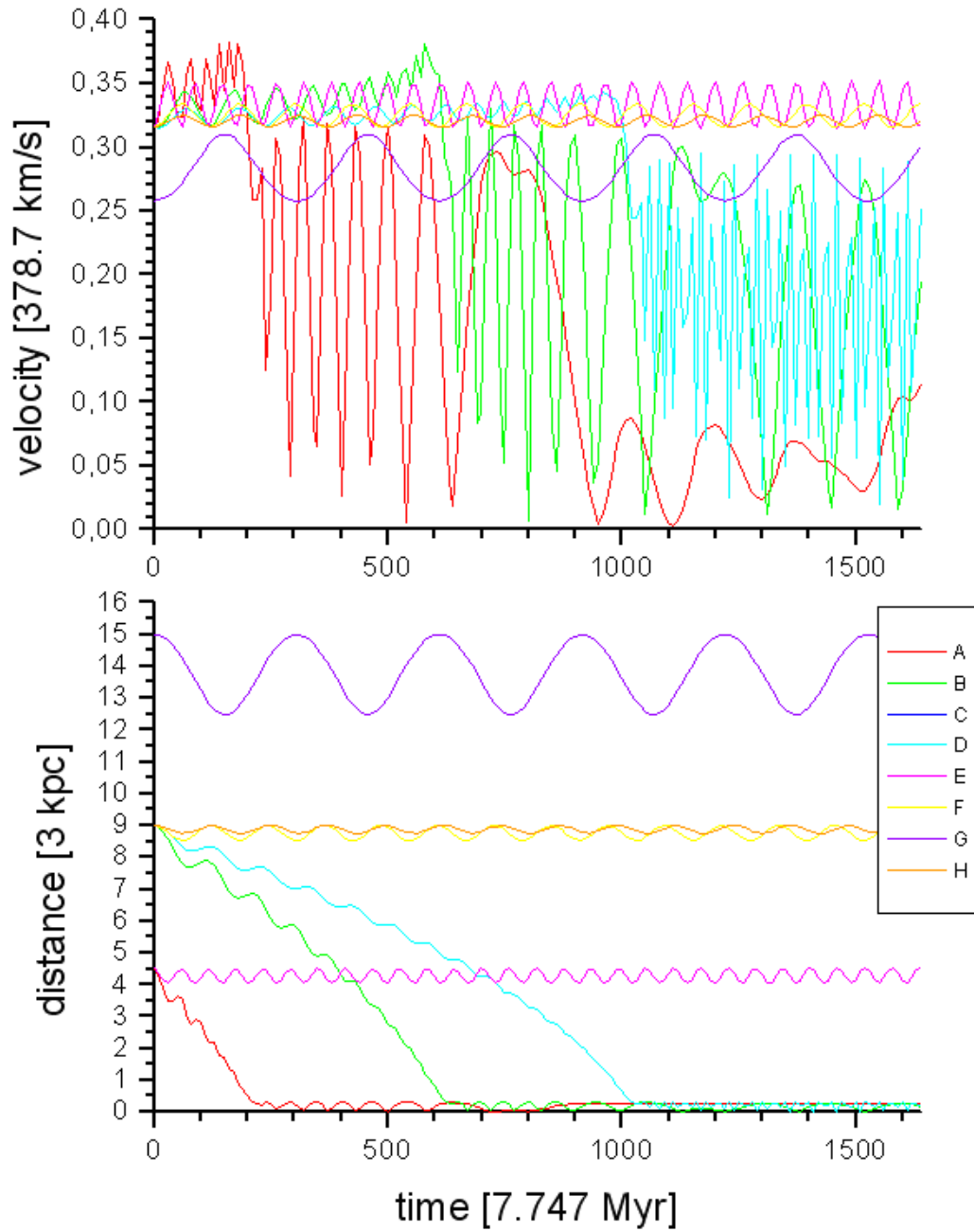


Figure 5.2: Dynamical friction in the case of massive particles. Note the different infall times depending on the particle's parameters.

5.2.3 Hubble Expansion

The next feature which had to be tested was the artificial Hubble-expansion. It is implemented similarly in *DeMonI* and *NewHEX* but because one cannot turn off the gravitation completely (both programmes require at least one massive particle (it may have a very small but finite mass) and one test particle), this feature needed to be examined carefully in both programmes. The setup for the tests of both programmes was quite simple. I just put a massive particle with a small mass into the origin and several test bodies at different distances from the centre. All particles were initially at rest and it started about 1.6 Gyr after the Big Bang and the test ran for 12 Gyr. When accomplishing these tests I had to face two difficulties: The first one is that the initial velocity of the test particles has been set to zero and therefore the first time steps do not lead to reliable values, though this small deviation is soon overwhelmed by the Hubble-expansion in the code. Furthermore both programmes, *NewHEX* and *DeMonI*, need at least one massive particle (and also one test particle) to work properly and therefore cannot get values for a pure undisturbed Hubble-expansion. Though I can minimize this effect by choosing the mass quite small ($2 \cdot 10^9 M_\odot$ in case of Newtonian gravity and $10^9 M_\odot$ in case of deep-MOND gravity with the units from table 5.1). As one can see in figure 5.3 it works very well for Newtonian gravity, because starting at a certain distance the gravity gets very weak and the Hubble expansion is by far dominant. Only at small distances the gravity wins and the test body falls back to the mass. In the case of deep-MOND gravity the problem is more severe.

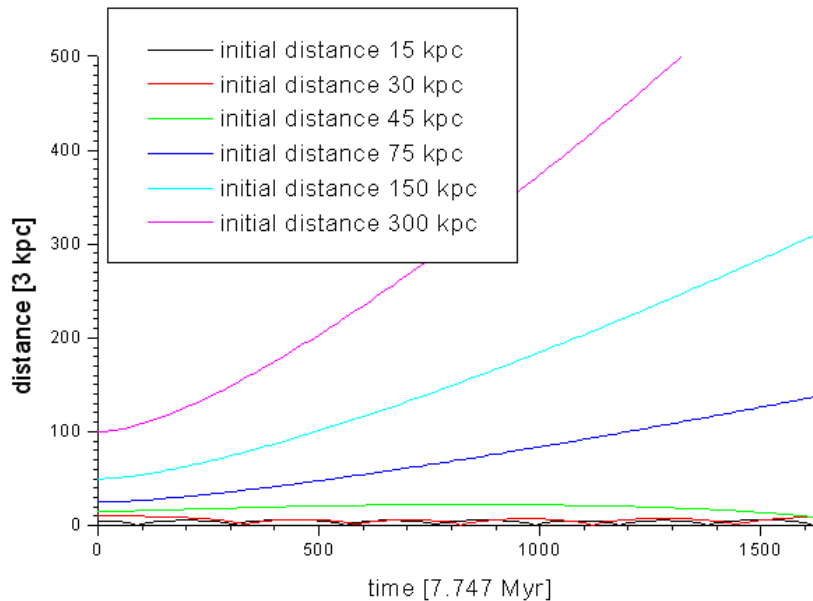


Figure 5.3: Hubble expansion with little Newtonian gravitation. Up to a certain distance the gravitation is still strong enough to prevent the particle from escaping.

Since the acceleration caused by the Hubble-expansion decreases with time (in the simple cosmological model which is used in these programmes) and the fact that MOND (and especially deep-MOND) does not have a finite escape velocity the gravitation will at last always win and in the long run the test body will fall back to the massive particle. This

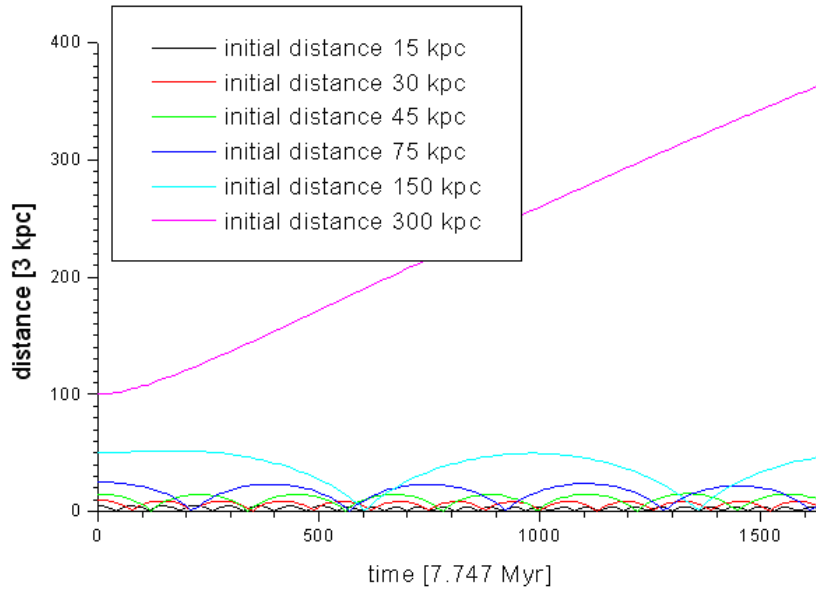


Figure 5.4: Hubble expansion with little deep-MONDian gravitation. One can see that gravity is at length stronger than the Hubble expansion.

is shown in figure 5.4. In case of the Newtonian gravity one can get very good values for the undisturbed Hubble expansion if one puts the starting positions of the test bodies far enough away from the massive particle. One can check the validity of implementation of the Hubble expansion in my programmes easily. One just needs to compare the velocity and the distance of the final time steps. As One can see in figure 5.5 there is a straight linear correlation between them, which also passes through zero only with a tiny deviation. So the programme can reproduce the expected Hubble relation (in the used cosmological model) of equation 2.32 very well. I get a present day Hubble constant of $(88.0 \pm 0.2) \text{ km } m.s^{-1} \text{ Mpc}^{-1}$ naturally out of my programme, which is an adequate value for my simple approach. The pure Hubble expansion is implemented in *NewHEXI* and *DeMonI* in exactly the same way and therefore it works correctly in both programmes. Though the disturbance due to the stronger gravitation in the MONDian run remains a problem but on the other hand only a bound system is considered my further simulations. In this case the gravitation is dominant anyway at length. The Hubble expansion is only an important effect during the first Gigayears in this case and there my approximation still is sufficient to simulate it.

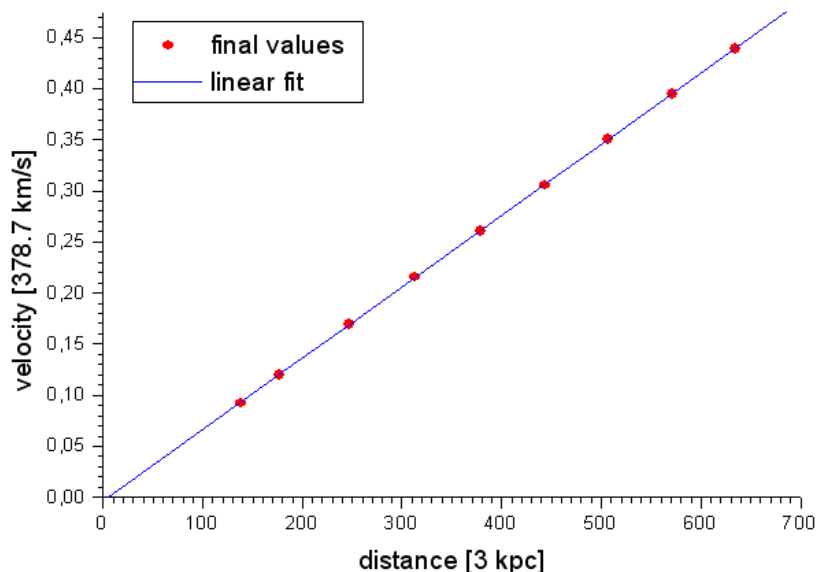


Figure 5.5: Hubble expansion: final distance vs. final velocity in case of unbound objects (in Newtonian gravitation). One gets the simple linear Hubble law.

5.2.4 Gravitation

The next feature which has to be examined is the very heart of these integrators itself: the calculation of the gravitation. The programme NewHExI uses normal Newtonian gravity and an isothermal halo with finite extension. Outside the halo the gravitation should exactly be like that of a point mass located in the centre of the halo because of the halo's spherical symmetry. This would be a Keplerian orbit but inside the halo it is a little different. The strength of the gravitation acting on an orbiting test body depends also on the enclosed mass. One reason for choosing a spherical isothermal halo was that this mass is given by a very simple formula: $M(r) = M \frac{r}{r_H}$. The variable $M(r)$ is the enclosed mass and the variable M stands for the total mass of the halo. The distance from the halo's centre to the orbiting object is given by r and r_H represents the scale-length of the halo which is equal to the halo's cut-off length in my definition. By using this formula and the equation for Newtonian Gravity one will see that the circular velocity v_{circ} inside the halo is constant or to be more exactly $v_{\text{circ}} = \sqrt{GM}$ with G representing the gravitation constant which is set 1 in our units. Outside the halo the circular velocity has to be the normal $v_{\text{circ}} = \sqrt{\frac{GM}{r}}$ for a massless test body. To test the correct strength of the gravitation I set up a simple model. I put one massive particle with $10^{11}M_{\odot}$ and halo of 30 kpc radius. In addition to that I put four massless test bodies at different distances from the centre of the halo (15 kpc (inside the halo), 30 kpc (at the edge of the halo), 45 kpc (outside the halo) and 75 kpc (outside the halo)). The initial velocities are calculated to be the circular velocities with the formulas above and their vectors are orthogonal to the radial vector. I expect the orbits of these test bodies to be stable and in fact they are (see figure 5.6). Although there are some minor fluctuations in the distance from the centre, they can be explained by numerical artefacts and the fact that the circular velocity is rounded to the three decimal and a tiny perturbation in the gravitation law caused by

the softening. Beside the numerical necessity of a softening to avoid the singularity in the centre, it also has a positive effect on the halo profile. The isothermal sphere has the problem of a central cusp, which is now smeared out by the softening to a core. Though this is of no real importance because at the softening length the detailed structure of the galaxy in the halo would become important and this is not resolved in the simulations anyway. The programme *DeMonI* uses deep-MOND gravity which is very different from the Newtonian gravity and therefore it has to be tested. In deep-MOND gravity the circular velocity v_{circ} is known to be constant at any distance. One can calculate it with this formula: $v_{\text{circ}} = \sqrt{4Ga_0M}$. For reasons of simplicity the gravitation constant G , the MONDian acceleration a_0 and the mass M have all been set to 1 and therefore the circular velocity is also 1 at all distances (in n-body units, for scaling relations in MOND see (Londrillo and Nipoti, 2008)). To check this I put four test bodies at different distances from the central mass, with an initial velocity orthogonal to the radial vector of 1. As one can see in figure 5.7 the distances remain approximately constant and also the velocities. Only the innermost orbit, which starts at an initial distance of 5, shows a small increase of its average distance to centre over time. Furthermore its velocity has obviously the largest fluctuations. The disturbance in the innermost orbit might be caused by the adaptive softening. In contrast to *NewHEXl* where I use a fixed softening length, the softening length r_{soft} in *DeMonI* is calculated for every massive particle individually using the formula $r_{\text{soft}} = \sqrt{GM}/a_0$. In this example the softening length is also 1 (in n-body units) and therefore has a small but visible influence on the test body orbiting at a distance of 5 (in n-body units). Despite this tiny disturbance the programme works very well and the deep-MOND gravitation is implemented correctly.

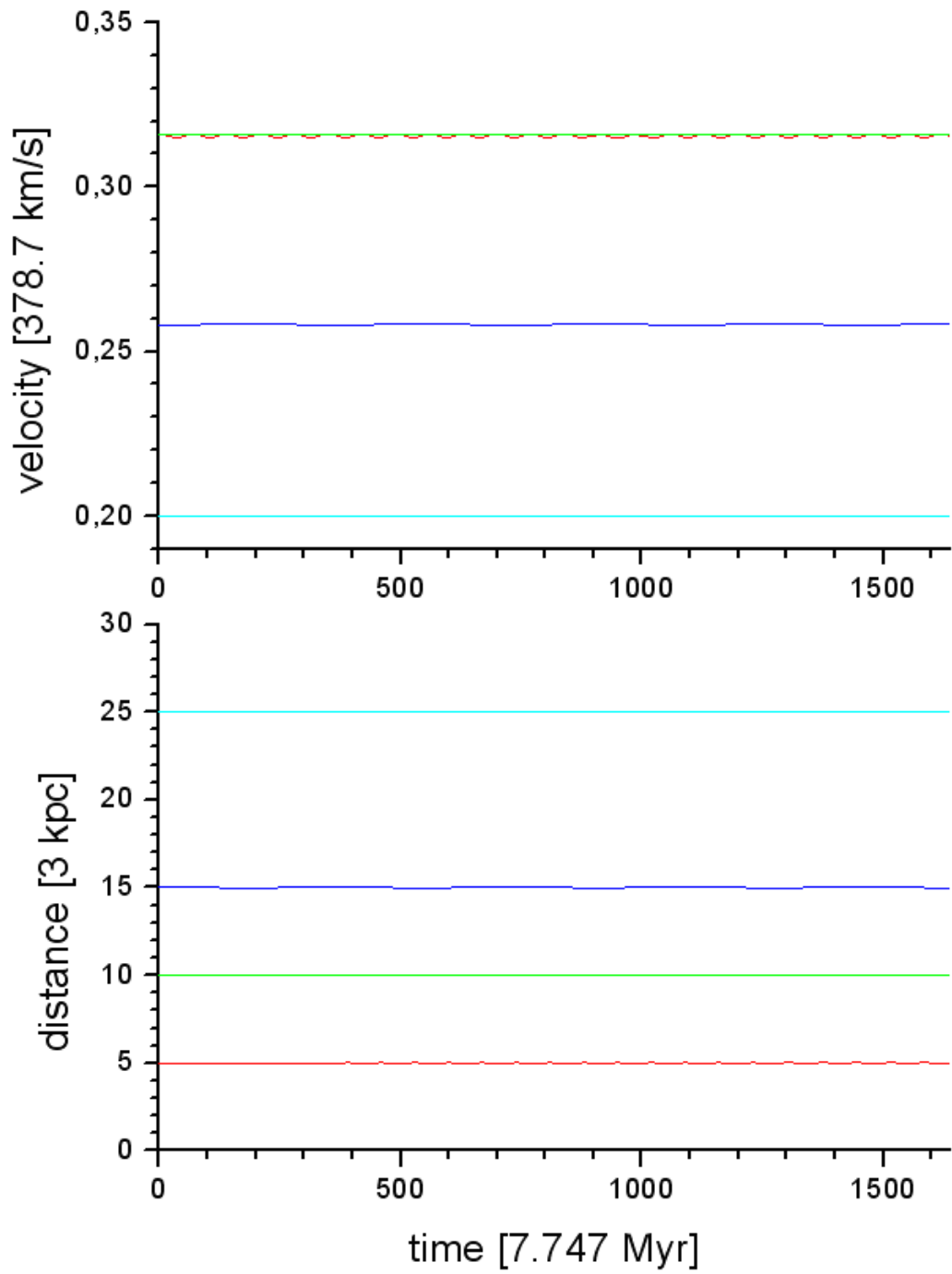


Figure 5.6: Orbits in Newtonian gravitation. Everything is stable as expected.

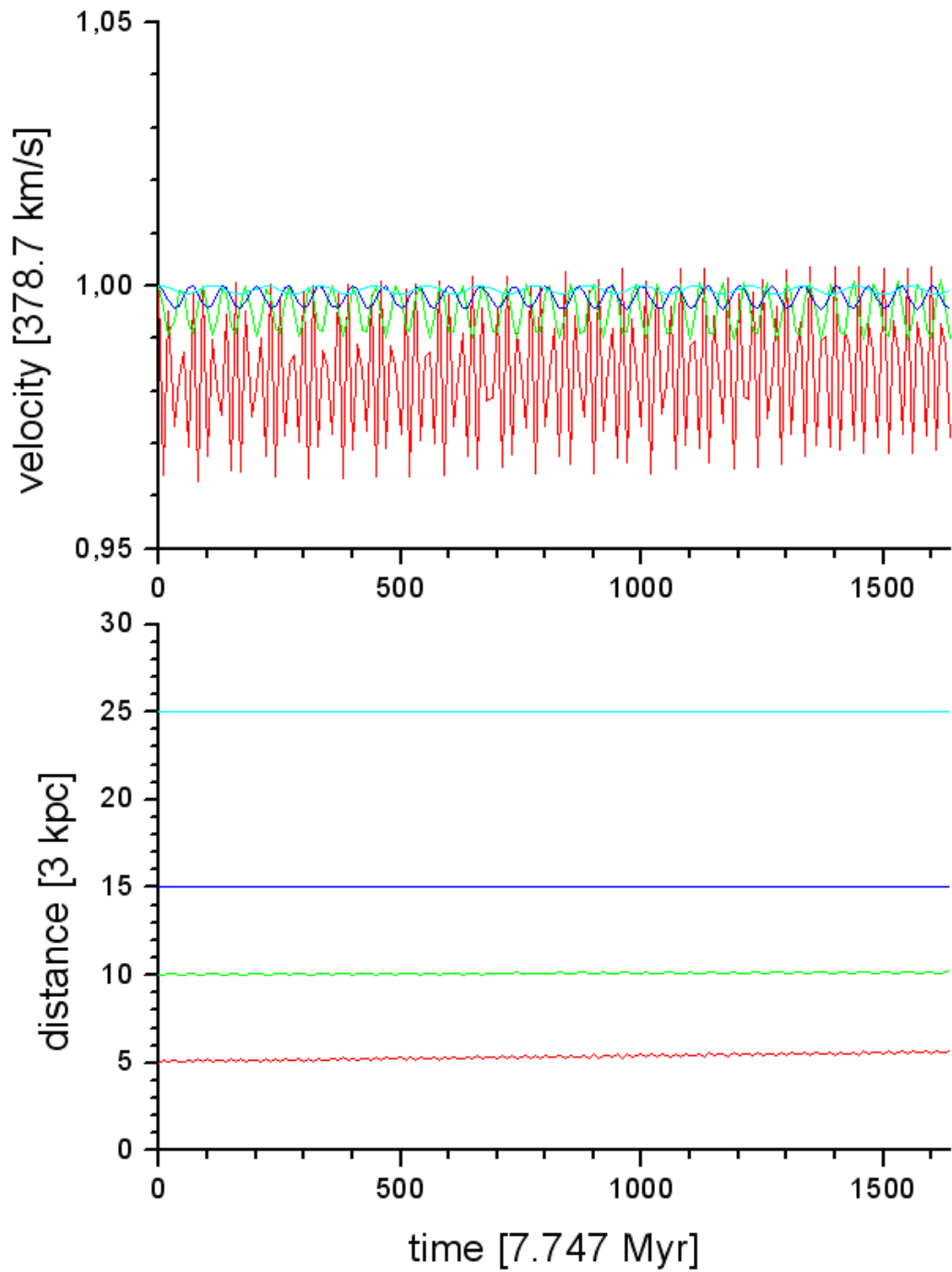


Figure 5.7: Orbits in MONDian gravitation. Everything is stable as expected.

5.3 A very simple Model.

5.3.1 Equal masses

The Local Group is dominated by two massive galaxies, the Milky Way and the Andromeda nebula. Hence the simplest possible model to study the dynamics will be a system consisting of two equal mass bodies which interact gravitationally. Of course this model is too simple, as the Milky Way and M31 have different masses though they are in the same order of magnitude. A few rough tests for the equal mass case have been run, because I have wanted to get a first impression. A far more thorough analysis for the more realistic non-equal mass case has been conducted. First I have tried to find a possible orbit for two objects with a mass of $2 \cdot 10^{12} M_{\odot}$ each. The Hubble-expansion, dynamical friction and the galactic halos have been enabled for the simulation in NewHExI. Both halos have a radius of 150 kpc and the simulation has been started about 12 billion years ago. Then the distance between both objects and their initial velocity (which has been set to have only a tangential component) have been changed manually. Two parameters (in the centre of mass system) need to be varied using the simple method of try and error. The final values of distance and radial velocity have been compared with nowadays values of the M31 - Milky Way's system. I have found one solution with both galaxies separated by an initial distance of 36 kpc and a initial velocity at the perigalacticum of 693 km/s. After 12 Gigayears the Andromeda Galaxy is located at a distance of 712 kpc and is approaching the Milky with -99 km/s. These values are not perfect (one would expect about 770 kpc and 117 km/s from observations) but sufficient for a first analysis. In the next step the behaviour of this system MOND is investigated. Therefore the same initial conditions have been used and the simulation has been run again with *DeMonI*. The mass has been the only parameter which has been varied. The results of this simple experiment is quite interesting. Within a reasonable mass range from 10^{12} to $2 \cdot 10^{10} M_{\odot}$ two possible solutions have been found. Both have not been very good but they have been the best which have been able to be obtained by this rough approach. At a mass ratio (compared to the Dark Matter model) of 1/22 (this means a mass of $9.1 \cdot 10^{10} M_{\odot}$ for each galaxy) I have found an orbit which has reached a distance of 1341 kpc and both galaxies have been approaching with a velocity of -180 km/s. In this case there has only been the initial close encounter between both galaxies but it is obvious that the values are too large. If the masses are decreased, both galaxies become very loosely bound and the Hubble expansion is still the dominant force at the end of the simulation. On the other hand the masses can increased and one finds another "good" parameter area around a mass ratio of 1/17 with a final distance of 642 kpc and a radial velocity of -201 km/s. This orbit has a second close encounter about 5.2 Gyr ago at a minimum distance of approximately 35 kpc. Although these results are very crude we can learn something from them. It is always a problem comparing dark matter models and MOND models, because the velocities at large distances are larger in MOND caused by the stronger gravitation. This results in a problem with two sides: either the distances have to be increased, because at the apogalacticum, the two galaxies have to be separated by much larger distances to get the same velocities or one has to increase the number of revolutions, because the galaxies can complete more orbits in the same time.

5.3.2 A realistic mass ratio for the dark matter case

After getting a crude overview of the situation and possible upcoming problems, it is logical to improve the model and make it more realistic. The first step in this direction is to choose a better mass ratio. The Milky Way gets $1.5 \cdot 10^{12} M_{\odot}$ and M31 $2.5 \cdot 10^{12} M_{\odot}$ in this new scenario, which yields a realistic mass ratio for these two galaxies. Instead of trying only a couple of models by varying the parameters manually, this has been automated. After a few smaller tests a big scan of the initial distance-velocity parameter space has been run with a resolution of 250×80 (distance \times velocity-resolution). The perigalacticum of their orbit has been assumed to be 12 Gyr ago and a radius of their dark matter halos of 80 kpc. The scan covered initial distances from 24 kpc to 64 kpc and initial velocities from 484 km/s to 726 km/s. After running all 20000 models the best fit models have been selected. This has been done by calculating the relative radial velocity and the distance between both galaxies at the last time step. I defined good models as those with a negative radial velocity and in which the galaxies are separated by a distance of 300 to 1200 kpc. The best models have a final radial velocity of -75.7 to -151.5 km/s and a distance of 720 to 810 kpc. From all 20000 models within the scanning range only 25 fulfil the conditions for the best models. All good models are located in a thin area in the parameter space. As one can see in figure 5.8 it is possible to find a solid correlation between the initial velocity and the initial distance. The tenuity of this area can be explained in a very simple way. If the initial distance for given velocity gets too large the Hubble expansion will push both galaxies so far from each other that they become unbound. On the other hand if the initial distance is too small they will not ever reach the required distance to be consistent with the observational data and in the worst case they come so close that the galaxies merge due to dynamical friction. I used the fitting parabola to optimize the initial conditions in the main models, because the other massive objects which were added in my full model of the Local Group only have masses of less than $(1/30)^{\text{th}}$ of one of the two biggest galaxies. Therefore the orbits of the Milky Way and M31 stay the same with some small tolerance.

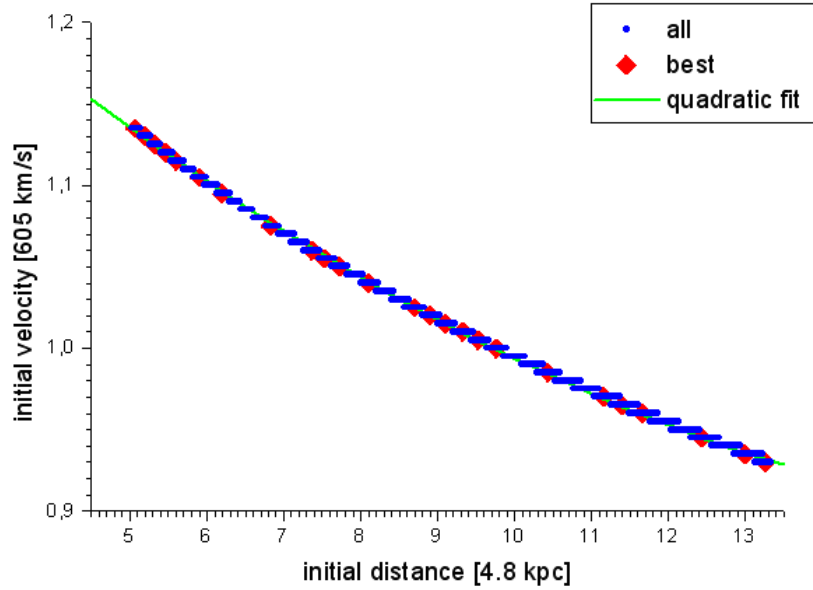


Figure 5.8: Results of a scan in the parameter space in the case of a mass of $1.5 \cdot 10^{12} M_{\odot}$ for the Milky Way and $2.5 \cdot 10^{12} M_{\odot}$ for the Andromeda Galaxy, with Newtonian gravity and Dark Matter halos of 80 kpc radius.

5.3.3 Masses in the MONDian case

In the case of deep MOND gravity similar simulations have been run. I have tried several different masses for the Milky Way and the Andromeda Galaxy. First only the masses from the previous Newtonian model have reduced by a factor 5, then 10, 20 and 50. After some quick scans I adapted the scanning range. For 1/5 of the Dark Matter mass one can already find some excellent orbits at low resolution like 250×80 . In figure 5.9 one can see that the good orbits (the definition is still the same as in the previous section) are not restricted to a small area in the parameter space like in the Newtonian case. There are a couple of bands where the initial conditions approximately reproduce the observed values but only in one of them, which corresponds to three revolutions, the best orbits can be found, which all lie on the parabola again. The other bands represent different numbers of revolutions. In the next run the masses have been reduced to $1.5 \cdot 10^{11} M_{\odot}$ and $2.5 \cdot 10^{11} M_{\odot}$. One can find the same bands like in the previous run, but one cannot find any best orbits with a resolution of 250×80 (see figure 5.10). In case of a ratio of 1/20 for the baryonic mass (compared to the Dark Matter mass) one gets several bands of good orbits again and also a strong correlation for the best orbits (see figure 5.11). If decreasing the masses further to only 1/50 one can find some bands of good orbits but no best orbits anymore with a resolution of 250×80 (see figure 5.12). In the last scan the observed values for the baryonic masses of the Milky Way and the Andromeda nebula of $5 \cdot 10^{10} M_{\odot}$ and $8 \cdot 10^{10} M_{\odot}$ have been used. First I did not get any best orbits although I found a couple of bands of good orbits, but then the resolution has been increased up to 999×1000 and 5 results for best orbits has been found, which are all located in the same band (see figure 5.13). Because I only got a few best orbits the quadratic fitting curve is not very good. The general behaviour with deep-MOND gravity is similar to

the already calculated behaviour for the equal mass case. One can find excellent orbits only for certain masses. A general problem of all runs is that one only gets the best orbits, if there are more than one close encounter of the Milky Way and M31 in the history of our galaxy group. In case of the very high baryonic masses of $1/5$ of the Dark Matter mass (note that in MOND, there is no Dark Matter though one can compare the masses with the Dark Matter model), which is quite unrealistic, there are three passages through the perigalacticum (the initial one and two more) before the galaxies reach their nowadays positions. In the $1/20$ case and in the case with the measured masses there are two perigalactic passages in the whole history of the Local Group. Although the fitting parabola is not very good for the real masses I used it to optimize the initial conditions for the main simulations but with a larger tolerance.

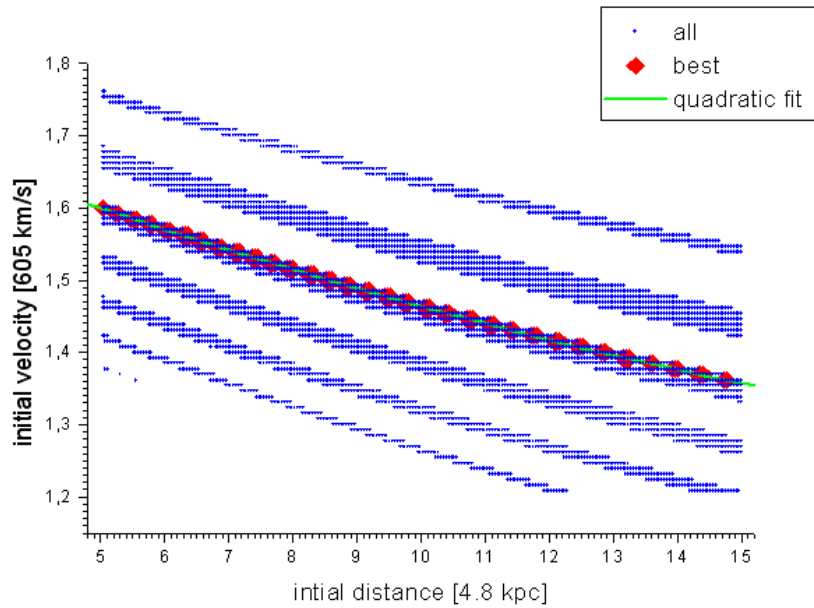


Figure 5.9: Results of a scan in the parameter space in the case of a mass of $3 \cdot 10^{11} M_{\odot}$ for the Milky Way and $5 \cdot 10^{11} M_{\odot}$ for the Andromeda Galaxy, with deep MOND gravity. One can find a parabola consisting of best orbits in the third band (corresponding to the third revolution).

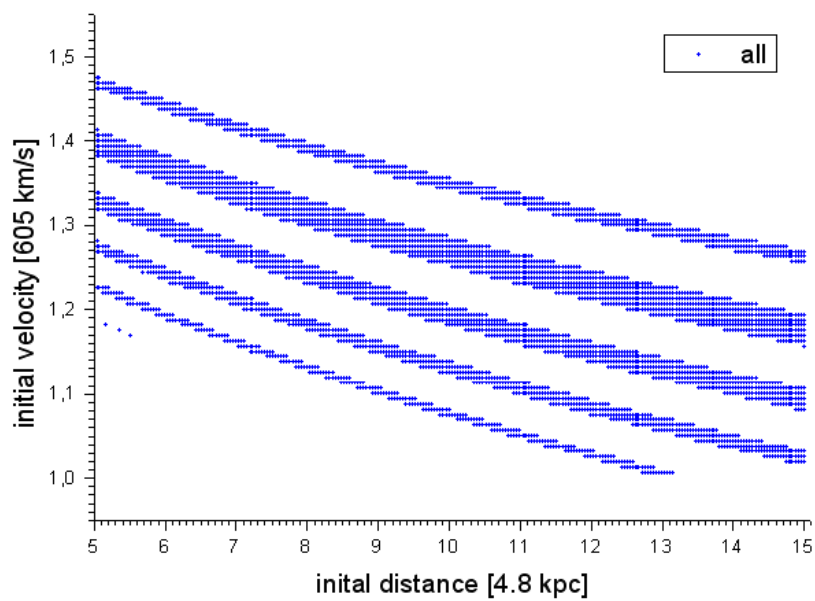


Figure 5.10: Results of a scan in the parameter space in the case of a mass of $1.5 \cdot 10^{11} M_{\odot}$ for the Milky Way and $2.5 \cdot 10^{11} M_{\odot}$ for the Andromeda Galaxy, with deep MOND gravity. Despite there are several bands of good orbits, one cannot find any orbit which parameters are really close to the observational values.

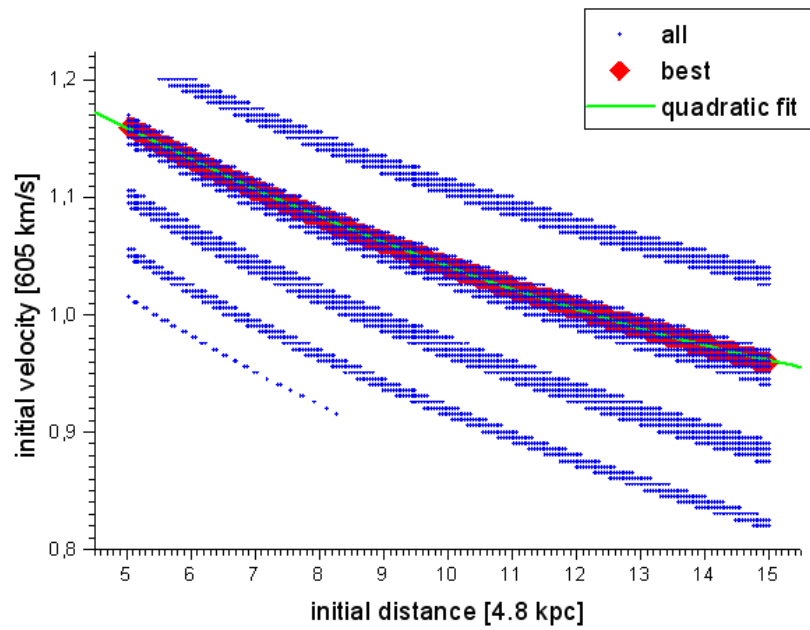


Figure 5.11: Results of a scan in the parameter space in the case of a mass of $7.5 \cdot 10^{10} M_{\odot}$ for the Milky Way and $1.25 \cdot 10^{11} M_{\odot}$ for the Andromeda Galaxy, with deep MOND gravity. One can find a parabola consisting of best orbits in the second band (corresponding to the second revolution).

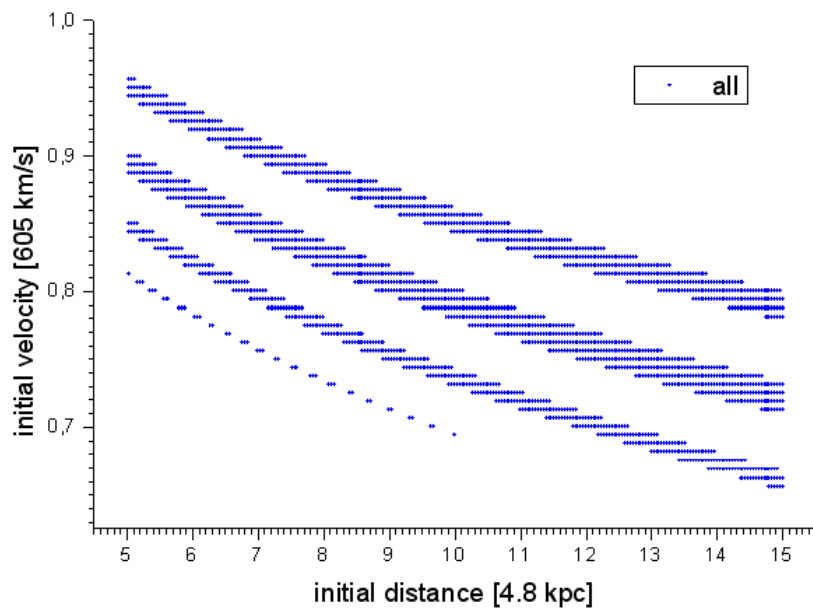


Figure 5.12: Results of a scan in the parameter space in the case of a mass of $3 \cdot 10^{10} M_{\odot}$ for the Milky Way and $5 \cdot 10^{10} M_{\odot}$ for the Andromeda Galaxy, with deep MOND gravity. Despite there are several bands of good orbits, one cannot find any orbit which parameters are really close to the observational values.

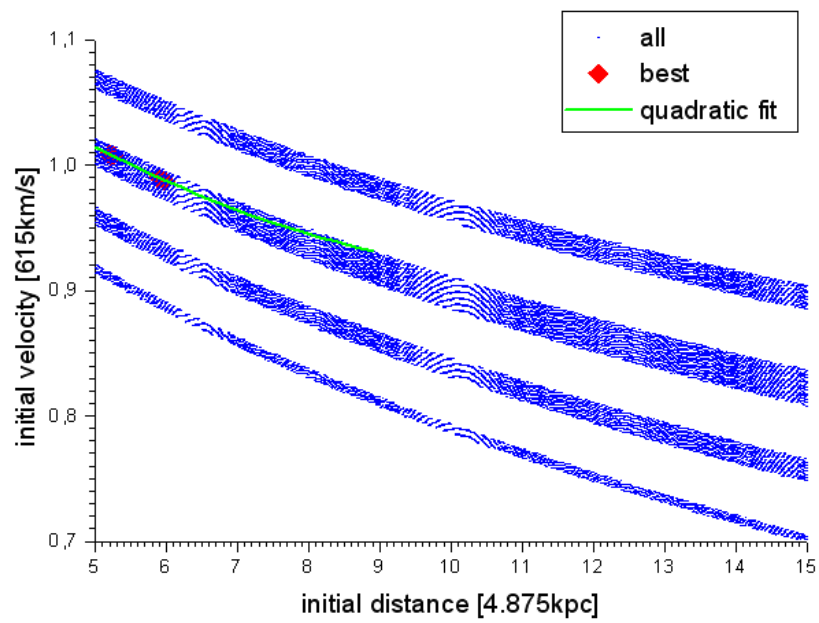


Figure 5.13: Results of a scan in the parameter space in the case of a mass of $5 \cdot 10^{11} M_{\odot}$ for the Milky Way and $8 \cdot 10^{11} M_{\odot}$ for the Andromeda Galaxy, with deep MOND gravity. One can only find five best orbits, which are located in the second band (corresponding to the second revolution).

5.4 The main models

I set up 11 different main models for my thesis. Six of them are based on Newtonian gravity with dark matter while the other five are based on deep-MOND gravity. For all models a Genetic Algorithm has been run for 20 generations with 1000 individual models per generation. The simulations have been started 12 billion years ago, which means 1.6 billion years after the Big Bang. Sawa and Fujimoto let their simulation start 10 Gyr ago (Sawa and Fujimoto, 2005), but speculated about other times too. They suggested that 12 Gyr might be a better time for the close encounter between the Milky Way and the Andromeda nebula and therefore I choose it for my simulations. But to leave the door open for another slightly different time of the first close encounter between the two galaxies, I allowed the initial velocity to be not exactly tangential at the beginning. For my simulations I used following scaling parameters (see table 5.1). With these units and a measured MONDian acceleration a_0 of $1.2 \cdot 10^{-10} \text{m s}^{-2}$, the value of a_0 in the programme *DeMonI* had to be set to $7.770 \cdot 10^{-2}$ in my units.

unit length	r_{scale}	3 kpc
unit time	t_{scale}	7.747 Myr
unit mass	M_{scale}	$10^{11} M_{\odot}$
unit velocity	v_{scale}	378.669 km/s

Table 5.1: Scaling parameters for all models.

The initial distances were randomly set to be between 24 kpc and 150 kpc for the first generation of all models, which covers the results of Sawa and Fujimoto which was about 150 kpc. The initial velocities were calculated according to the fitting parabolas (Newton and MOND) from the two body simulations of the Milky Way and the Andromeda Galaxy. The values from the fits have got some additional small random errors to avoid narrowing the parameter space to much. The other massive galaxies were distributed randomly around the area of the main galaxies. For the galaxies, which are treated massless in the calculation, a test particle cloud consisting of 25 particles each has been added for every "massless" galaxy. I set the efficiency of the Hubble expansion to 1 and the efficiency of the dynamical friction to 0.5 in the models with Newtonian gravity. In total 6 different models with Newtonian gravity have been run. The so called *Newton Main* model (NM) is the model which creates an improved version of the *Sawa and Fujimoto model*. In NM there are 5 galaxies treated as massive: the Milky Way, the Andromeda Galaxy, the Triangulum Nebula, the Large Magellanic Cloud and the Small Magellanic Cloud (for the masses see table 5.2). The mass of the test bodies, which is only used for the dynamical friction, is set to $10^9 M_{\odot}$ for all Newtonian models. The dark matter halos have a radius of 240 kpc for the Milky Way and M31, 60 kpc for M33, 36 kpc for the LMC and 12 kpc for SMC. In NM, like in 9 of 11 models, the values from table (5.5) have been used to compare the results with the observed distribution of galaxies in the Local Group. One of the two exceptions is the model *Newton New* (NN), where I applied the more recent values listed in table 5.6. Beside this difference both models (NM and NN) are identical. The number of massive galaxies has been changed in the models *Newton 4 massive* (N4M) and *Newton 2 massive* (N2M) while all other parameter have stayed the same as in NM. In N2M only the Milky Way and the Andromeda galaxy are treated as massive particles, while all other galaxies are test bodies. N4M is the one which resembles the *Sawa-Fujimoto model* most. Like in their simulation the Milky Way and M31 as well

as both Magellanic Clouds are treated as massive particles while all other members of the Local Group (including M33) are just test bodies. I have also created two more Newtonian models with the usual five massive galaxies but other radii of their Dark Matter halos. In the model *Newton Big Halo* (NBH) the halo radii has been increased for all massive galaxies. The Milky Way's halo and the halo of M31 have a radial extension of 360 kpc. M33's halo had a radius of 90 kpc, while the one of the LMC had 54 kpc and the halo of the SMC 18 kpc. In the other model *Newton Small Halo* (NSH) the radii of the galaxies' halos have been reduced and therefore become more compact. The Milky Way's and the Andromeda's dark matter halo only reaches out up to 120 kpc and the one of M33 to 30 kpc. The radii of the Magellanic clouds' halos ends up on 18 kpc for the LMC and 6 kpc for the SMC. All other parameters in NBH and NSH remained the same as in NM.

galaxy	mass [M_{\odot}]
Milky Way	$1.5 \cdot 10^{12}$
Andromeda Galaxy (M31)	$2.5 \cdot 10^{12}$
Triangulum Nebula (M33)	$5 \cdot 10^{10}$
Large Magellanic Cloud (LMC)	$2 \cdot 10^{10}$
Small Magellanic Cloud (SMC)	$7 \cdot 10^9$

Table 5.2: Masses of the massive galaxies used in the Newtonian models with Dark Matter.

Because there are no Dark Matter halos to analyse I only have to ran 5 models for deep-MOND gravity. The first thing to be mentioned concerning the difference between MOND and Dark Matter is that all galaxies have different total masses. The values in table 5.3 have been used for the massive galaxies in all but one MONDian simulations. These values are estimates of the baryonic mass content of the 5 most massive members of the Local Group. The first MONDian model *Mond Main* (MM) has consisted of 5 massive galaxies (the Milky Way, M31, M33, LCM and SMC) and all other galaxies from table 5.5 have been treated as test bodies. Since the model uses MONDian gravity there are no Dark Matter halos needed. Another model has been totally equivalent to MM but it has used the values from table 5.6 for all galaxies. This model has been called *Mond New* (MN). Furthermore the model *Mond 4 massive* (M4M) has been calculated, in which the Milky Way, the Andromeda galaxy and both Magellanic Clouds have been massive galaxies but with this exception all other settings have been the same as in MM. The next model have been called *Mond 2 massive* (M2M) and it has been the MONDian equivalent to N2M, where only the two dominant galaxies, the Milky Way and the Andromeda galaxy, have been treated as massive particles, while all other galaxies of the Local Group have been test bodies. For the last model, which has been called *Mond Heavy* (MH), the same configurations like in MM with the exception of the masses have been used. The values from table 5.4 have been used for the masses. One can see that only the masses of the Milky Way and M31 have been changed to values, which are exactly $(1/20)^{\text{th}}$ of the dark matter halo's mass from the Newtonian models. The reason for doing this is the very successful two-body simulation with these masses in a previous test (see figure (5.11)).

I cover a vast range of possible scenarios with my eleven models. One can investigate the dependence of the dynamics on the radii of the Dark Matter halos as well as the dependence of the orbits in our galaxy group on different theories of gravity (Dark Matter and MOND).

galaxy	mass [M_{\odot}]
Milky Way	$5 \cdot 10^{10}$
Andromeda Galaxy (M31)	$8 \cdot 10^{10}$
Triangulum Nebula (M33)	$9 \cdot 10^9$
Large Magellanic Cloud (LMC)	$5 \cdot 10^9$
Small Magellanic Cloud (SMC)	$1.6 \cdot 10^9$

Table 5.3: Masses of the massive galaxies used in most of the MONDian models.

galaxy	mass [M_{\odot}]
Milky Way	$7.5 \cdot 10^{10}$
Andromeda Galaxy (M31)	$1.25 \cdot 10^{11}$
Triangulum Nebula (M33)	$9 \cdot 10^9$
Large Magellanic Cloud (LMC)	$5 \cdot 10^9$
Small Magellanic Cloud (SMC)	$1.6 \cdot 10^9$

Table 5.4: Masses of the massive galaxies used in the "heavy" MONDian.

name of the galaxy	galactic longitude [°]	galactic latitude [°]	distance in kpc	radial velocity in km/s
Milky Way	0.0	0.0	8.5	0.0
M31	121.2	-21.6	770	-297
M33	133.6	-31.3	840	-181
LMC	280.5	-32.9	49	274
SMC	302.8	-44.3	58	148
WLM	75.9	-73.6	925	-123
NGC55	332.7	-75.7	1480	124
IC10	119.0	-3.3	825	-342
NGC147	119.8	-14.3	725	-193
And III	119.3	-26.2	760	-355
NGC185	120.8	-14.5	620	-204
NGC205	120.7	-21.1	815	-229
M32	121.2	-22.0	805	-197
And I	121.7	-24.9	805	-380
Sculptor	287.5	-83.2	79	102
LGS3	126.8	-40.9	810	-272
IC1613	129.8	-60.6	700	-234
And II	128.9	-29.2	525	-188
Phoenix	272.2	-68.9	445	56
Fornax	237.1	-65.7	138	53
UGCA92	144.7	+10.5	1300	-87
Carina	260.1	-22.2	101	224
Leo A	196.9	+52.4	690	26
Sextans B	233.2	+43.8	1345	303
NGC3109	262.1	+23.1	1250	404
Antlia	263.1	+22.3	1235	361
Leo I	226.0	+49.1	250	286
Sextans A	246.2	+39.9	1440	325
Sextans	243.5	+42.3	86	277
Leo II	220.2	+67.2	205	76
GR8	310.7	+77.0	1590	215
Ursa Minor	105.0	+44.8	66	-248
Draco	86.4	+34.7	82	-293
Sagittarius	5.6	-14.1	24	140
SagDIG	21.1	-16.3	1060	-79
NGC6822	25.3	-18.4	490	-54
Aquarius	34.0	-31.3	800	-137
IC5152	343.9	-50.2	1590	124
Tucana	322.9	-47.4	880	130
UGCA438	11.9	-70.9	1320	62
Pegasus	94.8	-43.5	955	-182

Table 5.5: Observational values of the Local Group galaxies used by Sawa and Fujimoto in 2005 based on the work of Mateo (Mateo, 1998).

name of the galaxy	galactic longitude [°]	galactic latitude [°]	distance in kpc	radial velocity in km/s
Milky Way	0.0	0.0	8.5	0.0
M31	121.2	-21.6	760	-301
M33	133.6	-31.3	795	-182
LMC	280.5	-32.9	50	283
SMC	302.8	-44.3	59	158
WLM	75.9	-73.6	925	-116
NGC55	332.9	-75.7	1480 1	23
IC10	119.0	-3.3	660	-345
NGC147	119.8	-14.3	660	-203
And III	119.3	-26.3	760	-355
NGC185	120.8	-14.5	660	-204
NGC205	120.7	-21.1	760	-254
M32	121.2	-22.0	760	-206
And I	121.7	-24.8	810	-380
Sculptor	287.5	-83.2	87	108
LGS3	126.8	-40.9	620	-286
IC1613	129.7	-60.6	725	-234
And II	128.9	-29.2	700	-188
Phoenix	272.2	-68.9	395	-13
Fornax	237.1	-65.7	138	49
UGCA92	144.7	+10.5	1300	-99
Carina	260.1	-22.2	100	223
Leo A	196.9	+52.4	800	24
Sextans B	233.2	+43.8	1345	301
NGC3109	262.1	+23.1	1250	404
Antlia	263.1	+22.3	1235	362
Leo I	226.0	+49.1	250	248
Sextans A	246.1	+39.9	1440	335
Sextans	243.5	+42.3	86	226
Leo II	220.2	+67.2	210	2
GR8	310.7	+77.0	1590	214
Ursa Minor	105.0	+44.8	63	-235
Draco	86.4	+34.7	79	-288
Sagittarius	5.6	-14.1	24	142
SagDIG	21.1	-16.3	1180	-79
NGC6822	25.3	-18.4	500	-48
Aquarius	34.0	-31.3	1025	-136
IC5152	343.9	-50.2	1590	116
Tucana	322.9	-47.4	895	130
UGCA438	11.9	-70.9	1320	62
Pegasus	94.8	-43.5	760	-184
Cetus	101.4	-72.9	775	?
And V	126.2	-15.1	810	-403
Cassiopeia	109.5	-9.9	690	?
Pegasus II	106.0	-36.3	815	-354

Table 5.6: Updated observational values of the Local Group galaxies based on the work of several different authors (Mateo, 1998; van den Bergh, 2000; van den Bergh, 2003) and some data from the SIMBAD Astronomical Database.

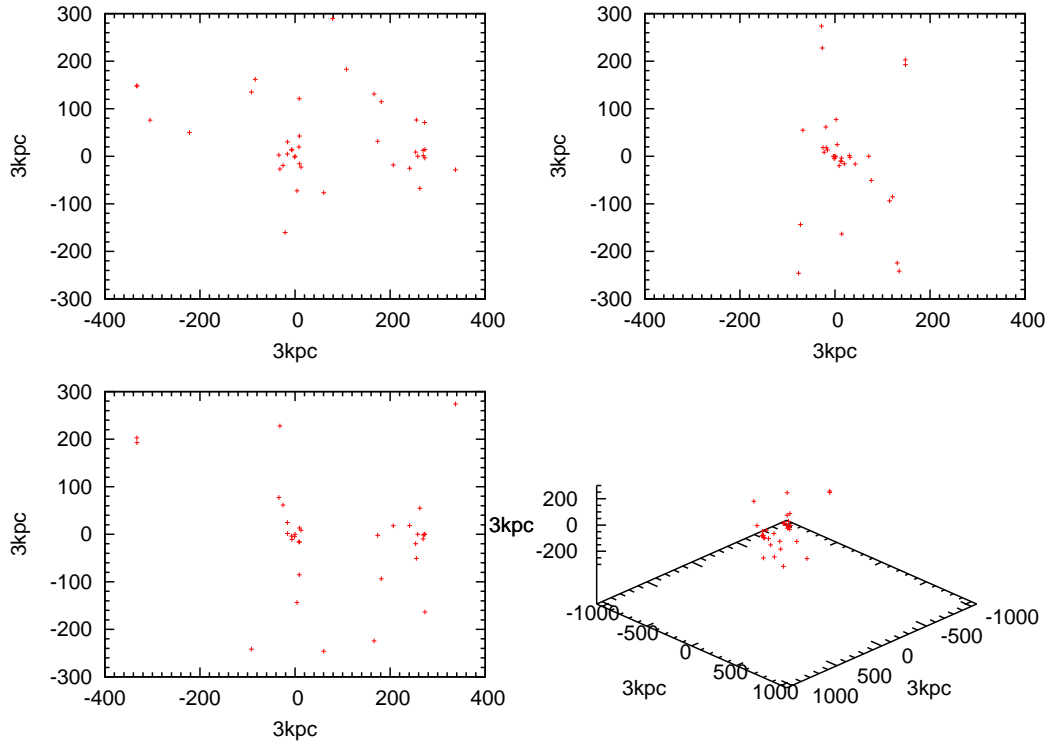


Figure 5.14: The observed spatial distribution of galaxies in the Local Group due to table 5.5. It has been rotated that the plane of the Milky Way, M31 and M33 corresponds to the xy-plane. The image in the upper-left corner is the view on the xy-plane, in the upper-right corner one finds the view on the yz-plane, in the lower-left corner there is a view on the xz-plane and in the lower-right corner one can find a 3D view along the first median.

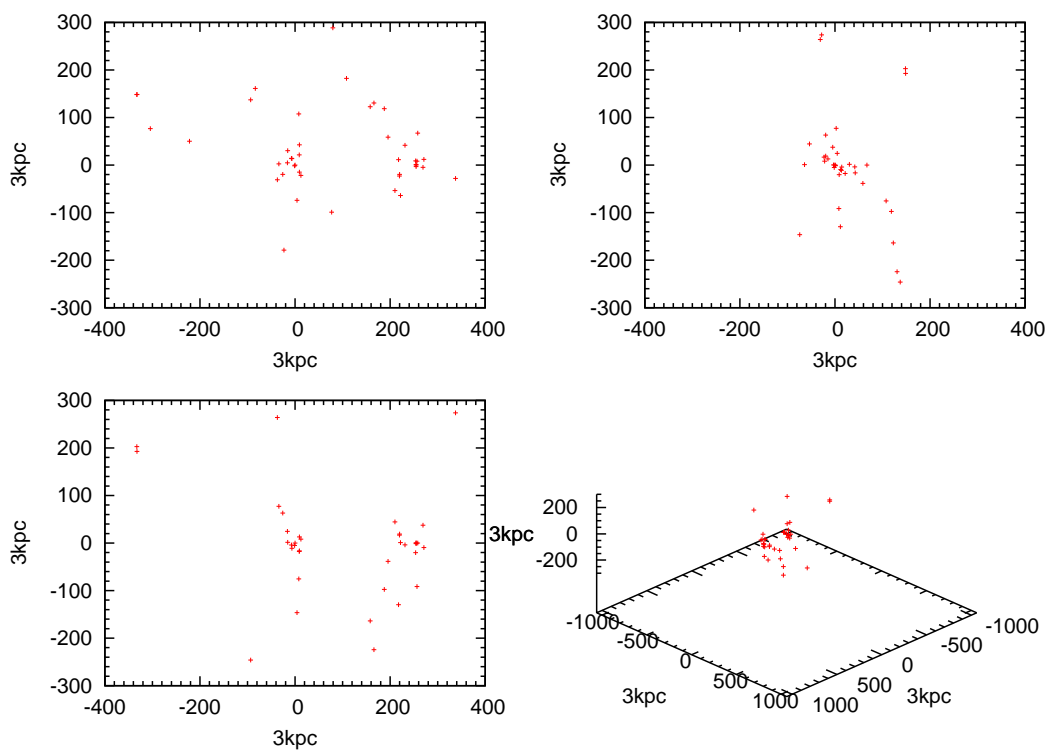


Figure 5.15: Same as figure 5.14, but using the data given in table 5.6.

Chapter 6

Results

6.1 Convergence of the genetic algorithm

It is important to test the convergence of the genetic algorithm that has been used, to see how much the results have been improved by it. Before doing the main run the algorithm has been tested with less optimized models and one has got an improvement between the first and the last generation of about a factor (convergence factor) of 50 to 100 and the largest part of it has occurred during the first 10 generations. During the last generations only the positions of the dwarf galaxies (test particles) improved a little, because of the test particle cloud trick. I set the statistical weights in the fitness function of my genetic algorithm (see equation A.4) to following values: $g_{\text{mpos}} = 200$, $g_{\text{mvel}} = 100$, $g_{\text{tbpos}} = 2$ and $g_{\text{tbvel}} = 1$ for all my simulations. The convergence of the final models with optimized initial conditions is significantly less compared to the first tests. If one excludes the outlier of the NBH model, one gets an average convergence factor of 20.7. The NBH model has an exceptional convergence factor of 1158, but it should be noted that it has had very bad initial conditions and therefore a very large value of the fitness function during the first generations. The largest convergence occurs during the first ten generations (see figure (6.1)). The reason for the bad average convergence are the already optimised initial conditions, like setting the orbit parameters of the main galaxies (Milky Way and M31). They have been set to values, which produce reasonable distances and radial velocities for today. Another problem, which one encounters, is that there are a few cases where the genetic algorithm shows a short divergence, in contrast to the expected monotonic convergence. It did not occur during the first tests. The best results of the concerned generations have been checked and one notices a huge change in the parameters of the respectively best result. But the value of the fitness function of this "best result" is worse than of the best result in the previous generation and should not become the new "best result", because the best results of the predecessor generation are always kept. Therefore I have double-checked the code of the *GeneAl* programme for any errors, but have not been able to find anything that would explain this strange behaviour. This problem remains an unsolved mystery. One might have noticed that in figure (6.1) some models have in general smaller values for their fitness function than others. These models consist of fewer massive particles and since the static weight of one massive particle is by a factor of 100 greater than that of a test body. Consequently models with fewer massive particles have lower values for their fitness functions in general. In addition to that, the convergence for models with fewer particles is better in general. One can also see that the average convergence of Newtonian models (average convergence factor of 27.6)

is greater than that of MONDian models (average convergence factor of 13.8). On the other hand, the final values of the fitness function for MONDian models is always less than those of Newtonian models with a similar configuration. One can explain these behaviours of the genetic algorithm by having a look at figures 5.8, 5.11 and 5.13 again. In case of Newtonian gravity, one always has a very small area in parameter space (a thin parabola) of possible initial conditions for a certain mass that leads to the desired final values. This is different to the case of deep-MOND gravity. There one finds several bands of possible initial conditions, which yields results of moderate quality. But due to the previous optimisation of these initial conditions, the genetic algorithm starts in the band (or near), where the best initial conditions can be found. In both cases the algorithm starts relatively close to the best initial conditions, but in the Newtonian case a small deviation from these initial conditions yields much worse values of the fitness function than in the MONDian case. Therefore one already gets small values of the fitness function in the first generation for MOND and consequently there cannot be as much improvement as in the Newtonian case. Nevertheless deep-MOND gravity can reproduce the distribution of the Local Group's galaxies better than Newtonian gravity with Dark Matter in the assumed scenario.

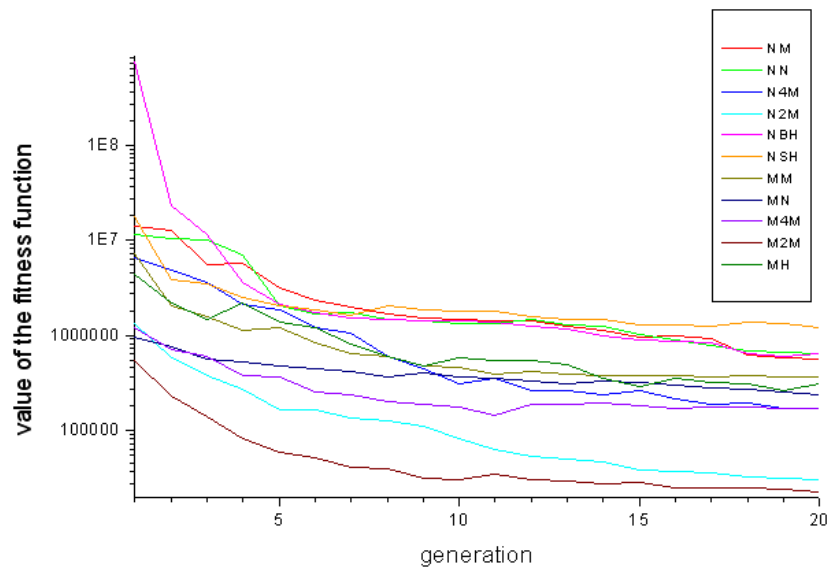


Figure 6.1: Convergence of the genetic algorithm for all eleven models.

6.2 Results of all models

6.2.1 NM

The analysis starts with a look on the very best results from every model. In NM, the values of the fitness function for the five best results are: 567136, 650519, 750015, 805293 and 844501. In figures 6.2, 6.3, 6.4, 6.5 and 6.6 one can find the corresponding distribution of galaxies. It shall be noted that these figures only show the spatial distribution. The radial velocity, which also contributes to the fitness function, is not displayed here. The deviation of the calculated radial velocities from the observed values for the five best results can be found in table 6.1, as well as the difference between the calculated and the observed positions of all Local Group galaxies. It should be noted that the velocities are fitted quite badly in this model. This might be caused by a relatively small statistic weight of the radial velocities in the fitness function. One may have noticed that some of the five best results, a certain galaxy can fit the observations very well, while in another result the calculated positions and velocities of the same galaxy can be totally wrong. Mainly galaxies outside the Milky Way and Andromeda subgroups are affected by behaviour. In contrast to these quite different final distributions, the initial distribution of galaxies are very similar in all five best results (see figures 6.8, 6.9, 6.10, 6.11 and 6.12). For the NM-models, it is always a very compact agglomeration (less than 100 kpc) around the two most massive galaxies, which shows an extension (up to 500 kpc) normal to the connection vector between the Milky Way and M31 (in the orbital plane of these two galaxies). The initial distance between these two galaxies is between 60 and 75 kpc. Since the angle of M31's velocity has been left variable, the exact time of its close encounter with the Milky Way is also variable. In case of this model the assumed time for the first encounter of 12 Gigayears ago has been shown to be in agreement with the working hypothesis within small deviations (<100 Myrs). A general problem is that the Magellanic Clouds always merge with Milky Way and M33 in some cases experiences a similar fate with the Andromeda Galaxy or gets at least by far too close to its host galaxy. Furthermore some of the outer galaxies of the Local Group cannot be fitted very well, like UGCA92 or IC5152. In a qualitative picture, most features of the Local Group's galaxy distribution can be reproduced with this model. One can see in figure 6.7, that the plane of galaxies is inclined to the orbital plane of the two most massive galaxies by roughly 30° . This is interesting, because one expects that both planes have to correspond to create a planar distribution. But the simulation has shown that this is not necessary.

name of the galaxy	spatial deviation [kpc] best result	velocity deviation [km/s] best result	spatial deviation [kpc] 2 nd best result	velocity deviation [km/s] 2 nd best result	spatial deviation [kpc] 3 rd best result	velocity deviation [km/s] 3 rd best result	spatial deviation [kpc] 4 th best result	velocity deviation [km/s] 4 th best result	spatial deviation [kpc] 5 th best result	velocity deviation [km/s] 5 th best result
Milky Way	0	0	0	0	0	0	0	0	0	0
M31	15	66	53	63	82	50	132	90	89	76
M33	77	59	132	264	118	61	86	166	125	281
LMC	49	229	48	287	49	306	49	390	49	268
SMC	55	274	55	120	56	136	55	196	55	174
WLM	340	99	77	7	119	48	195	31	395	79
NGC55	214	73	98	53	293	9	186	35	184	36
IC10	60	54	112	53	54	78	11	183	95	135
NGC147	77	140	82	44	24	114	47	120	33	123
And III	20	303	63	13	65	58	84	341	34	26
NGC185	31	193	26	39	55	36	95	41	53	75
NGC205	28	140	53	126	38	29	46	275	34	44
M32	50	92	19	96	31	173	39	100	20	98
And I	53	69	62	31	64	7	40	185	29	40
Sculptor	32	66	19	139	12	67	9	94	15	26
LGS3	69	51	137	96	70	51	34	184	55	163
IC1613	48	154	96	86	291	82	184	26	47	32
And II	41	62	49	60	217	200	151	142	103	155
Phoenix	75	1	227	120	117	56	74	106	82	24
Fornax	46	12	29	51	115	21	43	57	20	11
UGCA92	569	65	509	65	356	17	166	79	500	126
Carina	40	165	13	4	13	10	20	188	15	38
Leo A	303	13	140	12	182	80	235	28	88	24
Sextans B	306	45	280	71	442	74	141	54	187	49
NGC3109	322	99	220	55	69	94	146	60	280	137
Antlia	309	56	216	11	69	51	170	17	301	94
Leo I	145	224	46	132	52	200	54	181	84	256
Sextans A	286	21	252	6	438	60	184	2	116	71
Sextans	30	98	108	256	13	107	11	189	23	289
Leo II	92	62	49	95	43	21	33	33	61	73
GR8	133	25	284	13	113	72	578	56	174	3
Ursa Minor	26	122	34	129	43	18	62	174	10	71
Draco	29	224	11	127	15	186	76	129	26	101
Sagittarius	16	171	18	144	16	156	19	205	7	50
SagDIG	356	35	162	43	222	30	295	89	229	70
NGC6822	69	27	94	73	126	145	173	28	93	77
Aquarius	204	23	199	88	198	47	172	88	240	26
IC5152	292	46	210	45	195	70	241	22	224	17
Tucana	382	16	66	49	197	87	260	98	184	3
UGCA438	267	11	136	43	223	37	140	11	509	26
Pegasus	143	71	142	149	162	103	135	77	118	55

Table 6.1: Deviation of the positions and radial velocities for the five best NM results.

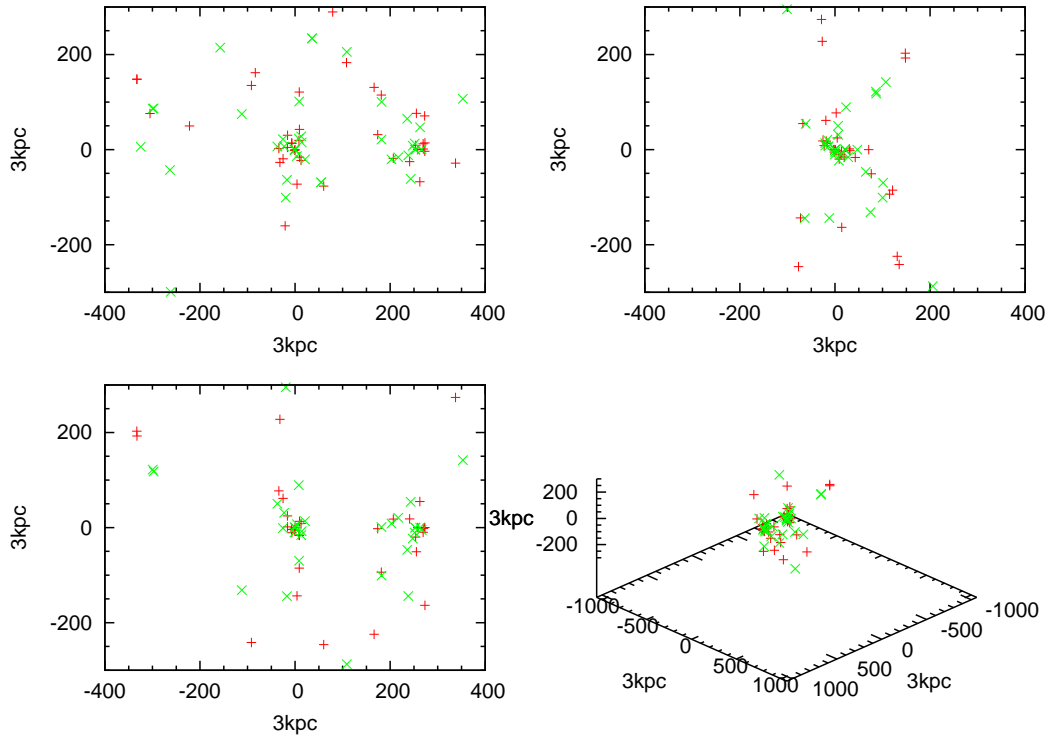


Figure 6.2: The spatial distribution of the best NM result (green \times) is compared with the observed distribution of the Local Group's galaxies (red $+$). Note the big differences of the calculated distribution, compared to the other results (see figures 6.3, 6.4, 6.5 and 6.6) of NM with only little worse values for their fitness functions compared to this result. The image in the upper-left corner is the view on the xy-plane, in the upper-right corner one finds the view on the yz-plane, in the lower-left corner there is a view on the xz-plane and in the lower-right corner one can find a 3D view along the first median.

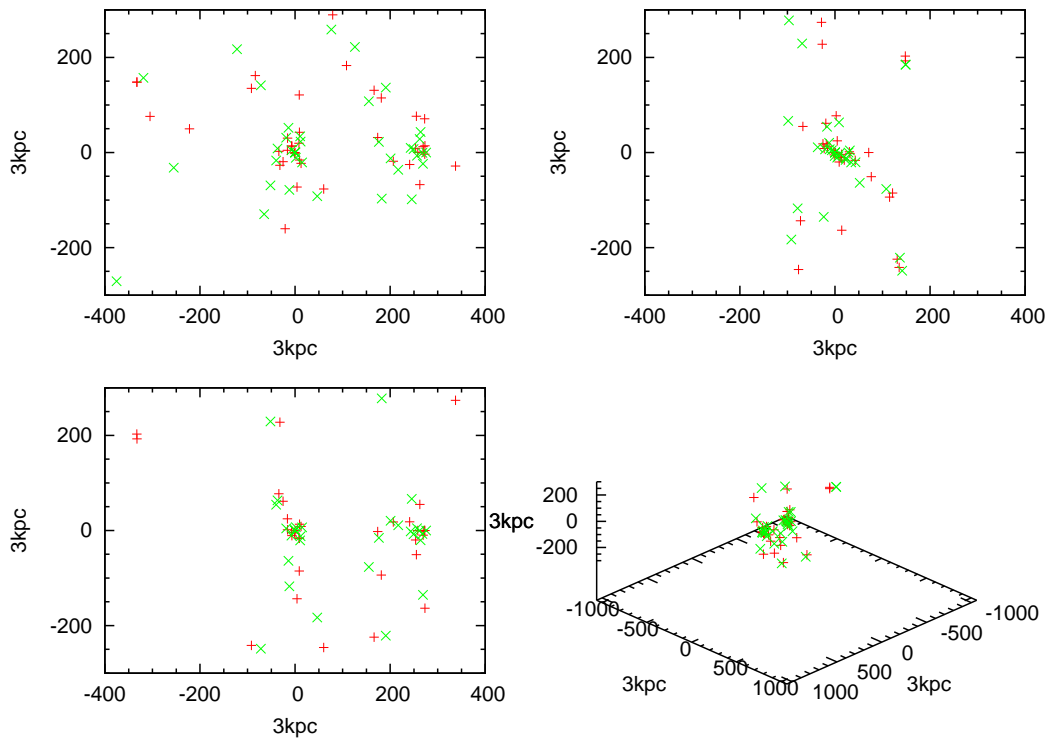


Figure 6.3: Same as figure 6.2, but for the second best NM result.

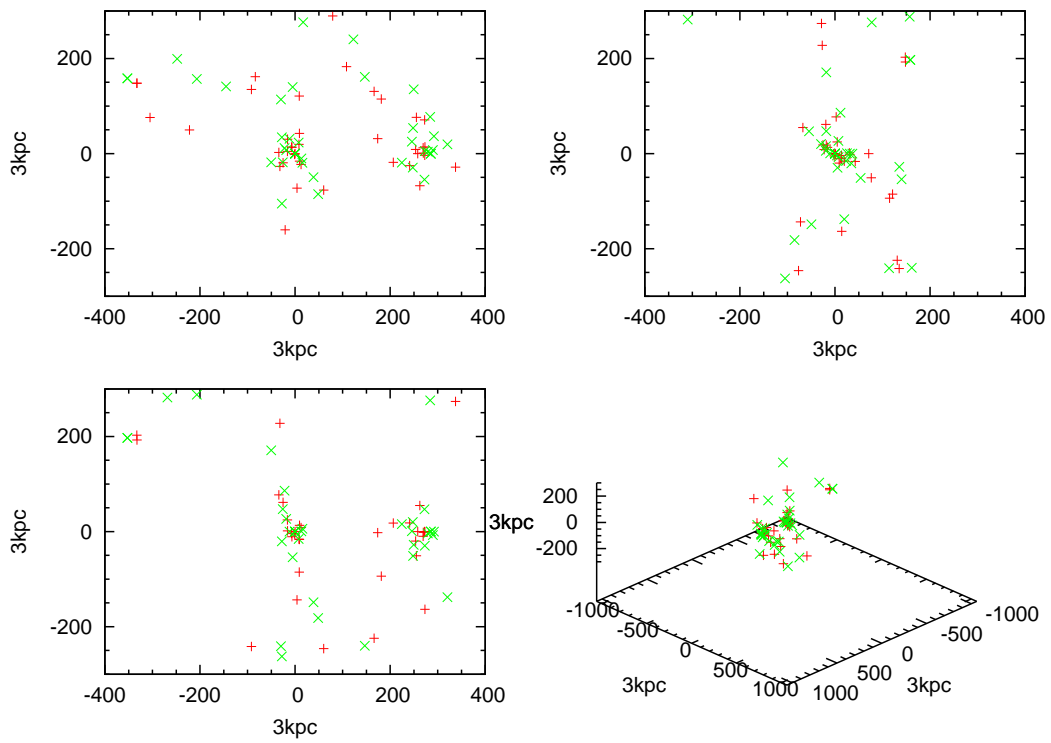


Figure 6.4: Same as figure 6.2, but for the third best NM result.

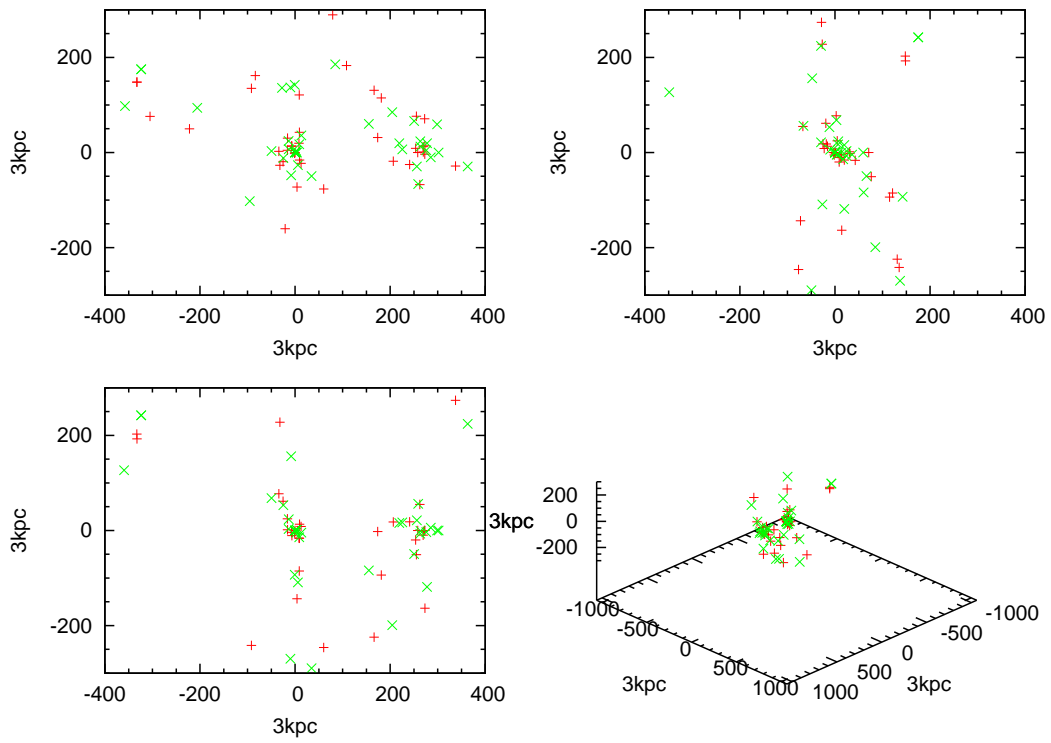


Figure 6.5: Same as figure 6.2, but for the fourth best NM result.

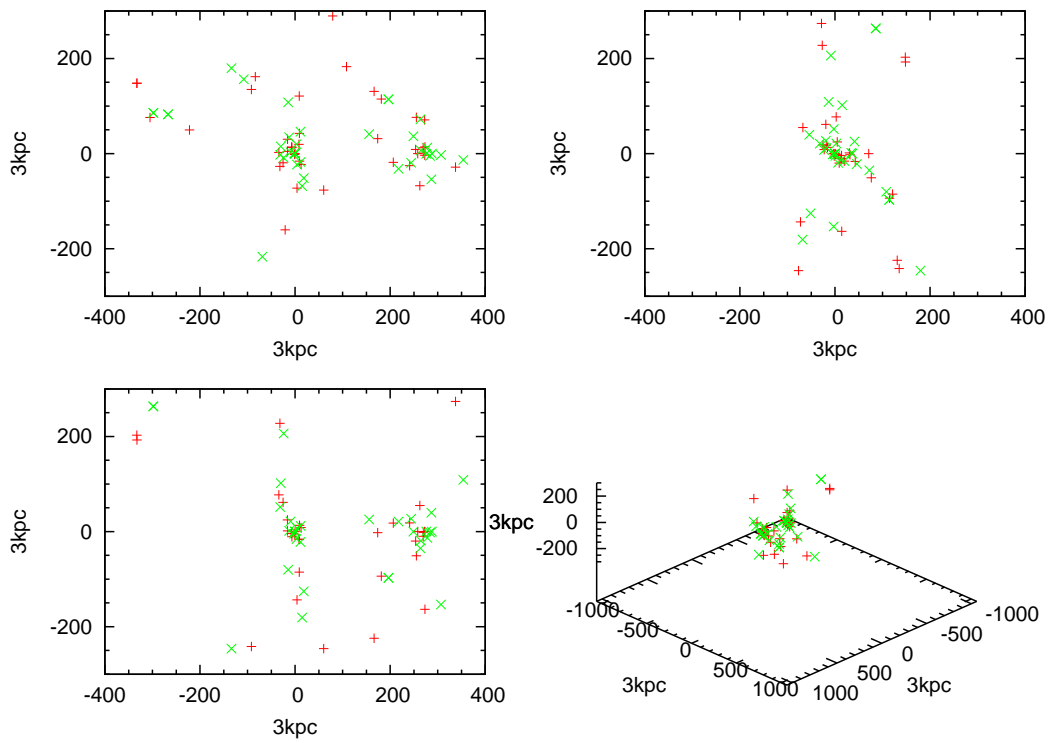


Figure 6.6: Same as figure 6.2, but for the fifth best NM result.

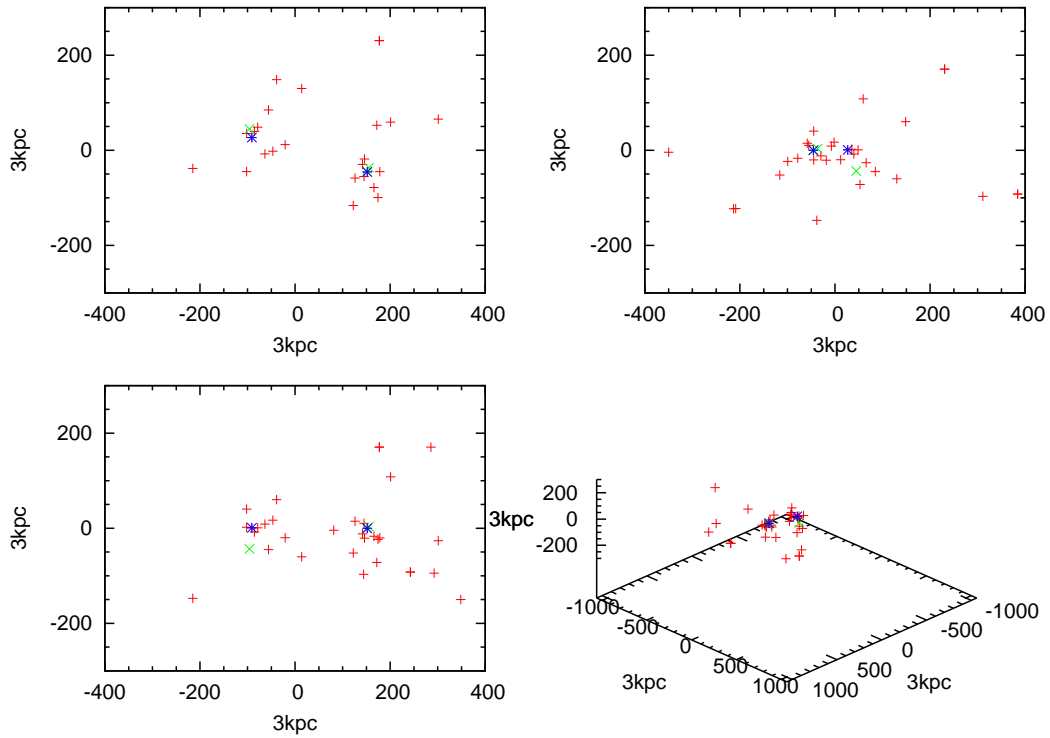


Figure 6.7: The spatial distribution of the best NM result. The Milky Way and the Andromeda galaxy are represented by a blue $*$, the other massive galaxies are shown as green \times and all the massless galaxies are represented by red $+$. Note that the plane of galaxies is inclined to the orbital plane of the Milky Way and M31, which is very close to the xy -plane. The image in the upper-left corner is the view on the xy -plane, in the upper-right corner one finds the view on the yz -plane, in the lower-left corner there is a view on the xz -plane and in the lower-right corner one can find a 3D view along the first median.

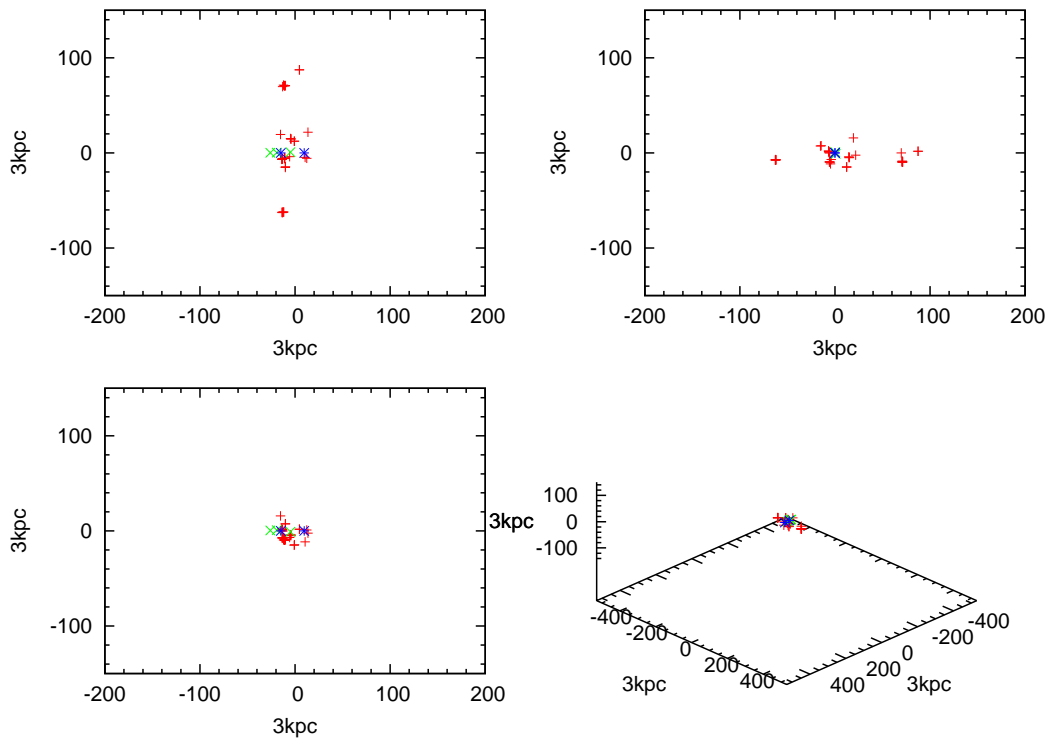


Figure 6.8: The initial distribution of the best NM result's galaxies (12 Gyr ago). The Milky Way and the Andromeda galaxy are represented by a blue *, the other massive galaxies are shown as green \times and all the massless galaxies are represented by red +. The image in the upper-left corner is the view on the xy-plane, in the upper-right corner one finds the view on the yz-plane, in the lower-left corner there is a view on the xz-plane and in the lower-right corner one can find a 3D view along the first median.

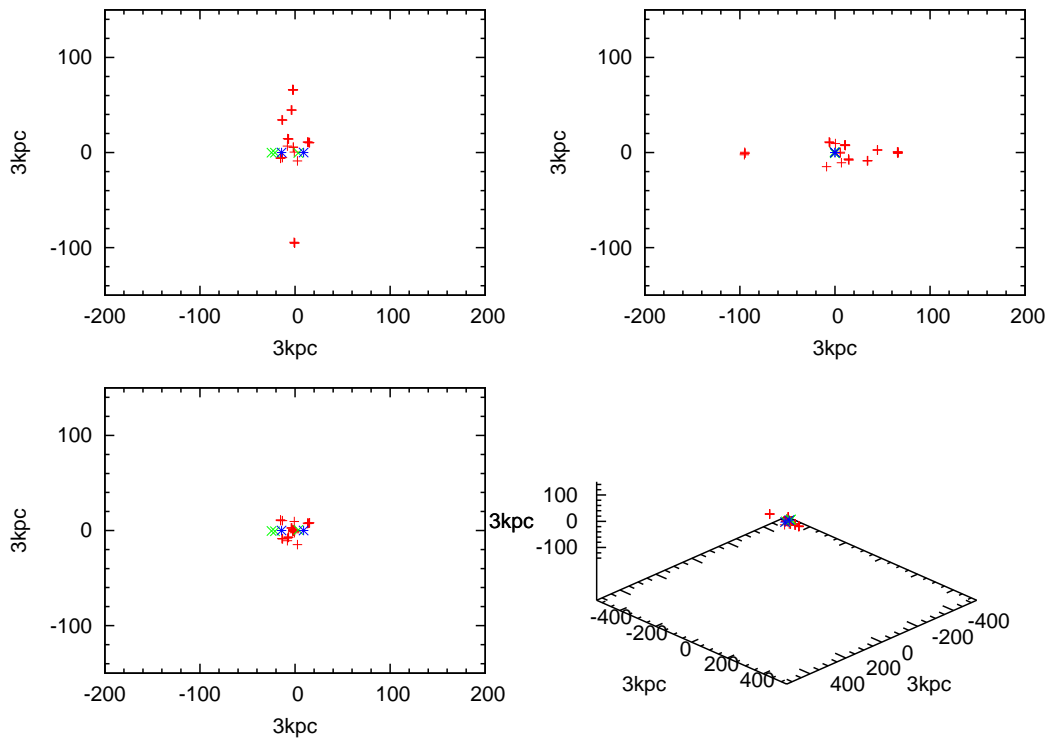


Figure 6.9: Same as figure 6.8, but for the second best NM result.

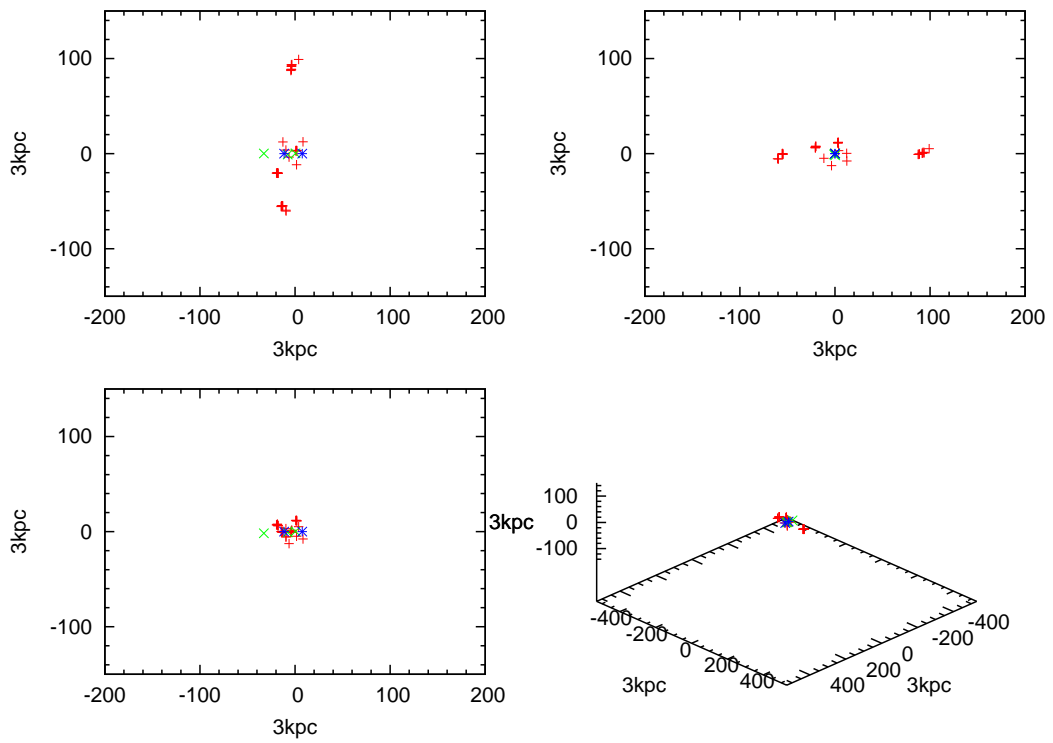


Figure 6.10: Same as figure 6.8, but for the third best NM result.

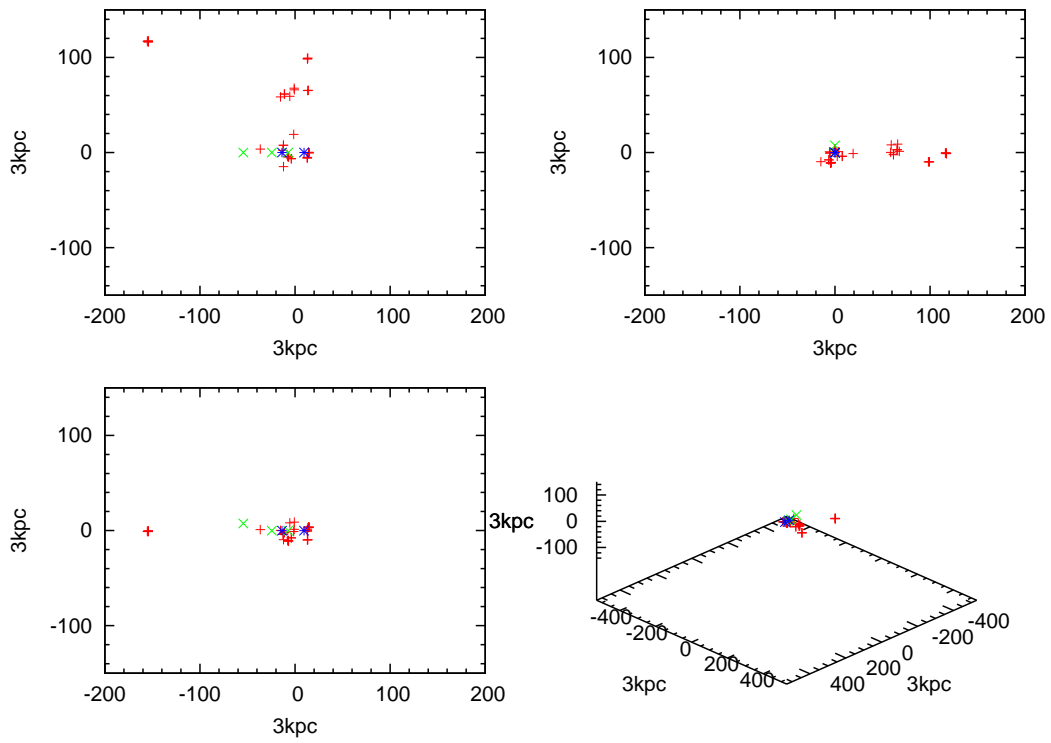


Figure 6.11: Same as figure 6.8, but for the fourth best NM result.

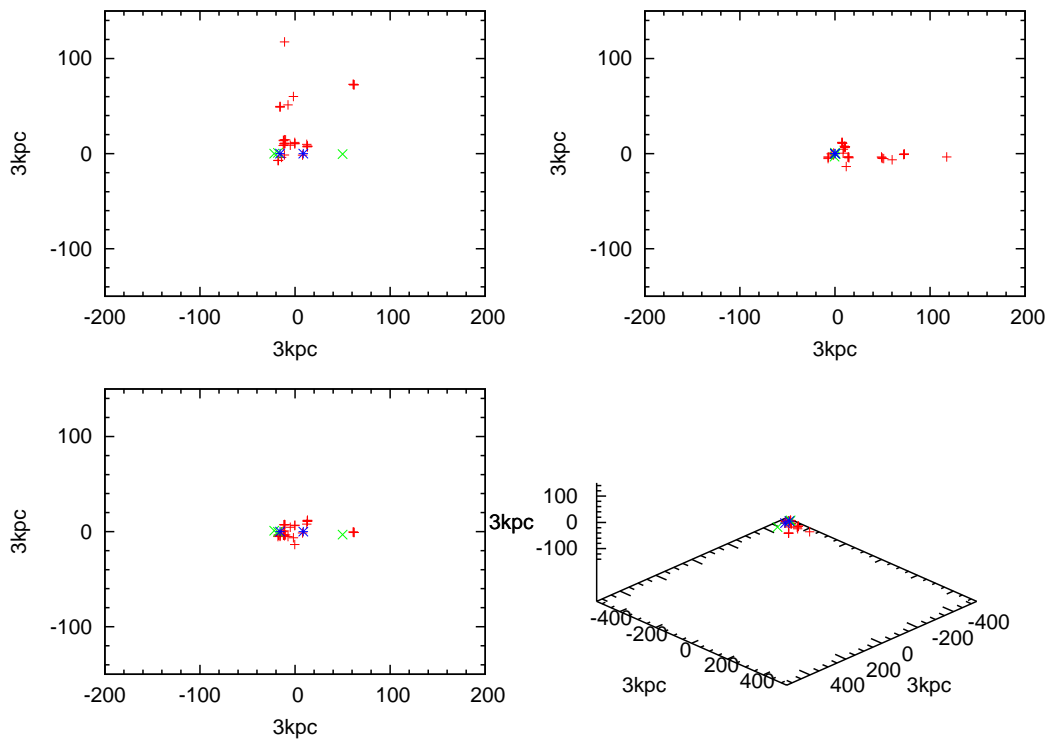


Figure 6.12: Same as figure 6.8, but for the fifth best NM result.

6.2.2 NN

The best result for the NN-model has a value of 644603 and therefore provides a little worse fit than the best result of the previous model (already taking into account that the NN model has more galaxies to fit). Though its best result is still better than the second best result of NM. This model (NN) uses more recent observational data for the Local Group's galaxies and also some newly discovered members of our galaxy group. Nevertheless it has very similar problems and advantages as the previous model (NM). The LMC and the SMC merge with the Milky Way in this model too, and M33 also ends up too deep into the Andromeda nebula's halo, though it does not merge. But in contrast to NM, NN does better in fitting the outer galaxies of the Local Group, although the improvement is not that good (see table 6.2). 12 Gigayears ago the distance between M31 and the Milky Way has been 70 kpc in the best result for this model. But the first (and only) close encounter between the two massive galaxies has taken place earlier at a smaller distance due to the best result. The second and third best result of NN tend to confirm the time of the close encounter of 12 Gigayears ago. The initial distribution of galaxies for this model (see figure 6.15) is a compact agglomeration with a similar tail like in the previous model (see figures 6.8 to 6.12). Though there is also an important and very interesting difference. The galaxy M33 starts approximately 150 kpc away of the Milky Way, but on the side opposite to the Andromeda galaxy and therefore M33 is not part of the tail. Furthermore, the Triangulum nebula has been moving away with 250 km/s from our galaxy group's centre of mass, but after several billion years it is captured by M31. Despite some problems, NN can qualitatively reproduce the basic structure of the Local Group (see figure 6.13). If one takes a closer look at the second, third, etc. best results of NN, one may notice that they look very different, despite the fact, that there is hardly any difference in the value of the fitness function. Each result fits some galaxies extremely well, while failing in fitting others. On the other hand the initial conditions of all good results are very similar. This strong dependence on the exact initial conditions is typical for highly dynamical (chaotic) systems, like the Local Group and therefore no surprise. One encounters this phenomenon with every model, not only NM and NN. Furthermore one may notice that there is an angle of about 45° between the orbital plane of the Milky Way and M31 and the plane of the galaxy distribution (see figure 6.14).

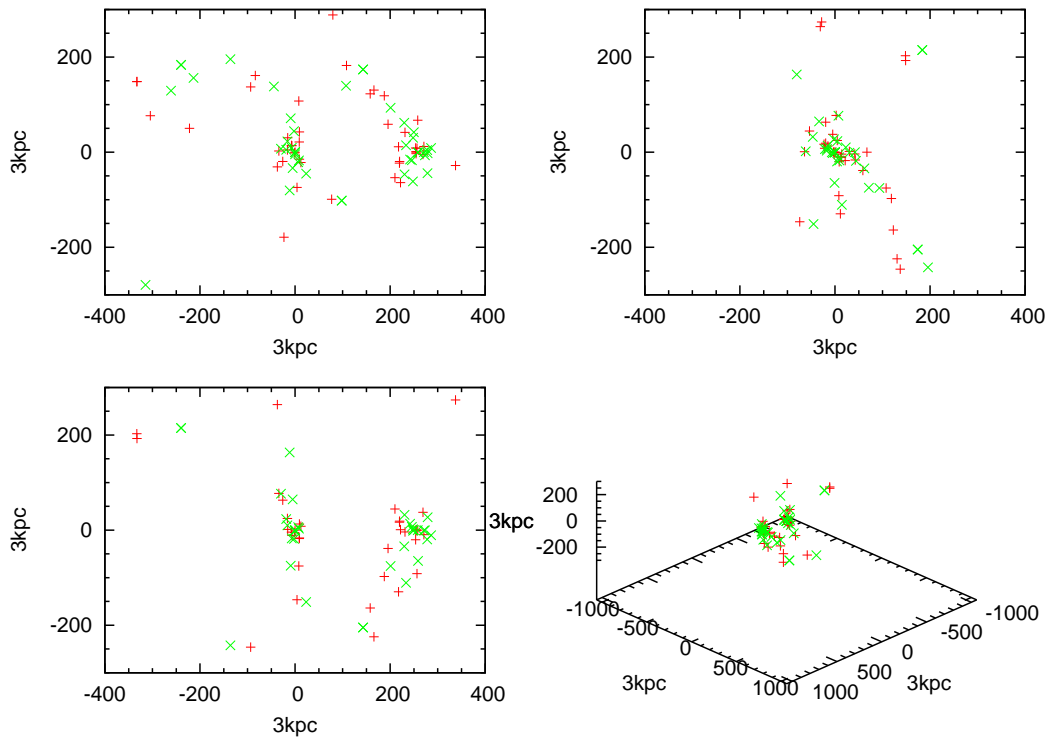


Figure 6.13: The spatial distribution of the best NN result (green \times) after the integration is compared with the observed distribution of the Local Group's galaxies (red $+$). The image in the upper-left corner is the view on the xy-plane, in the upper-right corner one finds the view on the yz-plane, in the lower-left corner there is a view on the xz-plane and in the lower-right corner one can find a 3D view along the first median.

name of the galaxy	spatial deviation [kpc]	velocity deviation [km/s]
Milky Way	0	0
M31	10	51
M33	80	68
LMC	49	224
SMC	56	196
WLM	159	8
NGC55	267	102
IC10	73	145
NGC147	71	20
And III	74	129
NGC185	86	97
NGC205	57	19
M32	49	137
And I	46	69
Sculptor	60	125
LGS3	103	72
IC1613	108	3
And II	62	49
Phoenix	120	177
Fornax	35	69
UGCA92	260	1
Carina	34	139
Leo A	345	74
Sextans B	387	47
NGC3109	301	140
Antlia	305	98
Leo I	20	280
Sextans A	277	72
Sextans	8	77
Leo II	75	49
GR8	129	6
Ursa Minor	30	49
Draco	18	245
Sagittarius	13	197
SagDIG	434	53
NGC6822	106	18
Aquarius	76	4
IC5152	177	12
Tucana	217	14
UGCA438	133	85
Pegasus	74	177
Cetus	202	108
And V	43	295
Cassiopeia	79	259
Pegasus II	85	82

Table 6.2: Deviation of the positions and radial velocities for the best NN result.

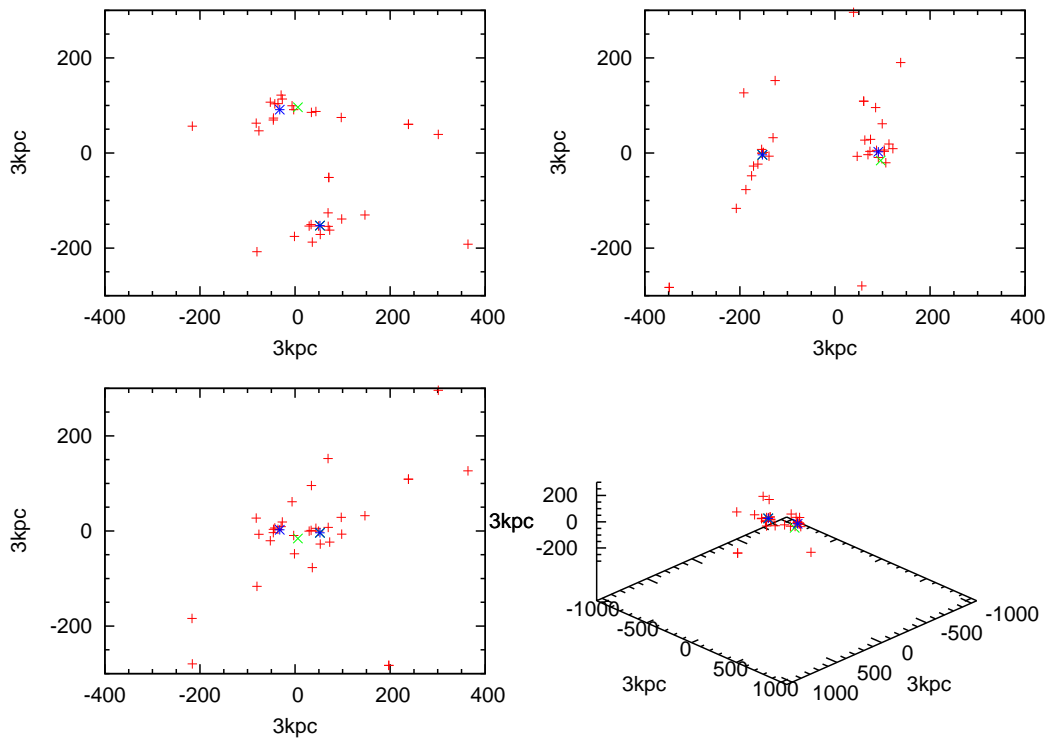


Figure 6.14: The spatial distribution of the best NN result. The Milky Way and the Andromeda galaxy are represented by a blue *, the other massive galaxies are shown as green \times and all the massless galaxies are represented by red +. Note that the plane of galaxies is inclined to the orbital plane of the Milky Way and M31, which is very close to the xy-plane. The labelling of the images is identical to figure 6.13.

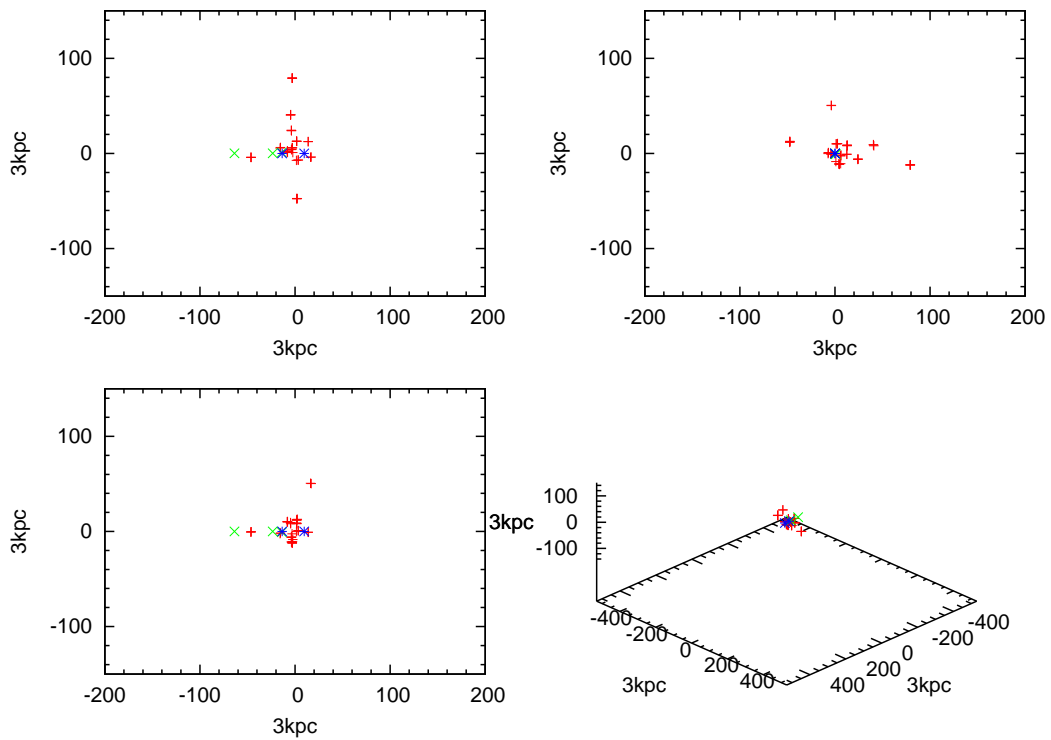


Figure 6.15: The initial distribution of the best NN result's galaxies (12 Gyr ago). The Milky Way and the Andromeda galaxy are represented by a blue *, the other massive galaxies are shown as green \times and all the massless galaxies are represented by red +. The labelling of the images is identical to figure 6.13.

6.2.3 N4M

The analysis of the N4M model has shown that the best result has a value of the fitness function of 170939. This is much better than the results of the previous models, but on the other hand, there is one massive galaxy less in N4M, which also reduces the value of the fitness function. As you can see in figure (6.16) the model can reproduce the spatial structure of the Local Group very well. Since this model is an improved, but very similar version (though different masses) of the Sawa-Fujimoto model, one can compare the results of both models. The Milky Way and M31 are fitted very well, but the Magellanic clouds only moderately, because they get too close to the Milky Way again. The SMC merges and the LMC orbits the Milky Way at a distance of about 30 kpc at the end of the integration. Sawa and Fujimoto have found that IC10, NGC147, NGC185, NGC205, M32, M31, the SMC, Sculptor, LGS3, IC1613, M33, Phoenix, Fornax, LMC, Carina, Leo I, Sextans, Leo II, Ursa Minor, Draco, the Milky Way, Sagittarius and Pegasus are in agreement with their model (Sawa and Fujimoto, 2005). The galaxies of N4M's results will be categorised in four classes: excellent, good, moderate and bad. Galaxies with a spatial deviation of less than 30 kpc and a radial velocity deviation of less than 50 km/s will be called "excellent". A galaxy will be designated "good", if it has a spatial deviation of less than 60 kpc and a radial velocity deviation of less than 100 km/s. A galaxy with a spatial deviation less than 120 kpc and a radial velocity deviation of less than 200 km/s will be called "moderate". All galaxies, which fit worse, will be designated "bad". Note that this categorisation is quite generous, especially concerning the radial velocity. The problems of fitting the radial velocity have already been discussed in subsection 6.2.1. There are 5 excellent galaxies in the best result of N4M (see table 6.3), which are: the Milky Way, M31, IC10, NGC185 and Carina. 5 galaxies fall into the category "good" and they are NGC205, M32, Leo II, Draco and Pegasus. There are also 15 moderate galaxies, which are: the LMC, the SMC, M33, NGC147, And I, LGS3, IC1613, And II, Fornax, Leo A, Leo I, GR8, Ursa Minor, NGC6822 and Aquarius. All other 16 galaxies fall into the category "bad". It is interesting, that all galaxies, which are in the categories "excellent" and "good", can also be fitted by the Sawa-Fujimoto model. All other galaxies except Sextans and Sculptor (only because of their totally wrong radial velocities, their positions would be excellent), which have been well fitted by Sawa and Fujimoto are categorised as "moderate". Despite the problems with the Magellanic Clouds, there are many similarities between the results of N4M and the Sawa-Fujimoto model. The initial distribution (see figures 6.18) of the N4M model is similar to the previous models. It shall be noted that the Small Magellanic Cloud starts very close to the Milky Way and the Large Magellanic Cloud significantly farther away. This is the reason, why the SMC merges and LMC not, though it is too close to our Galaxy after 12 Gigayears integration. The initial distance between the Milky Way and the Andromeda galaxy has been approximately 73 kpc and the time of the close encounter 12 Gigayears ago is in a close agreement with N4M. The orbital plane of the Milky Way and M31 is inclined by approximately 50° to the plane of the galaxy distribution (see figure 6.17).

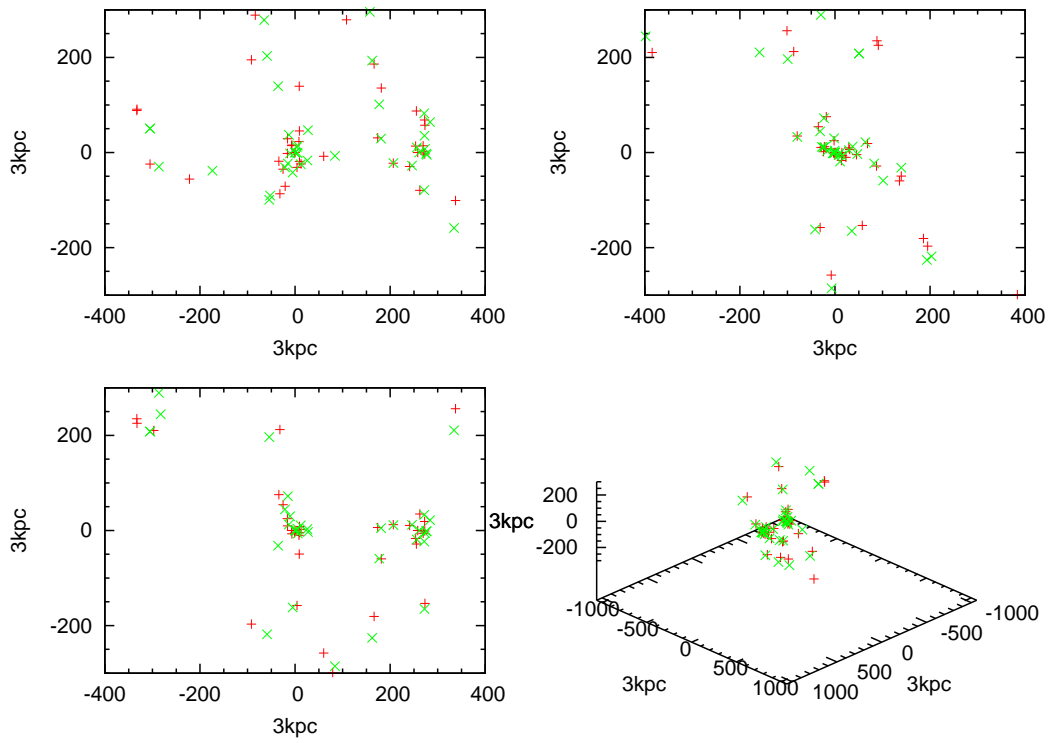


Figure 6.16: Same as figure 6.13, but for the best N4M result.

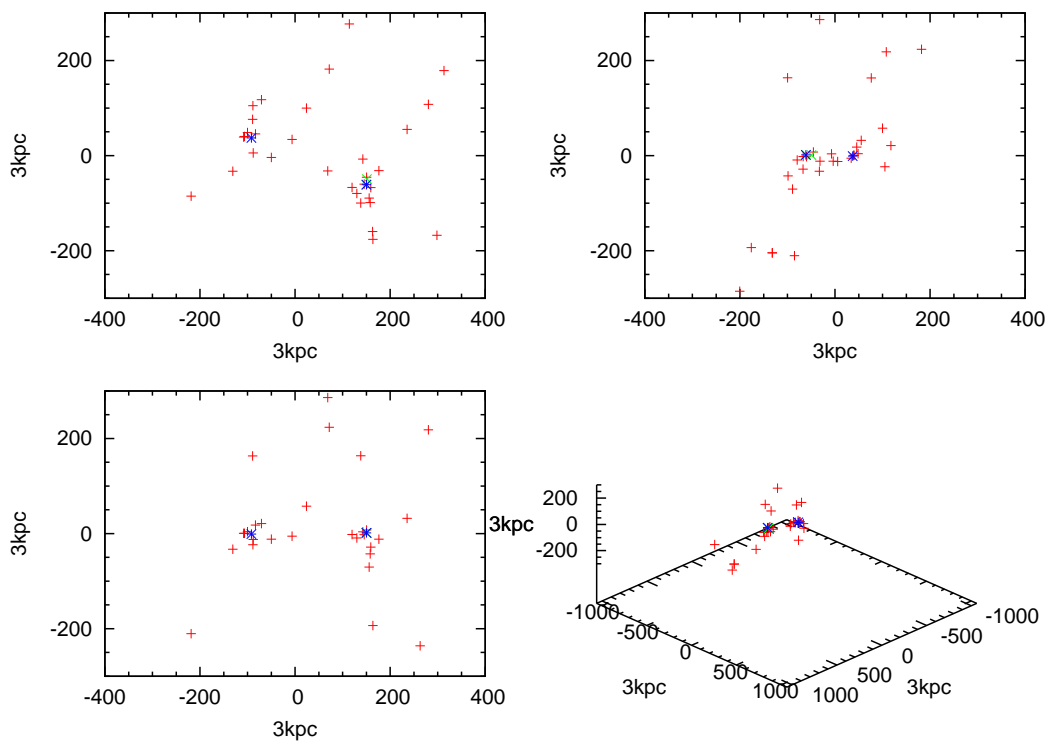


Figure 6.17: Same as figure 6.14, but for the best N4M result.

name of the galaxy	spatial deviation [kpc]	velocity deviation [km/s]
Milky Way	0	0
M31	9	47
LMC	34	187
SMC	56	176
M33	37	185
WLM	137	4
NGC55	181	84
IC10	28	5
NGC147	16	200
And III	13	208
NGC185	3	25
NGC205	13	78
M32	22	94
And I	24	150
Sculptor	29	220
LGS3	54	195
IC1613	105	23
And II	22	137
Phoenix	144	10
Fornax	54	108
UGCA92	221	68
Carina	28	6
Leo A	91	27
Sextans B	160	85
NGC3109	162	94
Antlia	156	51
Leo I	60	176
Sextans A	251	36
Sextans	22	275
Leo II	33	39
GR8	118	6
Ursa Minor	20	199
Draco	45	94
Sagittarius	32	494
SagDIG	162	55
NGC6822	43	109
Aquarius	109	24
IC5152	150	12
Tucana	121	80
UGCA438	161	91
Pegasus	75	30

Table 6.3: Deviation of the positions and radial velocities for the best N4M result.

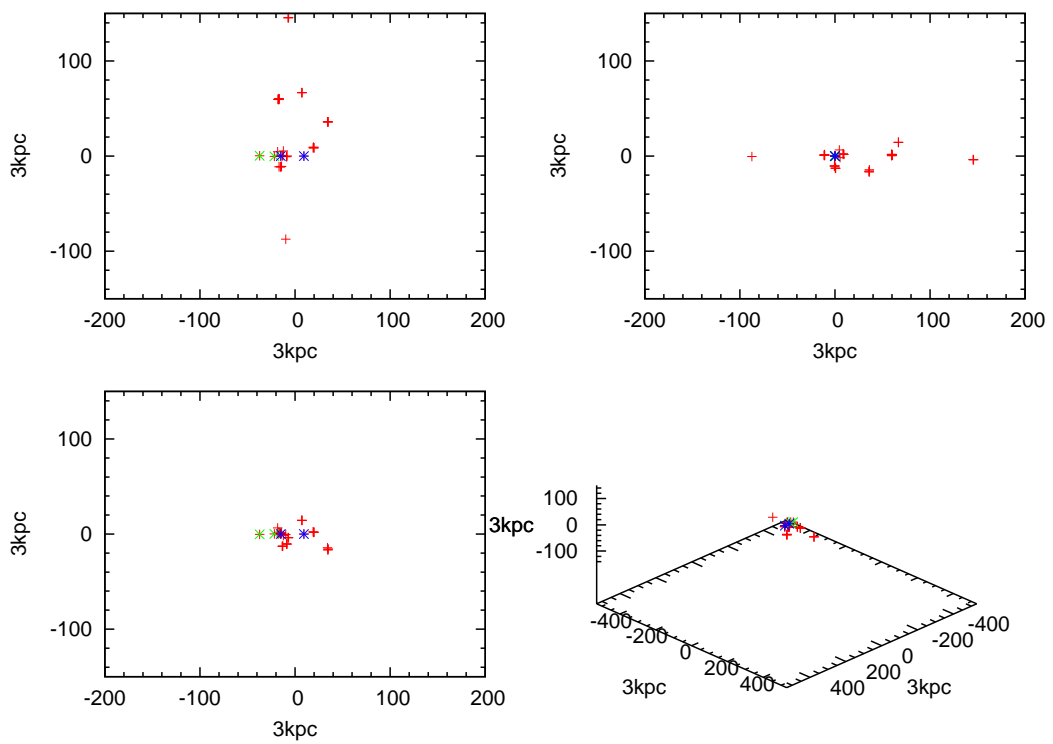


Figure 6.18: Same as figure 6.15, but for the best N4M result.

6.2.4 N2M

The simplest model with Newtonian gravity is N2M, where only the Milky Way and M31 are treated as massive particles with halos. With a value of only 30562 for the fitness function, this model shows the best of all models with Newtonian gravity, but one shall keep in mind that the statistic weights of massive galaxies are much larger than those of massless galaxies. Therefore a model with fewer massive galaxies has naturally a smaller value for the fitness function. Nevertheless the positions of most galaxies can be fitted very well (see figure 6.19). Again galaxies, which are located in the outer areas of the Local Group, like GR8, WLM, NGC55, UGCA438 and Aquarius, are fitted the worst (see table 6.4). The values of the other members of the Local Group are quite promising, even the SMC and M33 do not end up too deep in their host galaxies' potential. Though the LMC is not that lucky and merges with the Milky Way in the best N2M model. One can learn from the five best N2M results that at the encounter of the Milky Way and the Andromeda Galaxy, they have been separated by 50 to 60 kpc. The time, when this event happened, has been calculated to be about 12 Gyr or a little less ago. The initial distribution of the Local Group (see figure 6.21) at the time of the encounter is a compact agglomeration around the two main galaxies. In addition to that, there is also a tail reaching out 500 kpc in one direction and 200 kpc in the opposite direction. It is orientated normal to the connection vector of the Milky Way and M31, but in the orbital plane of both galaxies. Most (but not all) galaxies in these tails are members of the Local Group, which are located, nowadays, in the outer areas of our galaxy group. Even in this simple model, without the perturbation of other massive galaxies, one finds that the orbital plane of the Milky Way and M31 is inclined by a little more than 30° to the plane of the galaxy distribution (see figure 6.20).

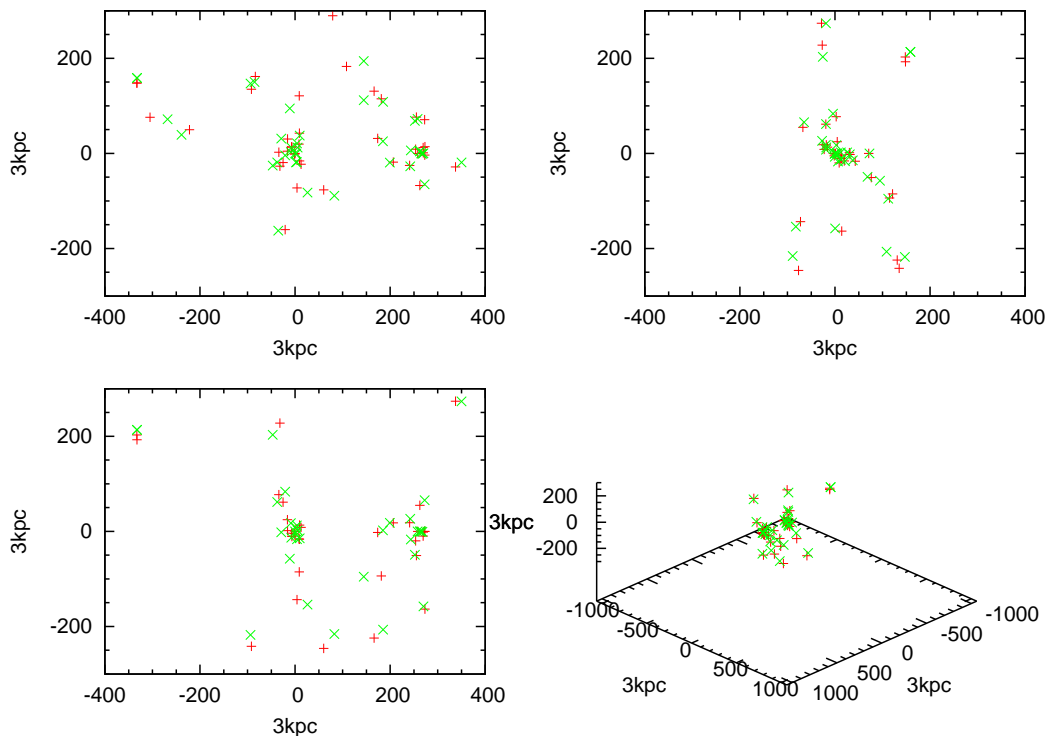


Figure 6.19: Same as figure 6.13, but for the best N2M result.

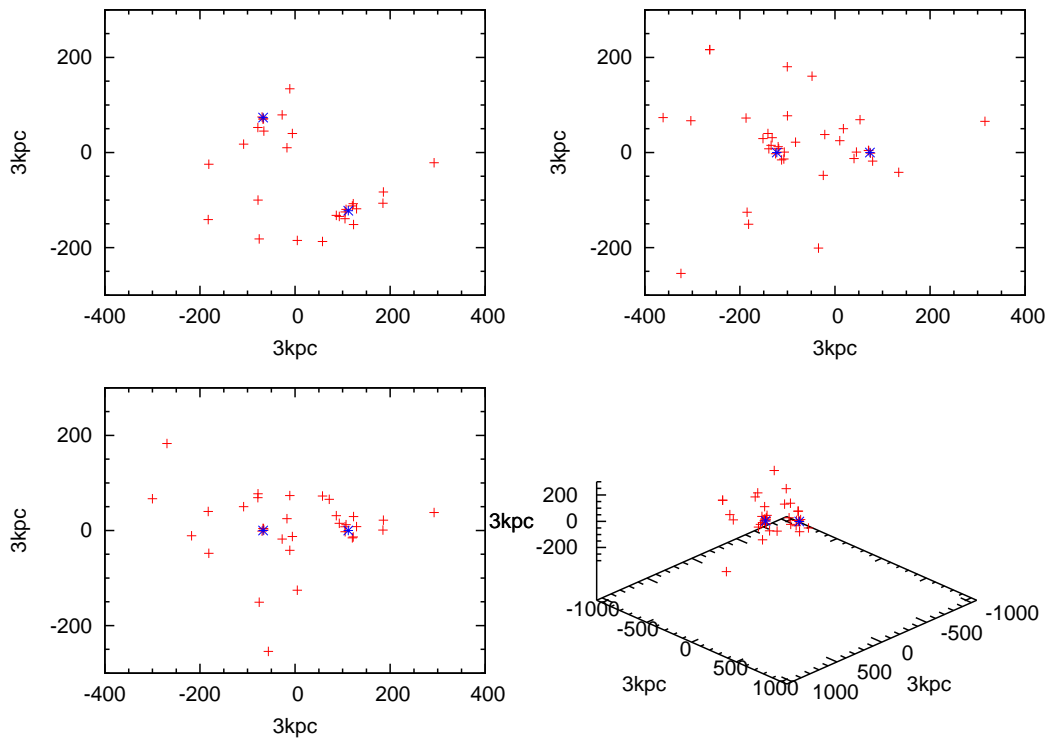


Figure 6.20: Same as figure 6.14, but for the best N2M result.

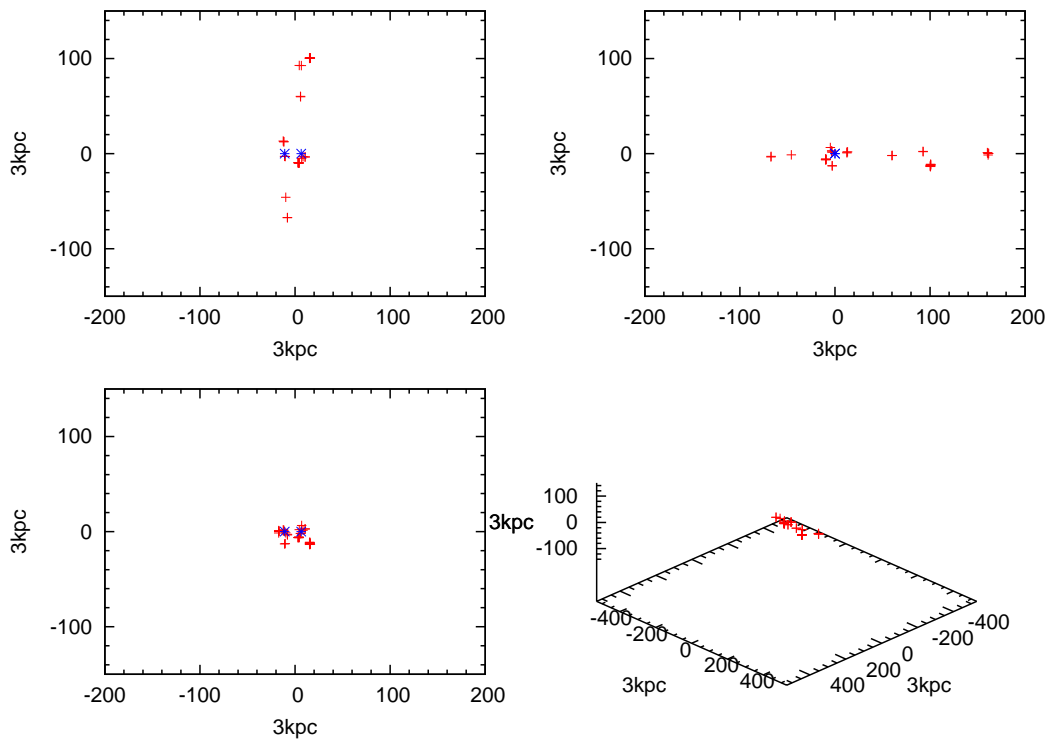


Figure 6.21: Same as figure 6.15, but for the best N2M result.

name of the galaxy	spatial deviation [kpc]	velocity deviation [km/s]
Milky Way	0	0
M31	22	52
M33	45	21
LMC	42	161
SMC	8	51
WLM	103	22
NGC55	130	11
IC10	45	236
NGC147	25	186
And III	33	72
NGC185	21	9
NGC205	18	3
M32	22	91
And I	43	175
Sculptor	14	178
LGS3	26	23
IC1613	111	216
And II	41	125
Phoenix	130	127
Fornax	17	122
UGCA92	47	100
Carina	41	94
Leo A	87	42
Sextans B	74	87
NGC3109	45	43
Antlia	69	0
Leo I	49	159
Sextans A	112	81
Sextans	31	182
Leo II	37	70
GR8	181	54
Ursa Minor	19	112
Draco	35	259
Sagittarius	13	197
SagDIG	61	63
NGC6822	79	15
Aquarius	119	7
IC5152	41	39
Tucana	81	13
UGCA438	114	49
Pegasus	46	6

Table 6.4: Deviation of the positions and radial velocities for the best N2M result.

6.2.5 NBH

The best results of NBH are very similar to the results of NM. The fitness function of the best NBH halo has a final value of 640314. This model only has very few galaxies, which are fitted badly (see table 6.5), like NGC55, GR8, SagDIG UGCA92, Leo A and UGCA438. NBH also faces the problem that both Magellanic Clouds merge with their host galaxy and that M33, although it is near M31, is by far not at the correct relative position. One can see that most features of the general structure of the Local Group can be reproduced qualitatively (see figure 6.22). The initial distribution (see figure 6.24) shows the same features like the previous models, but with an important difference. M33 is located a little outside the central agglomeration approximately 90 kpc away from the Andromeda Galaxy. The close encounter of the Milky Way and M31 has taken place at a distance of only 37 kpc a little more than 12 Gyr ago in the best result of the NBH model. The orbital plane of the Milky Way and M31 is inclined by slightly more than 45° to the plane of the galaxy distribution (see figure 6.23).

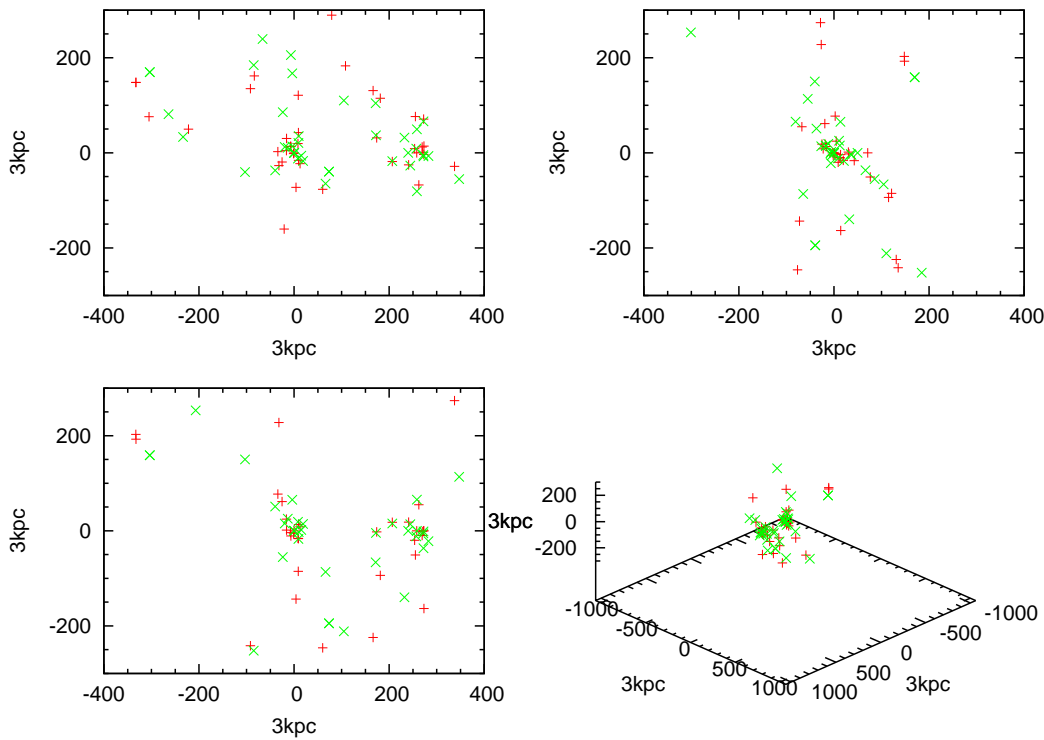


Figure 6.22: Same as figure 6.13, but for the best NBH result.

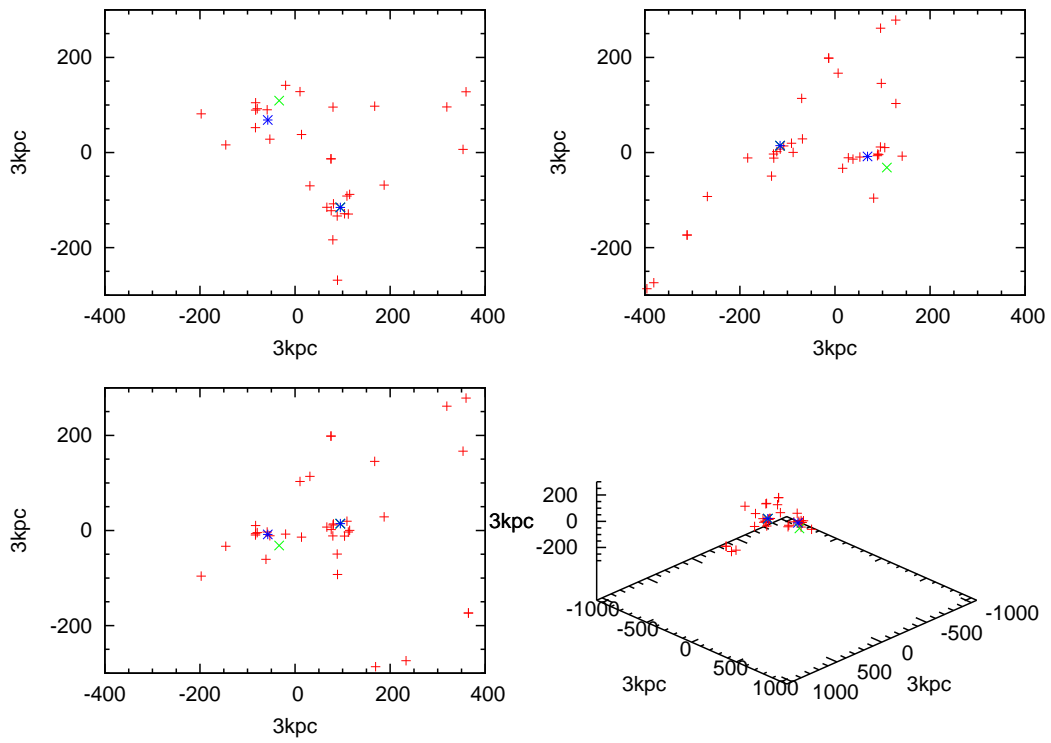


Figure 6.23: Same as figure 6.14, but for the best NBH result.

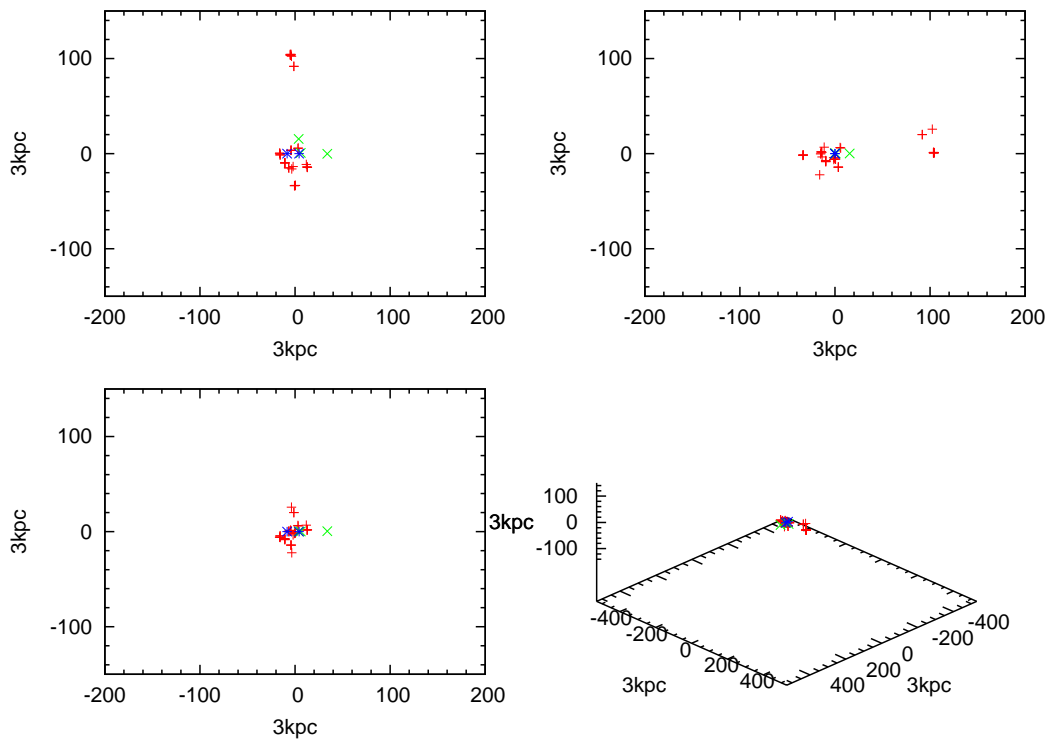


Figure 6.24: Same as figure 6.15, but for the best NBH result.

name of the galaxy	spatial deviation [kpc]	velocity deviation [km/s]
Milky Way	0	0
M31	54	19
M33	78	113
LMC	49	252
SMC	56	115
WLM	198	6
NGC55	360	45
IC10	52	69
NGC147	17	133
And III	27	58
NGC185	8	211
NGC205	14	4
M32	22	115
And I	79	109
Sculptor	6	127
LGS3	73	20
IC1613	93	108
And II	18	182
Phoenix	170	152
Fornax	48	10
UGCA92	488	195
Carina	70	56
Leo A	319	36
Sextans B	142	58
NGC3109	172	67
Antlia	148	24
Leo I	104	253
Sextans A	203	47
Sextans	19	71
Leo II	75	71
GR8	316	78
Ursa Minor	21	168
Draco	31	160
Sagittarius	55	306
SagDIG	579	142
NGC6822	254	274
Aquarius	195	83
IC5152	269	32
Tucana	153	19
UGCA438	348	12
Pegasus	152	112

Table 6.5: Deviation of the positions and radial velocities for the best NBH result.

6.2.6 NSH

The model NSH has with 1218751 the highest, and therefore worst value, for its fitness function. The main reason for this is, that M33 merges completely with the Andromeda Galaxy. The LMC and the SMC share the same fate with respect to the Milky Way. Furthermore, there are also some extremely bad fitted galaxies like Leo I and Leo II (see table 6.6). One may notice that in this model most galaxies have a large spatial deviation, especially outside the relatively compact Andromeda- and Milky Way-subgroups. NSH does not fit the Local Group very well (see figure 6.25). Since the masses of the halos are the same as in all other models with Newtonian gravity, their small radii make them denser. Therefore the dynamical friction becomes to strong and causes significant problems for this model. Another interesting feature of NSH is that initial distribution does hardly show any tail-like structure (see figure 6.27). It is a more loosely agglomeration with less striking features compared to the other Newtonian models. Furthermore, the initial distance between our Galaxy and M31 is with approximately 100 kpc, greater than in all other models which are using Newtonian gravity. The time, which has passed since the close encounter, is a little more than 12 Gigayears in the NSH model. In contrast to the previous models, the orbital plane of the Milky Way and M31 is inclined by less than 20° to the plane of the galaxy distribution (see figure 6.26).

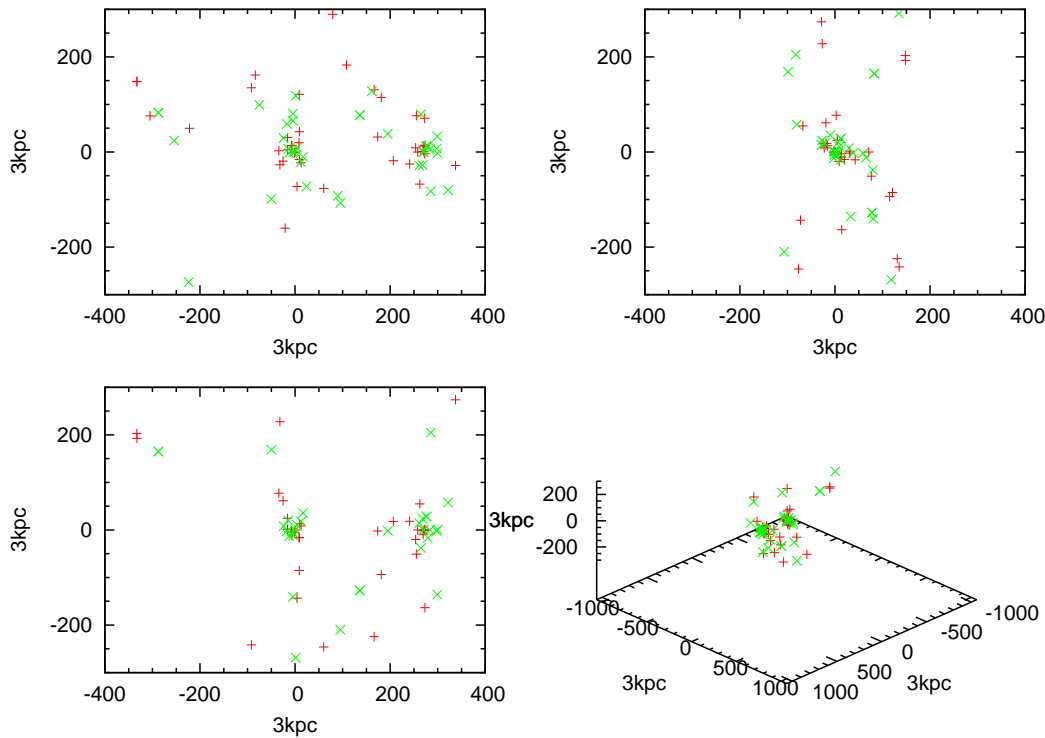


Figure 6.25: Same as figure 6.13, but for the best NSH result.

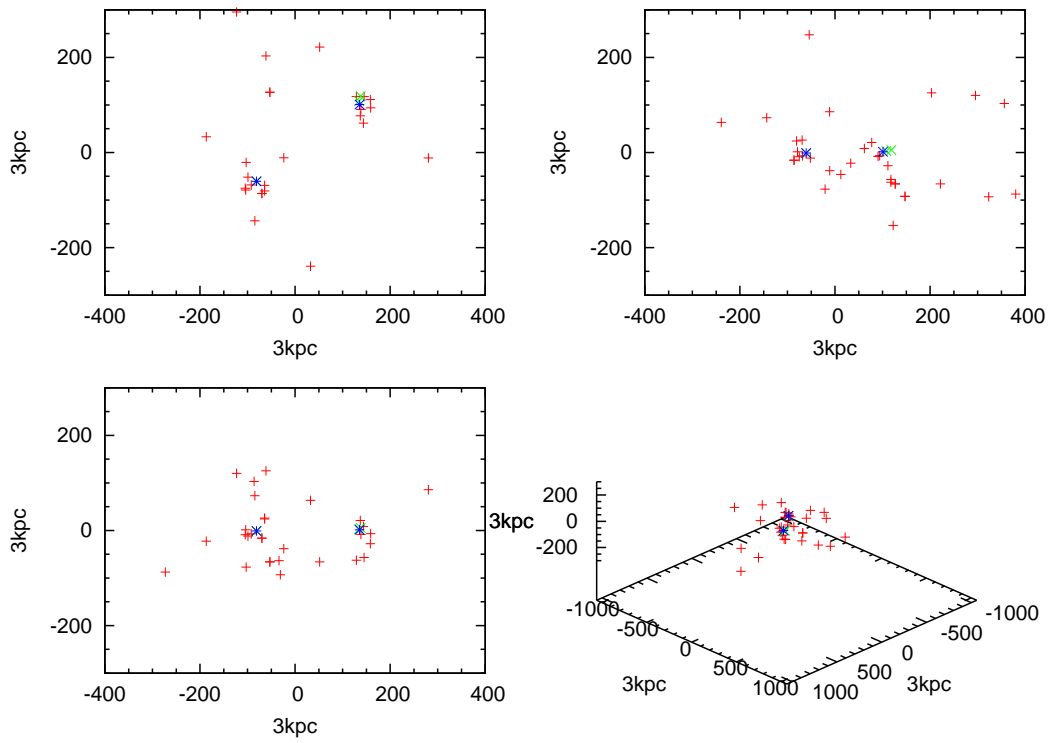


Figure 6.26: Same as figure 6.14, but for the best NSH result.

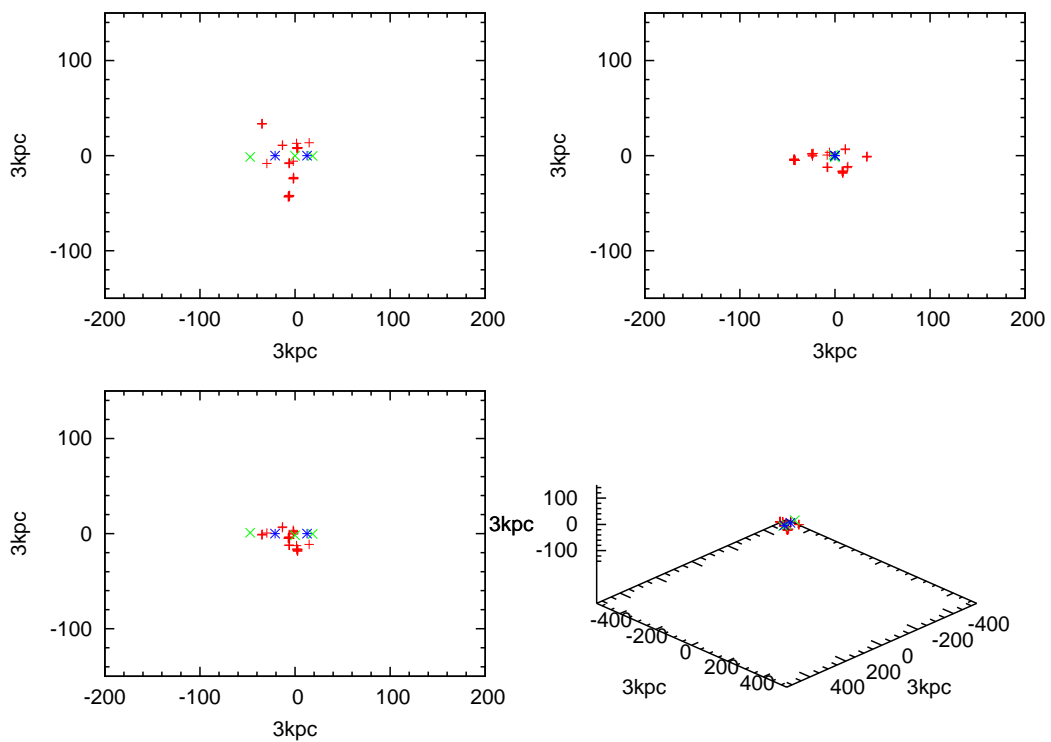


Figure 6.27: Same as figure 6.15, but for the best NSH result.

name of the galaxy	spatial deviation [kpc]	velocity deviation [km/s]
Milky Way	0	0
M31	37	87
M33	213	186
LMC	58	300
SMC	45	216
WLM	343	51
NGC55	481	5
IC10	182	54
NGC147	84	96
And III	78	417
NGC185	167	428
NGC205	79	24
M32	44	215
And I	90	18
Sculptor	146	23
LGS3	48	217
IC1613	202	162
And II	67	11
Phoenix	210	104
Fornax	80	15
UGCA92	307	125
Carina	32	42
Leo A	285	10
Sextans B	280	53
NGC3109	264	113
Antlia	253	70
Leo I	944	268
Sextans A	417	7
Sextans	15	244
Leo II	916	58
GR8	268	66
Ursa Minor	72	250
Draco	30	162
Sagittarius	60	91
SagDIG	313	12
NGC6822	354	145
Aquarius	242	20
IC5152	403	56
Tucana	295	130
UGCA438	320	97
Pegasus	126	109

Table 6.6: Deviation of the positions and radial velocities for the best NSH result.

6.2.7 MM

In general the fitness functions of all MONDian models are better (lower) than the fitness functions of their corresponding Newtonian models. In the case of MM, the fitness function has a value of 366189, which is about 35% less than the value of NM. This is due the fact, that the positions of nearly all of the galaxies can be fitted very well (see figure 6.28). But there is also a big problem: the radial velocities (see table 6.7) are fitted extremely poorly in the MM model, because all galaxies are moving significantly too fast in MOND. Though one shall keep in mind, that the fitting of radial velocities has always been a problem in this genetic algorithm, because the statistic weights of the radial velocities have been set to too small values. An interesting feature of the final distribution of the Local Group's galaxies in this model, is that both Magellanic Clouds get extremely close to the Milky Way (perigalacticum of 15 kpc) and orbit their host galaxy on a highly eccentric orbit (apogalacticum of 130 kpc (LMC) and of 105 kpc (SMC)). The first close encounter of our Galaxy and M31 has taken place at a distance of 90 kpc approximately 12 Gyr ago in MM. In this model there is also a second encounter of both galaxies, which has happened two Gigayears ago. At this time the two galaxies have been separated by 75 kpc. It shall be noted, that despite giving a reasonable distance of the Andromeda galaxy from the Milky Way, M31 is not approaching our Galaxy in this model, but it is departing with a velocity of about 350 km/s. This is a big contrast to the observations and to the Newtonian models, where the two galaxies have always been approaching at the end of the integration, though maybe not exactly with the correct velocity. The initial distribution of the Local Group's galaxies is surprisingly similar to the one of most Newtonian models. It shows an agglomeration around the two most massive galaxies and the already well known tail-like structure (see figure 6.30). Furthermore one may notice that there is an angle of roughly 30° between the orbital plane of the Milky Way and M31 and the plane of the galaxy distribution (see figure 6.29).

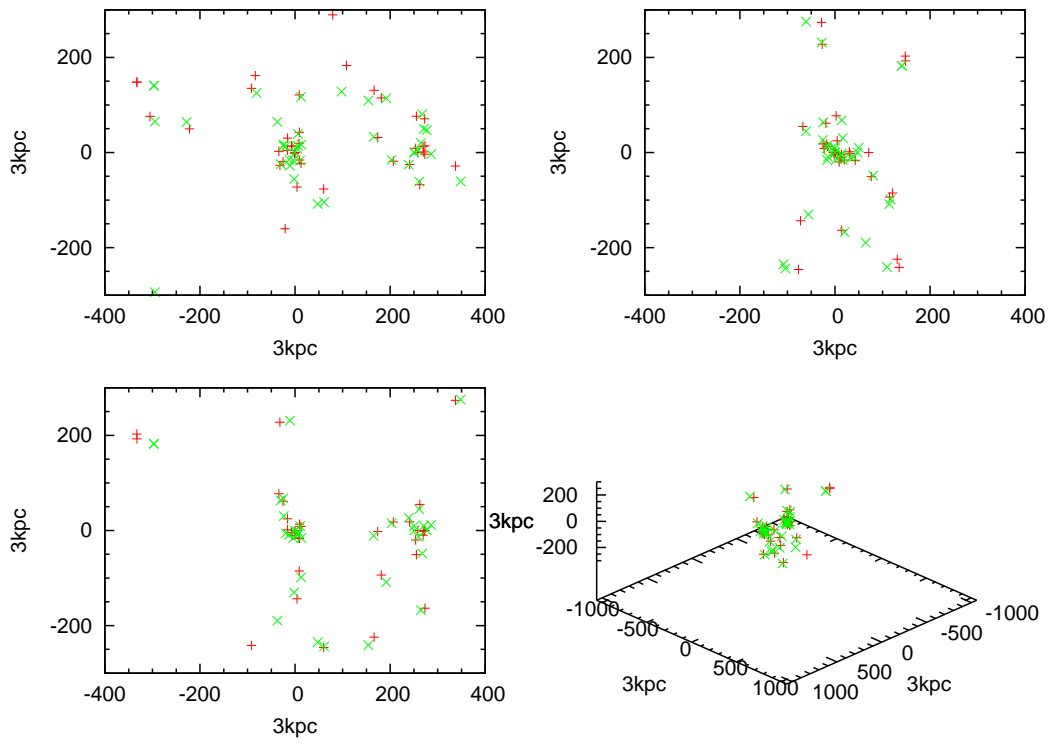


Figure 6.28: Same as figure 6.13, but for the best MM result.

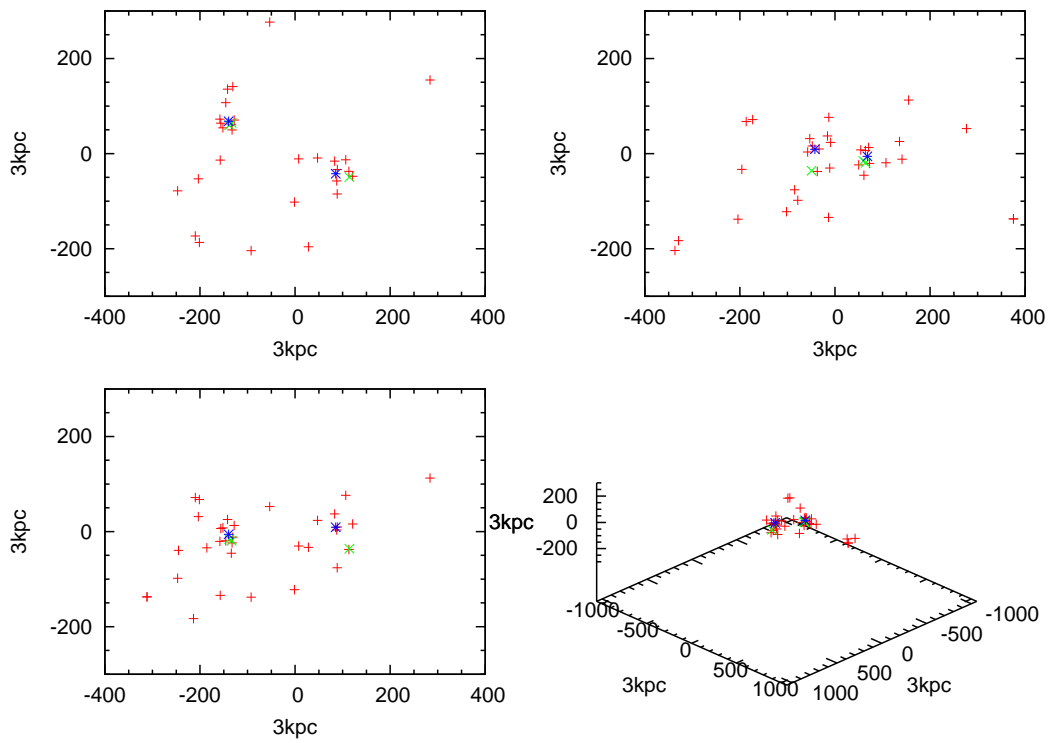


Figure 6.29: Same as figure 6.14, but for the best MM result.

name of the galaxy	spatial deviation [kpc]	velocity deviation [km/s]
Milky Way	0	0
M31	20	462
M33	73	337
LMC	41	73
SMC	35	268
WLM	89	201
NGC55	259	221
IC10	36	498
NGC147	26	197
And III	161	576
NGC185	15	361
NGC205	52	715
M32	66	368
And I	39	664
Sculptor	18	3
LGS3	40	567
IC1613	54	394
And II	36	309
Phoenix	42	198
Fornax	26	56
UGCA92	102	93
Carina	58	314
Leo A	64	247
Sextans B	115	392
NGC3109	127	521
Antlia	114	478
Leo I	54	313
Sextans A	57	402
Sextans	45	342
Leo II	22	159
GR8	73	396
Ursa Minor	12	135
Draco	90	287
Sagittarius	53	169
SagDIG	345	65
NGC6822	66	124
Aquarius	84	142
IC5152	116	311
Tucana	310	59
UGCA438	185	275
Pegasus	33	302

Table 6.7: Deviation of the positions and radial velocities for the best MM result.

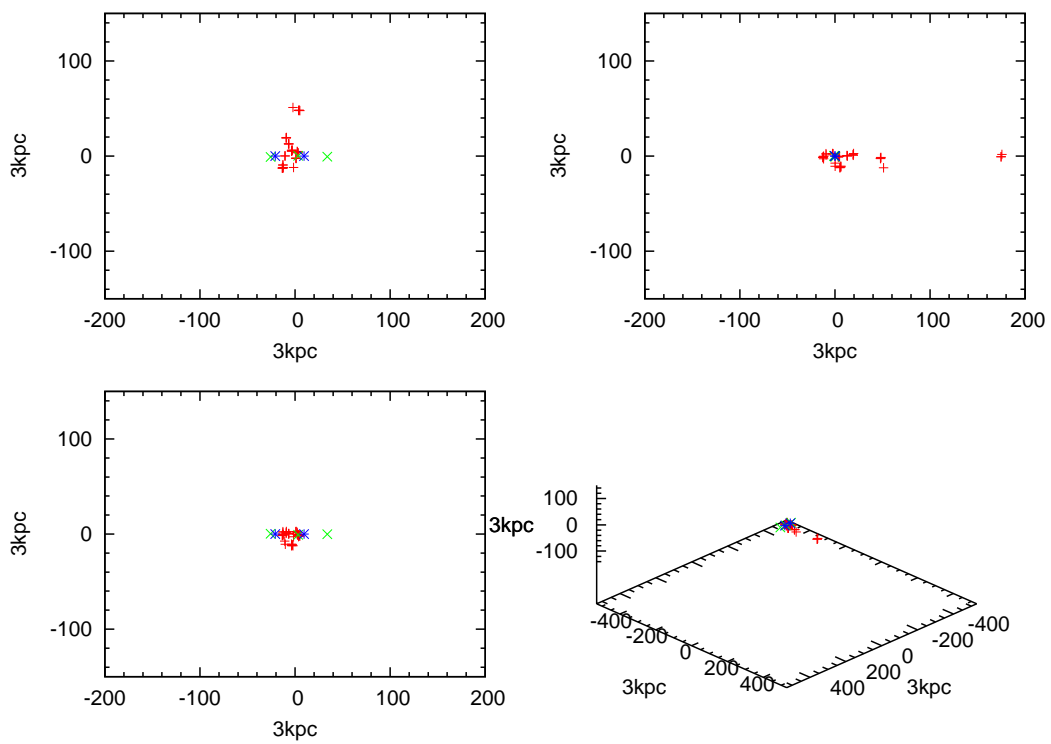


Figure 6.30: Same as figure 6.15, but for the best MM result.

6.2.8 MN

The value of the fitness function of the best MN result is 233898. This value is 64% less than the one of NN and even better than the value of MM, though MN has more galaxies to fit. MN can reproduce the spatial distribution (see figure 6.28) of the Local Group's members very well, but again at the high cost of a poor fitting of the radial velocities (see table 6.8), though it is partly a little better than in MM. The problem that the Andromeda galaxy is departing from the Milky Way also remains. The distance between M31 and Milky Way has been 80 kpc 12 Gyr ago. But the closed encounter has been about 150 Myrs early at an extremely short distance. There has been also a second encounter of both galaxies 1.8 Gyr ago, where the Milky Way and the Andromeda Galaxy have been separated by only 12 kpc. The initial distribution of the Local Group's galaxies is an agglomeration with a diameter of about 200 kpc. In contrast to most previous model, there are no peculiar features, except that a small group of six galaxies (And I, Sextans B, NGC3109, Antlia, Sextans A and GR8) is located 600 kpc outside the centre outside the main agglomeration (see figures 6.30). The orbital plane of the Milky Way and M31 is inclined by approximately 50° to the plane of the galaxy distribution (see figure 6.32).

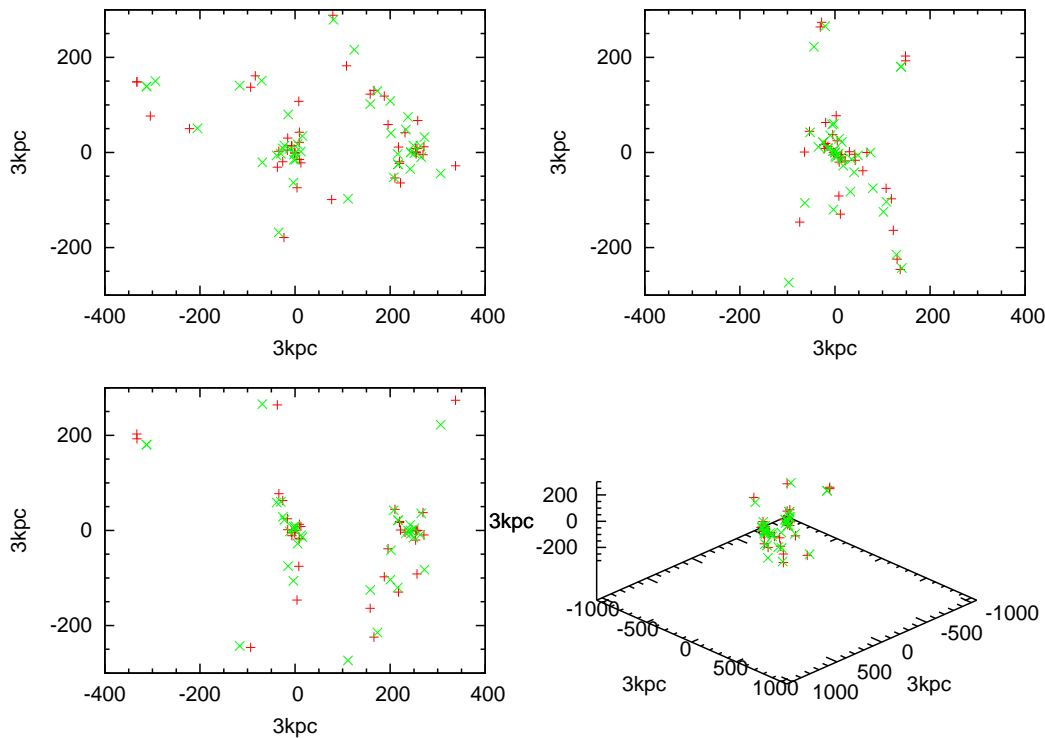


Figure 6.31: Same as figure 6.13, but for the best MN result.

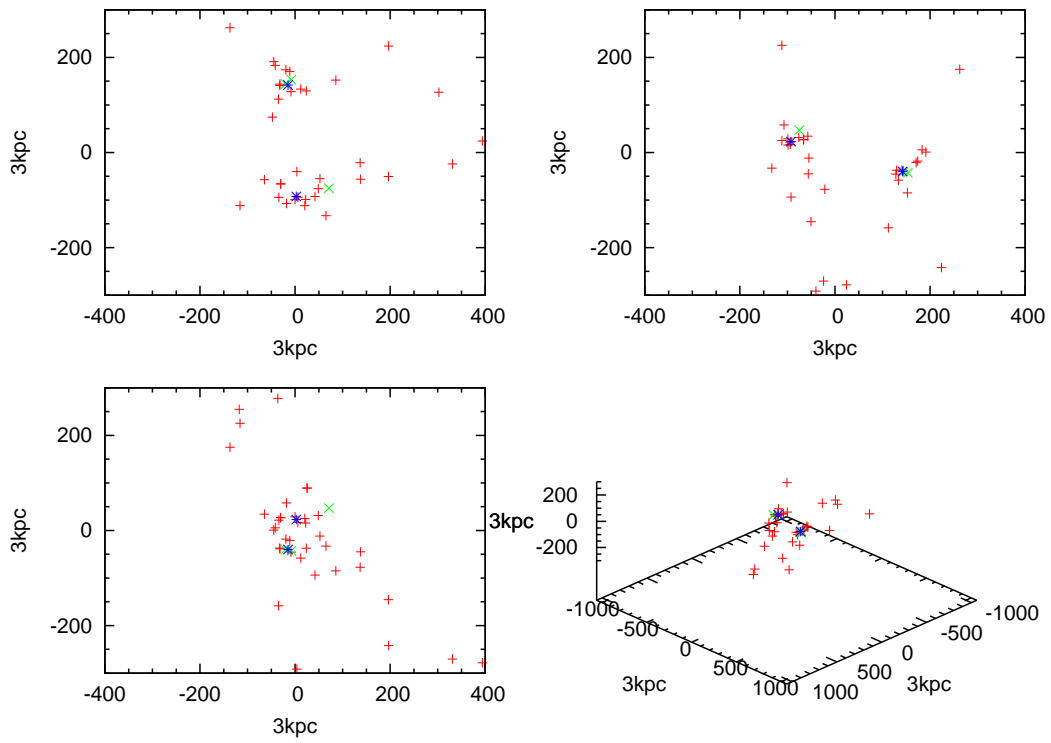


Figure 6.32: Same as figure 6.14, but for the best MN result.

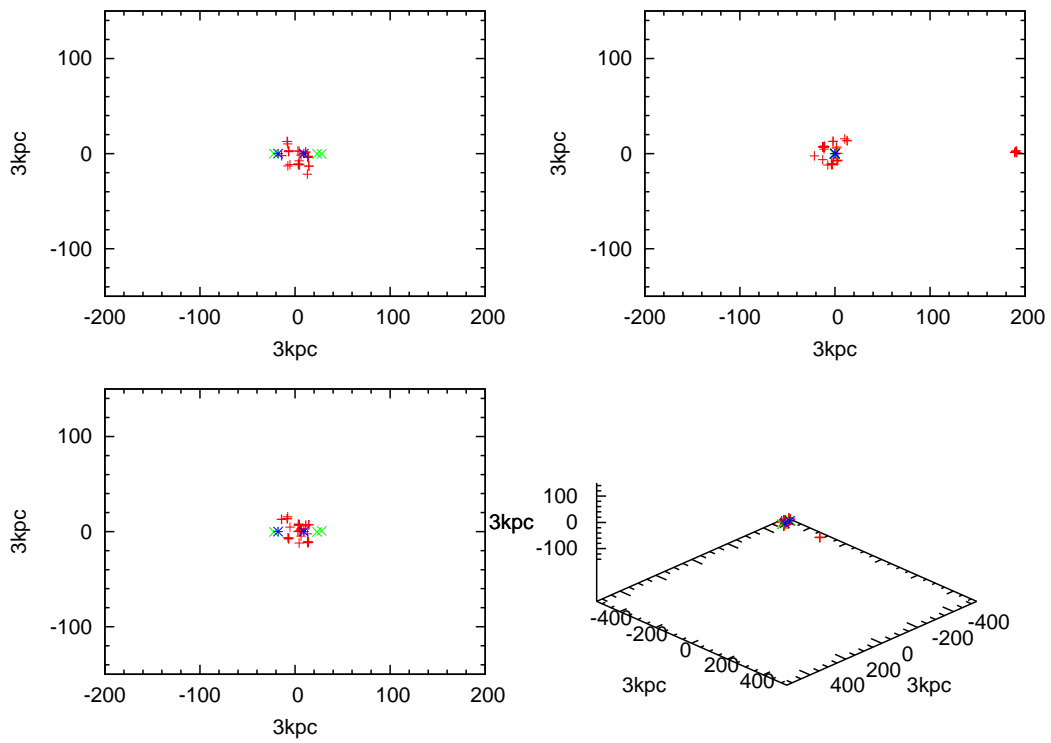


Figure 6.33: Same as figure 6.15, but for the best MN result.

name of the galaxy	spatial deviation [kpc]	velocity deviation [km/s]
Milky Way	0	0
M31	34	400
M33	65	331
LMC	61	423
SMC	35	24
WLM	36	172
NGC55	29	271
IC10	10	335
NGC147	18	4
And III	27	580
NGC185	19	3
NGC205	18	795
M32	38	239
And I	23	162
Sculptor	34	172
LGS3	59	472
IC1613	52	410
And II	22	381
Phoenix	107	326
Fornax	31	30
UGCA92	187	321
Carina	80	210
Leo A	100	261
Sextans B	82	416
NGC3109	96	517
Antlia	77	475
Leo I	55	510
Sextans A	228	387
Sextans	33	24
Leo II	57	279
GR8	106	357
Ursa Minor	38	173
Draco	40	234
Sagittarius	44	343
SagDIG	50	247
NGC6822	127	26
Aquarius	163	239
IC5152	51	267
Tucana	70	353
UGCA438	119	251
Pegasus	52	345
Cetus	132	305
And V	19	797
Cassiopeia	112	116
Pegasus II	91	335

Table 6.8: Deviation of the positions and radial velocities for the best MN result.

6.2.9 M4M

With a value for the fitness function of 169550 the best result, M4M fits the Local Group only 1% better than the comparable Newtonian model N4M. The positions of most Local Group galaxies can be reproduced quite well in M4M (see figure 6.34), but the radial velocities (see table 6.9) can be fitted comparably well too, for a MONDian model with respect to all the problems, that have already been discussed. Even the radial velocity of the Andromeda Galaxy is correct, as well as its distance from the Milky Way. Like in all other MONDian models M31 is on its second orbit. It has had a close encounter about 12.1 Gyr ago, a distance of 71 kpc has been reached 12 Gyr ago. 4.5 Gyr ago M31 is separated by 57 kpc from the Milky Way in its second perigalacticum. Furthermore the Andromeda Galaxy has passed two apogalactica at 834 kpc about 8.7 Gyr ago and at 833 kpc 775 Myr ago. When taking a look on the initial distribution of galaxies (see figure 6.36), one notices that there are two small subgroups outside the central agglomeration. Both subgroups are located in the orbital plane of the Milky Way and M31 and have a distance of 400 to 450 kpc from the Local Group's centre of mass. One of these subgroups contains M33, LGS3, IC1613, GR8, Ursa Minor, NGC6822, Aquarius and Tucana, while the other consists of IC5152, UGCA438, NGC185, WLM and NGC55. This is interesting because most of these do not belong to the Milky Way or M31 subgroups, but form their own groups or are today located in the outermost areas of the Local Group. The central agglomeration has the neck of the tail structure, which has been found in many of the previous models. When taking a look at figure 6.35, one may notice that the orbital plane of the Milky Way and M31 is inclined by a little less than 40° to the plane of the galaxy distribution.

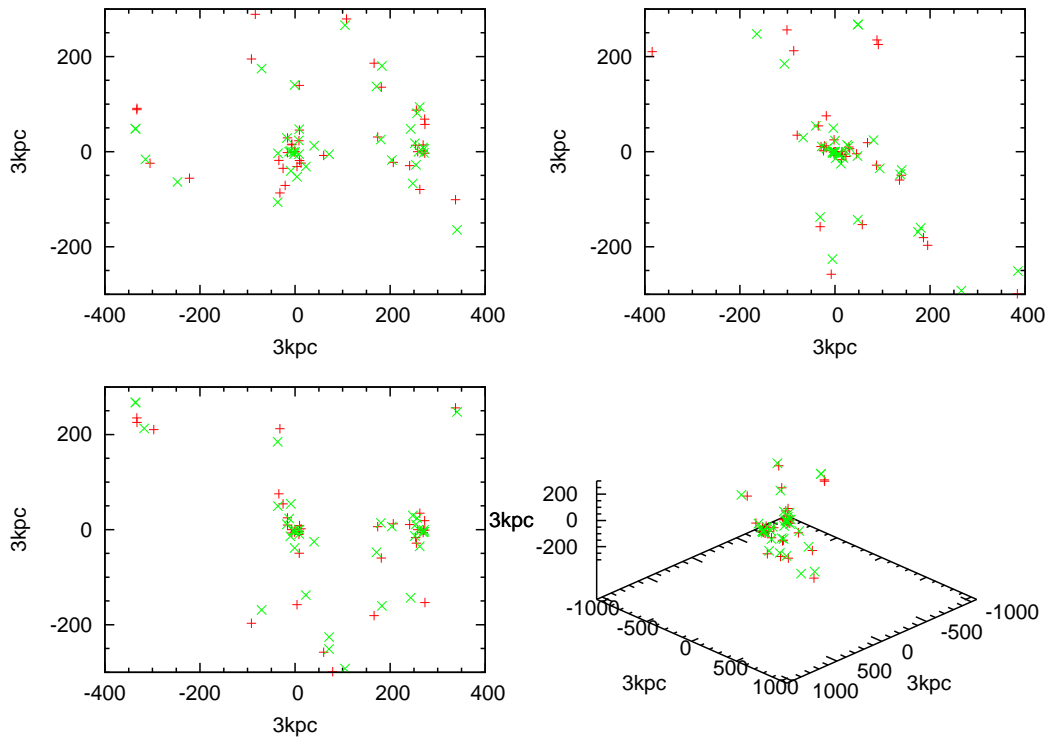


Figure 6.34: Same as figure 6.13, but for the best M4M result.

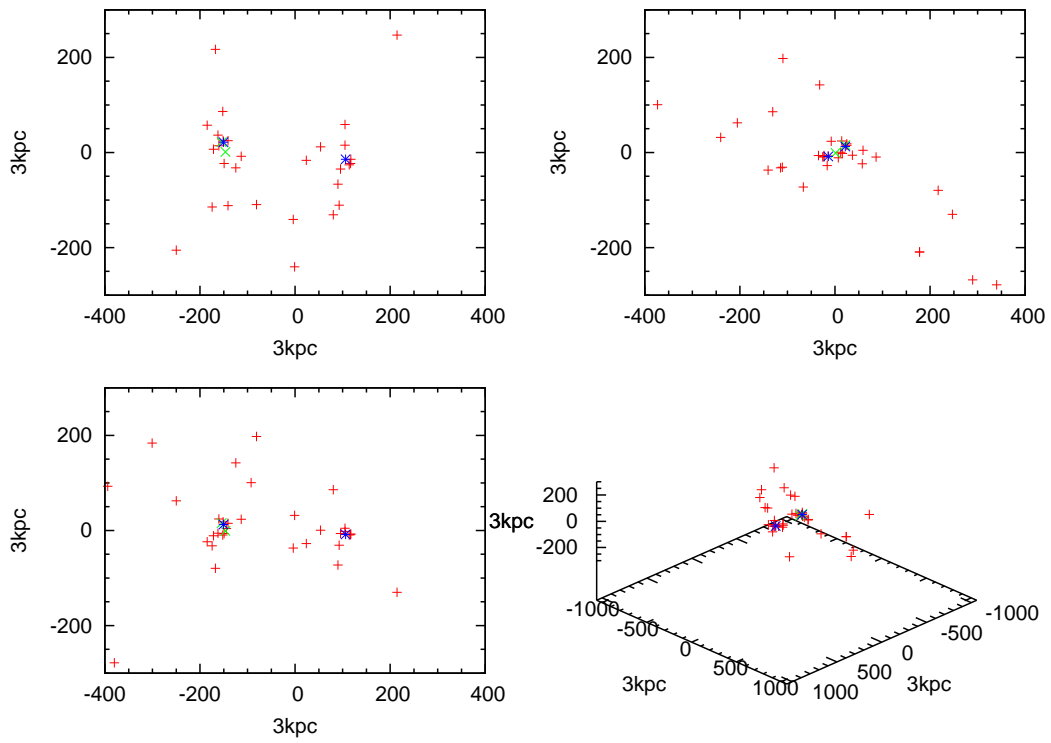


Figure 6.35: Same as figure 6.14, but for the best M4M result.

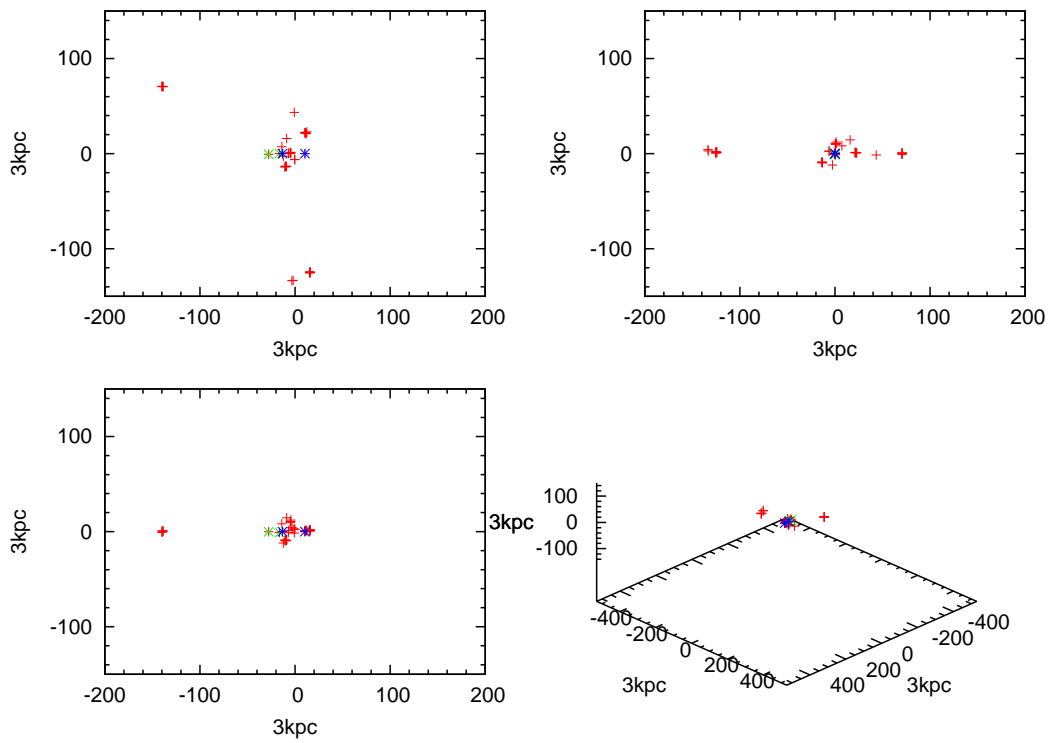


Figure 6.36: Same as figure 6.15, but for the best M4M result.

name of the galaxy	spatial deviation [kpc]	velocity deviation [km/s]
Milky Way	0	0
M31	6	2
LMC	53	385
SMC	52	159
M33	62	170
WLM	81	147
NGC55	145	245
IC10	60	94
NGC147	40	175
And III	17	143
NGC185	23	267
NGC205	6	91
M32	17	87
And I	17	196
Sculptor	89	264
LGS3	34	108
IC1613	47	230
And II	35	16
Phoenix	44	79
Fornax	15	6
UGCA92	193	115
Carina	6	12
Leo A	102	129
Sextans B	119	238
NGC3109	155	289
Antlia	181	246
Leo I	89	319
Sextans A	44	219
Sextans	13	215
Leo II	52	199
GR8	125	162
Ursa Minor	166	0
Draco	113	280
Sagittarius	17	211
SagDIG	120	205
NGC6822	83	142
Aquarius	101	198
IC5152	124	174
Tucana	122	102
UGCA438	96	253
Pegasus	99	253

Table 6.9: Deviation of the positions and radial velocities for the best M4M result.

6.2.10 M2M

The best result of the model M2M has a value for the fitness function of 22686. This is the smallest value of all fitness functions and it is 26% less than the value of the corresponding Newtonian model N2M. One might say that this is the best model, but there is a snag. Like in MM and MN, the Andromeda galaxy is departing from the Milky Way. Furthermore there are two close encounters of the two dominant galaxies: one a little less than 12 Gyr ago at a distance of 40 kpc and another one 2.5 Gyr ago at approximately the same distance. M31 has reached its apogalacticum at 960 kpc 7.4 Gyr ago. One can see that the positions of almost all galaxies can be fitted extremely well by M2M (see figure 6.37). The radial velocities are fitted poorly (see table 6.10) like in all MONDian models. The initial distribution consists of a group around the two main galaxies and two tails. Both are extending in the orbital plane of the Milky Way and M31, normal to their connection vector. They reach out up to 600 kpc in opposite directions (see figure 6.39). This is the only model, where there is (almost) no inclination between the orbital plane of the two dominant galaxies and the planar distribution of galaxies in the Local Group (see figure 6.38).

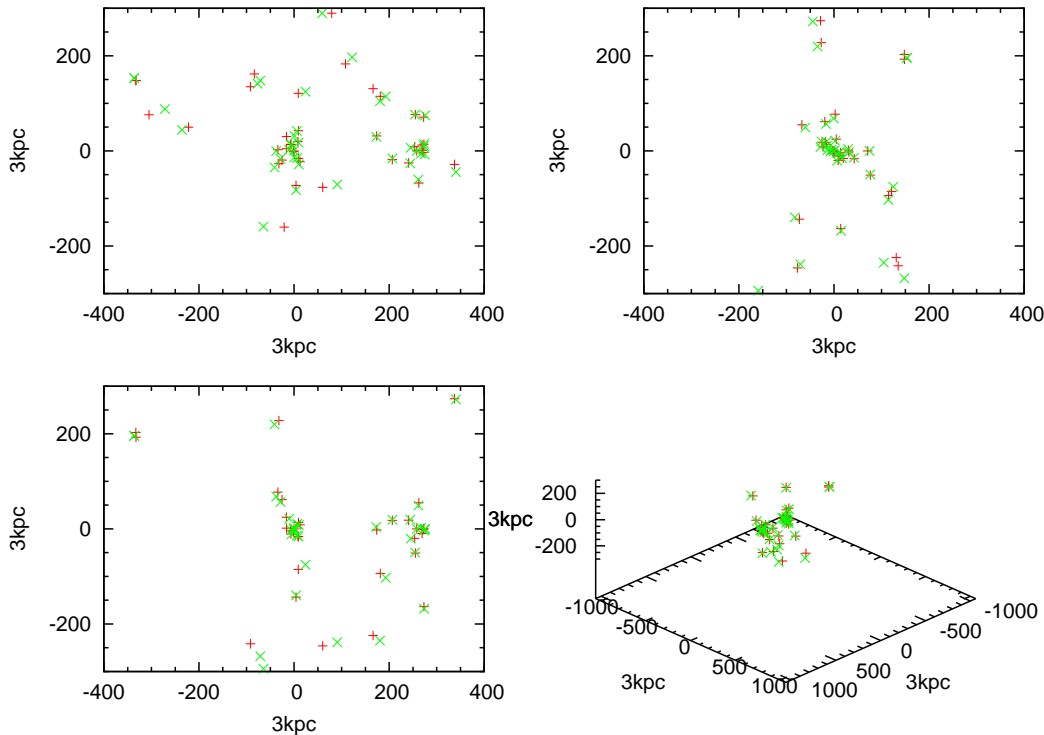


Figure 6.37: Same as figure 6.13, but for the best M2M result.

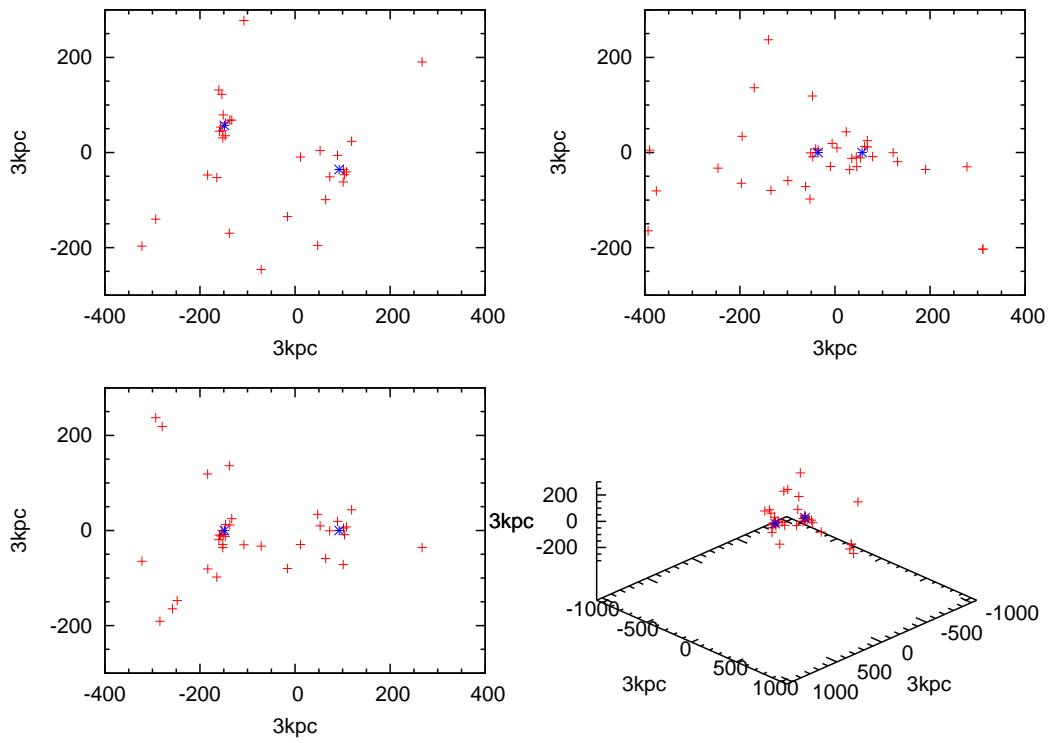


Figure 6.38: Same as figure 6.14, but for the best M2M result

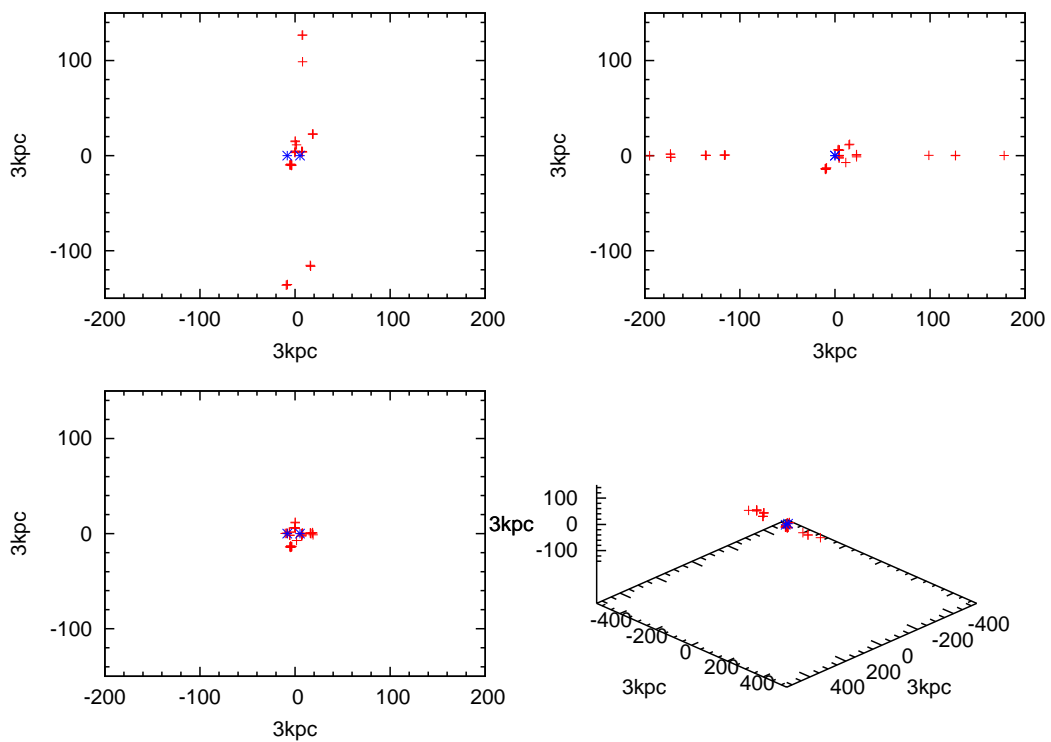


Figure 6.39: Same as figure 6.15, but for the best M2M result

name of the galaxy	spatial deviation [kpc]	velocity deviation [km/s]
Milky Way	0	0
M31	1	276
M33	14	389
LMC	7	103
SMC	5	159
WLM	95	87
NGC55	60	195
IC10	27	299
NGC147	12	66
And III	25	480
NGC185	9	160
NGC205	15	164
M32	25	65
And I	22	466
Sculptor	7	63
LGS3	4	360
IC1613	44	339
And II	20	75
Phoenix	55	32
Fornax	12	93
UGCA92	49	159
Carina	51	57
Leo A	44	327
Sextans B	80	256
NGC3109	29	312
Antlia	20	269
Leo I	31	141
Sextans A	108	253
Sextans	21	244
Leo II	19	47
GR8	37	253
Ursa Minor	12	68
Draco	19	189
Sagittarius	42	56
SagDIG	141	155
NGC6822	32	38
Aquarius	96	190
IC5152	70	188
Tucana	107	249
UGCA438	65	194
Pegasus	14	186

Table 6.10: Deviation of the positions and radial velocities for the best M2M result.

6.2.11 MH

In the MH model other masses for the Milky Way and the Andromeda galaxy are used, compared to the other MONDian models. The value of the fitness function of the best MH result is with 313457 better than the one of MM, which is (save the different masses) identical to MH. An advantage of MH is that the Andromeda galaxy is approaching the Milky Way in contrast to most other MONDian models. Already the simple two body simulations in subsection 5.3.3 have shown that it is easier to reproduce the dynamics of the main galaxies with the masses of the MH model. Like in all other MONDian models, M31 is already on its second orbit. The assumed time of the first encounter has been confirmed to be very close to 12 Gyr ago. The Milky Way and M31 have been separated by 77 kpc at this time. Around 8.7 Gyr ago the Andromeda Galaxy has reached its first apogalacticum at 995 kpc and it has passed through its second perigalacticum at 103 kpc 4.3 Gyr ago. M31 has reached its last apogalacticum at 845 kpc only 775 Myr ago and it is now slowly approaching the Milky Way again. Although this model yields an acceptable orbit for the Andromeda Galaxy, it does not fit the other massive galaxies well, though it does reproduce the positions of many massless (in the model) galaxies comparably well (see figure 6.40). There are problems with galaxies which are located at the outer areas of our galaxy group though, like in many other models. MH also faces the problem of getting reasonable values for the radial velocities and it performs poorly (see table 6.11) in this aspect like all other MONDian models. The initial distribution of the Local Group members (see figure 6.42) shows some very interesting features. The central agglomeration around the two main galaxies has three short (100 - 200 kpc) tails. Two of them are in the orbital plane of the Milky Way and the Andromeda galaxy, one of them extends normal to the connection vector of the two dominate galaxies and the other one is located in the elongation of this vector and contains the Triangulum Nebula. The third tail is orthogonal to the orbital plane and its base is near the Local Group's centre of mass. The galaxies at the end of this tail are IC10, And II, Leo A, Sextans B, Leo I, Sextans A, UGCA438 and Pegasus, but surprisingly those galaxies have nothing in common except being a member of the Local Group. An interesting feature of the MH model is that one finds that the orbital plane of the Milky Way and the Andromeda Galaxy is almost orthogonal to the plane of the galaxy distribution (see figure 6.41).

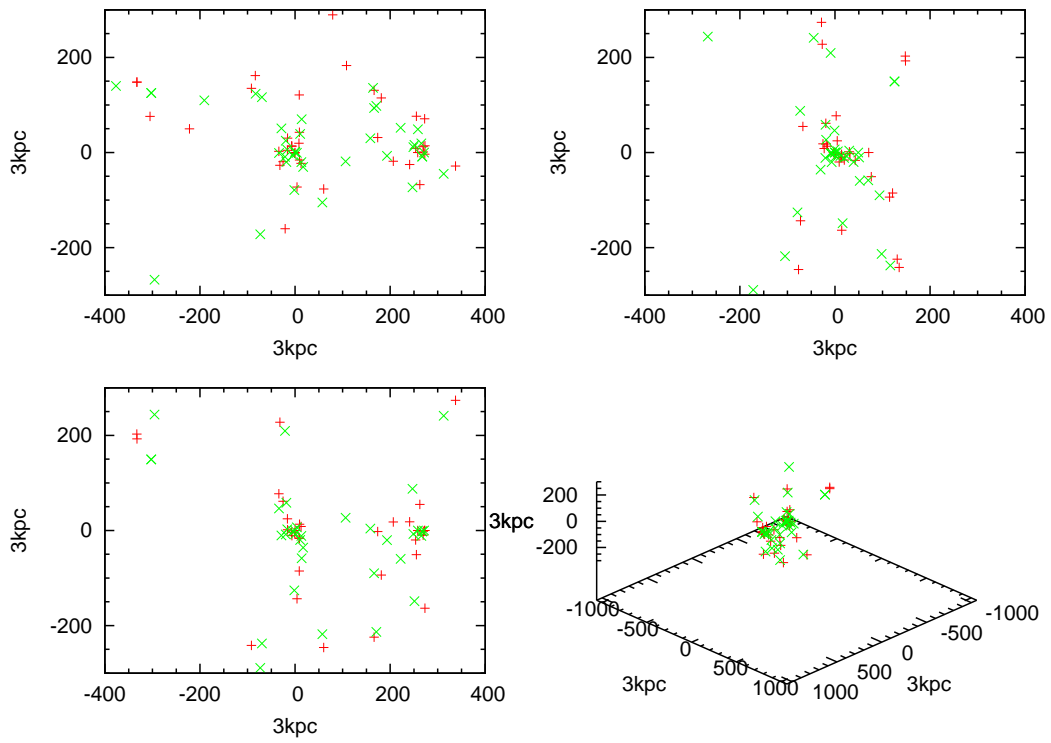


Figure 6.40: Same as figure 6.13, but for the best MH result.

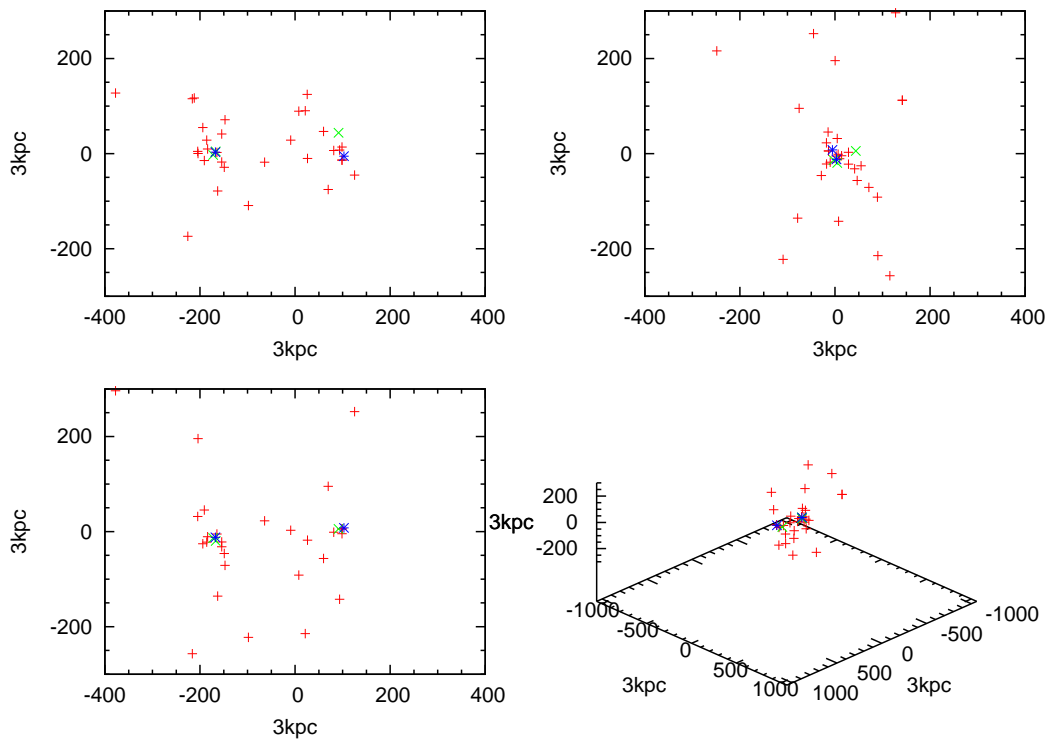


Figure 6.41: Same as figure 6.14, but for the best MH result.

name of the galaxy	spatial deviation [kpc]	velocity deviation [km/s]
Milky Way	0	0
M31	40	56
M33	79	233
LMC	44	311
SMC	65	84
WLM	104	76
NGC55	240	246
IC10	110	111
NGC147	192	70
And III	41	63
NGC185	301	74
NGC205	24	33
M32	30	65
And I	25	304
Sculptor	147	19
LGS3	126	45
IC1613	79	516
And II	50	199
Phoenix	174	432
Fornax	16	1
UGCA92	132	86
Carina	36	27
Leo A	83	112
Sextans B	275	358
NGC3109	196	46
Antlia	172	3
Leo I	94	244
Sextans A	333	250
Sextans	66	25
Leo II	23	81
GR8	232	312
Ursa Minor	53	218
Draco	60	104
Sagittarius	138	381
SagDIG	175	196
NGC6822	59	326
Aquarius	120	50
IC5152	127	252
Tucana	88	324
UGCA438	238	63
Pegasus	80	337

Table 6.11: Deviation of the positions and radial velocities for the best MH result.

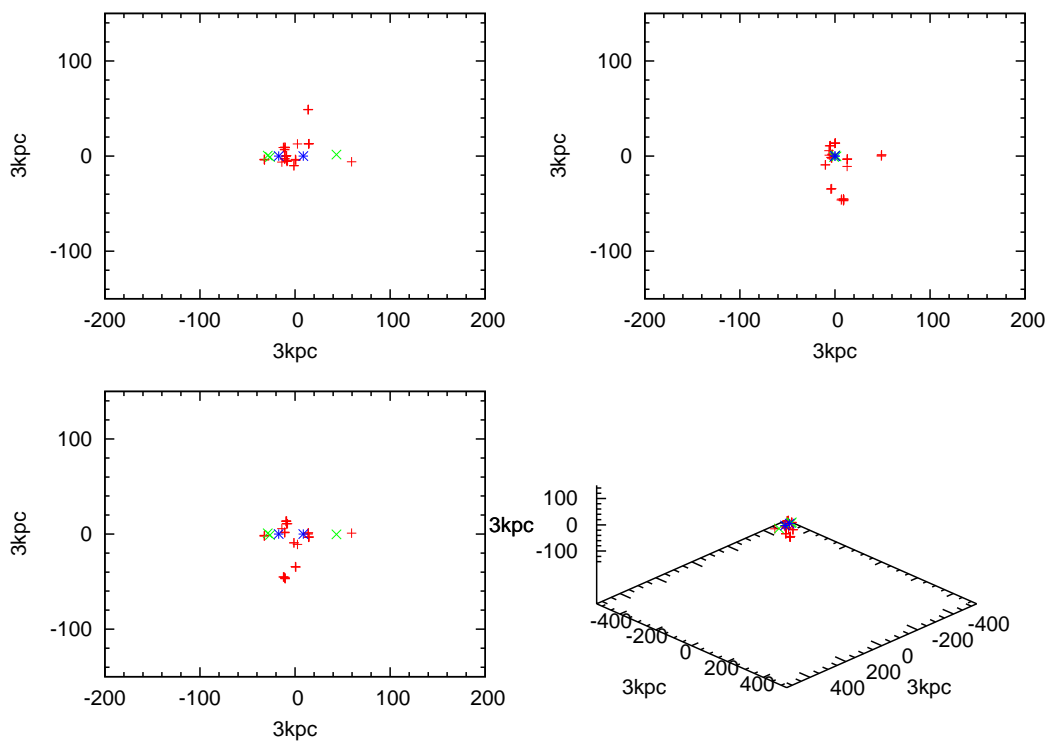


Figure 6.42: Same as figure 6.15, but for the best MH result.

6.3 Conclusions

As already seen in the previous section, the results of the simulations are very multifarious. In general the basic features of the Local Group's structure can be reproduced more or less in all models. The spatial distribution of the Local Group galaxies can be fitted quite well, though the outermost parts of our galaxy group have been problematic in all models. A problem is that the radial velocities of the galaxies can only be fitted poorly. A possible reason for this is that the statistic weights for the radial velocities have been set to too small values. The radial velocity problem becomes striking in MOND. Even the Milky Way and Andromeda Galaxy are not approaching in most MONDian models (all but M4M and MH). Moreover it has been shown that there are only certain masses allowed for the two dominant galaxies to get an orbit, which is in agreement with the observed radial velocity and distance. Furthermore, most of the other galaxies are moving significantly too fast in deep-MOND gravity. Another interesting feature, which has been discovered in the simulations, is that there have already been two passages of M31 through its perigalacticum in case of realistic baryonic masses for the two main galaxies and MONDian gravity. This is in agreement with the analysis of the Local Group timing by Shi (Shi, 2009). In contrast to this, the Milky Way and M31 have not completed their first orbit in Newtonian gravity yet. The problem with the radial velocities is also less striking in Newtonian gravity. At least the orbit of the two most massive galaxies can be reproduced with an acceptable quality (the galaxies are separated by approximately the correct distance and they are approaching each other). In contrast to the MONDian models, the spatial distribution cannot be fitted well, though it is not much worse too. This fact results in higher final values of the fitness functions in case of Newtonian gravity. But with respect to the problem of the Andromeda Galaxy's orbit in the case of MONDian gravity, this does not mean that the Newtonian models are worse. The model NSH has shown that small radii for halos can be ruled out. A general problem of the Newtonian models is that the Magellanic Clouds merge with the Milky Way due to dynamical friction. Also M33 gets too close to the Andromeda Galaxy. Somehow the genetic algorithm has not been able to find initial conditions for these galaxies, which protect them from this fate, though this does not necessarily mean that no such initial conditions exist. It may be useful to optimise the initial condition by additional calculation for these galaxies. All Newtonian models show very similar initial distributions at the time of the close encounter (12 Gyr ago) of the Milky Way and the Andromeda Galaxy. It consists of a compact agglomeration with a diameter of roughly 100 kpc which contains the Milky Way and M31 and most of the other galaxies. This agglomeration has a tail like structure, which is orientated in the orbital plane of the Milky Way and the Andromeda Nebula, but orthogonal to their connection vector. It can extend to several hundred kiloparsecs in both directions. This may indicate, that a combination of the interaction and the infall scenario, although it is quite unlikely, may be worth investigating. In contrast to that the initial distributions are very different in case of MONDian gravity, though there is also a tendency to some tail like structures in some models. The simulations also have shown that a time of 12 Gyr in the past, give or take 100 Myr, works as the time for the first, but determining, close encounter of the Milky Way and the Andromeda Galaxy. Sawa and Fujimoto got a distance of about 150 kpc (Sawa and Fujimoto, 2005), which has separated both galaxies at this time. My results yield values between 50 and 100 kpc, which is significantly less. Therefore the encounter is more violent in these simulations. The final distributions are very different in all models, and even in the individual results

of one model. Nevertheless all results can roughly reproduce the basic structure of the Local Group but with different deviations. The maybe most astonishing result of the simulations is that the plane of galaxies in the Local Group does not have to correspond to the orbital plane of the Milky Way - Andromeda system. In all, but one, models, these two planes are inclined by different angles (up to almost 90°). These results show, that the scattering process is more complicated than expected and that it strongly depends on the initial velocity distribution of the small Local Group galaxies. The spatial distribution also seems to contribute, because the largest differences in the inclinations occurred in the MONDian models, where the initial distributions are, in contrast to the Newtonian models, very multifarious.

The recalibration of the fitness function in *GeneAl* will be the first possible improvement of the whole set of simulations. This may solve or at least cut down the radial velocity problem. The programme *NewHEXl* has worked perfectly and a spherical halo with dynamical friction is a good description of a Dark Matter dominated galaxy at these scales. Another possible improvement for further studies would be to add some multipole moments to the galaxy model in *DeMonI*. It is only treated as a point mass in this programme and since the potential is shaped by baryonic matter only, the contribution of the galactic disc to potential can change the orbits of satellite galaxies. Furthermore, it would help much to know the full three-dimensional velocity of all Local Group galaxies, so that the models would not be restricted to radial velocities alone. One could learn a lot about the dynamics of our galaxy group through it, but one has to wait for upcoming missions like GAIA to get more information on this problem. The particle cloud technique has been a very successful trick and the efficiency of it would be definitely increased by increasing the number of particles per cloud and also the number of generations of the genetic algorithm. Another improvement would be better known masses. This means that the total masses of the massive galaxies have to be known more exactly. This can be done either by additional observational data (which is close to impossible for a Dark Matter halo) or by including the masses as free parameter for fitting in the genetic algorithm. Furthermore, since dynamical friction depends on the satellite's mass, it would be another possible improvement to use different masses (only for the dynamical friction, not for the gravity (they are still massless testparticles with respect to it)) for the dwarf galaxies. There are definitely many possibilities to improve the scenario further and with every improvement one will find more ways for additional optimisation.

The simulations have shown that the scenario of creating the planar distribution of Local Group galaxies by an early interaction between the Milky Way and the Andromeda Galaxy is possible. It is no surprise that the simulations do not yield a unique result, because the model is highly dynamical and there are numerous local minima, where the genetic algorithm can end up. There are problems in both used theories of gravity but each of them also has its advantages.

Acknowledgments

I want to thank all my colleagues from Christian Theis' working group for their help especially Harald Leibinger, Armin Liebhart, Christian Göschl, Hanns Petsch, Julia Weniger and Adam Ruzicka and my colleague from the office Jenny Feige. I am very thankful for many fertile discussions we had as well as for plenty of advices concerning programming and especially parallel computing and debugging. Furthermore I thank the University of Vienna for all the provided resources and I want to accentuate my thank for the possibility to use the Vienna Astro Cluster which reduced my calculation times essentially. I also want to express my gratitude for the patient of my fellow cluster users with me when I made my first clumsy steps in parallel computing. Moreover I want to thank all my friends for their support and especially Simon Dauth, Andreas Gabriel, Lisa Hofer, Armin Liebhart, Elentari Nepomucky, Simon Rothwangl, Patricia Schmidt and Bernhard Wenzel for proofreading my thesis. I also want to thank my advisor Christian Theis for his help and everything he taught me. Finally I want to express my gratitude to my grandparents and parents for their financial support which enabled me to do my studies.

Bibliography

- Aguirre, A., Schaye, J., and Quataert, E.: 2001, *ApJ* **561**, 550
- Alves, D. R.: 2004, *ApJ* **601**, L151
- Anderson, J. D., Laing, P. A., Lau, E. L., Liu, A. S., Nieto, M. M., and Turyshev, S. G.: 2002, *Phys. Rev. D* **65(8)**, 082004
- Baiesi Pillastrini, G. C.: 2009, *ArXiv e-prints*
- Bekenstein, J. and Milgrom, M.: 1984, *ApJ* **286**, 7
- Bekenstein, J. D.: 2004, *Phys. Rev. D* **70(8)**, 083509
- Bekenstein, J. D.: 2009, *Nuclear Physics A* **827**, 555
- Bekki, K.: 2008, *MNRAS* **390**, L24
- Bekki, K. and Stanimirović, S.: 2009, *MNRAS* **395**, 342
- Binney, J. and Tremaine, S.: 2008, *Galactic Dynamics*, Princeton University Press
- Burkert, A.: 1996, in R. Bender & R. L. Davies (ed.), *New Light on Galaxy Evolution*, Vol. 171 of *IAU Symposium*, pp 175–+
- Chandar, R., Bianchi, L., and Ford, H. C.: 1999a, *ApJ* **517**, 668
- Chandar, R., Bianchi, L., Ford, H. C., and Salasnich, B.: 1999b, *PASP* **111**, 794
- Chandrasekhar, S.: 1943, *ApJ* **97**, 255
- Chernin, A. D., Teerikorpi, P., Valtonen, M. J., Byrd, G. G., Dolgachev, V. P., and Domozhilova, L. M.: 2009, *ArXiv e-prints*
- Cioni, M.: 2009, *A&A* **506**, 1137
- Ciotti, L., Nipoti, C., and Londrillo, P.: 2007, *ArXiv Astrophysics e-prints*
- Clowe, D., Bradač, M., Gonzalez, A. H., Markevitch, M., Randall, S. W., Jones, C., and Zaritsky, D.: 2006, *ApJ* **648**, L109
- Corbelli, E., Lorenzoni, S., Waltherbos, R. A. M., Braun, R., and Thilker, D. A.: 2009, *ArXiv e-prints*
- de Freitas Pacheco, J. A.: 1986, *Revista Mexicana de Astronomia y Astrofisica*, vol. 12 **12**, 74
- Deeg, H. J., Munoz-Tunon, C., Tenorio-Tagle, G., Telles, E., Vilchez, J. M., Rodriguez-Espinosa, J. M., Duc, P. A., and Mirabel, I. F.: 1998, *A&AS* **129**, 455
- del Peloso, E. F., da Silva, L., Porto de Mello, G. F., and Arany-Prado, L. I.: 2005, *A&A* **440**, 1153
- Diemand, J., Kuhlen, M., Madau, P., Zemp, M., Moore, B., Potter, D., and Stadel, J.: 2008, *Nature* **454**, 735
- Frebel, A., Christlieb, N., Norris, J. E., Thom, C., Beers, T. C., and Rhee, J.: 2007, *ApJ* **660**, L117
- Fujimoto, M., Sawa, T., and Kumai, Y.: 1999, in J. E. Barnes & D. B. Sanders (ed.), *Galaxy Interactions at Low and High Redshift*, Vol. 186 of *IAU Symposium*, pp 31–+
- Giraud, E.: 2000, *ApJ* **539**, 155
- Gonidakis, I., Livanou, E., Kontizas, E., Klein, U., Kontizas, M., Belcheva, M., Tsalmantza, P., and Karamelas, A.: 2009, *A&A* **496**, 375

- Hartwick, F. D. A.: 2000, *AJ* **119**, 2248
- Jee, M. J., Ford, H. C., Illingworth, G. D., White, R. L., Broadhurst, T. J., Coe, D. A., Meurer, G. R., van der Wel, A., Benítez, N., Blakeslee, J. P., Bouwens, R. J., Bradley, L. D., Demarco, R., Homeier, N. L., Martel, A. R., and Mei, S.: 2007, *ApJ* **661**, 728
- Kallivayalil, N., Besla, G., Sanderson, R., and Alcock, C.: 2009, *ApJ* **700**, 924
- Klypin, A. and Prada, F.: 2009, *ApJ* **690**, 1488
- Komatsu, E., Dunkley, J., Nolta, M. R., Bennett, C. L., Gold, B., Hinshaw, G., Jarosik, N., Larson, D., Limon, M., Page, L., Spergel, D. N., Halpern, M., Hill, R. S., Kogut, A., Meyer, S. S., Tucker, G. S., Weiland, J. L., Wollack, E., and Wright, E. L.: 2009, *ApJS* **180**, 330
- Kuijken, K. and Dubinski, J.: 1995, *MNRAS* **277**, 1341
- Kunkel, W. E.: 1979, *ApJ* **228**, 718
- Li, Y. and Helmi, A.: 2008, *MNRAS* **385**, 1365
- Li, Y. and Helmi, A.: 2009, in J. Andersen, J. Bland-Hawthorn, & B. Nordström (ed.), *IAU Symposium*, Vol. 254 of *IAU Symposium*, pp 263–268
- Li, Y.-S. and White, S. D. M.: 2008, *MNRAS* **384**, 1459
- Libeskind, N. I., Frenk, C. S., Cole, S., Helly, J. C., Jenkins, A., Navarro, J. F., and Power, C.: 2005, *MNRAS* **363**, 146
- Loeb, A., Reid, M. J., Brunthaler, A., and Falcke, H.: 2005, *ApJ* **633**, 894
- Londrillo, P. and Nipoti, C.: 2008, *User Guide for N-MODY*
- Londrillo, P. and Nipoti, C.: 2009, *Memorie della Societa Astronomica Italiana Supplement* **13**, 89
- Magrini, L., Corbelli, E., and Galli, D.: 2007, *A&A* **470**, 843
- Mastropietro, C.: 2009, in J. T. van Loon & J. M. Oliveira (ed.), *IAU Symposium*, Vol. 256 of *IAU Symposium*, pp 117–121
- Mateo, M. L.: 1998, *ARA&A* **36**, 435
- McConnachie, A. W., Chapman, S. C., Ibata, R. A., Ferguson, A. M. N., Irwin, M. J., Lewis, G. F., Tanvir, N. R., and Martin, N.: 2006, *ApJ* **647**, L25
- Metz, M., Kroupa, P., Theis, C., Hensler, G., and Jerjen, H.: 2009, *ApJ* **697**, 269
- Milgrom, M.: 1983, *ApJ* **270**, 365
- Milgrom, M.: 2008, *ArXiv e-prints*
- Milgrom, M.: 2009, *ArXiv e-prints*
- Milgrom, M. and Sanders, R. H.: 2008, *ApJ* **678**, 131
- Moffat, J. W.: 2006, *Journal of Cosmology and Astro-Particle Physics* **3**, 4
- Moore, B., Ghigna, S., Governato, F., Lake, G., Quinn, T., Stadel, J., and Tozzi, P.: 1999, *ApJ* **524**, L19
- Navarro, J. F., Ludlow, A., Springel, V., Wang, J., Vogelsberger, M., White, S. D. M., Jenkins, A., Frenk, C. S., and Helmi, A.: 2010, *MNRAS* **402**, 21
- Nipoti, C., Ciotti, L., Binney, J., and Londrillo, P.: 2008, *MNRAS* **386**, 2194
- Nipoti, C., Londrillo, P., and Ciotti, L.: 2007a, *MNRAS* **381**, L104
- Nipoti, C., Londrillo, P., Zhao, H., and Ciotti, L.: 2007b, *MNRAS* **379**, 597
- Novati, S. C., De Luca, F., Jetzer, P., and Scarpetta, G.: 2006, *ASTRON.ASTROPHYS.* **459**, 407
- Peacock, J. A.: 1999, *Cosmological Physics*, Cambridge University Press
- Petsch, H. P.: 2007, *Master's thesis*, University of Vienna
- Press, W., Teukolsky, S., Vetterling, W., and Flannery, B.: 1997, *Numerical Recipes*, Cambridge University Press
- Pritchett, C. J. and van den Bergh, S.: 1999, *AJ* **118**, 883

- Putman, M. E., Peek, J. E. G., Muratov, A., Gnedin, O. Y., Hsu, W., Douglas, K. A., Heiles, C., Stanimirovic, S., Korpela, E. J., and Gibson, S. J.: 2009, *ApJ* **703**, 1486
- Raychaudhury, S. and Lynden-Bell, D.: 1989, *MNRAS* **240**, 195
- Rindler, W.: 2006, *Relativity: Special, General, and Cosmological*, Oxford University Press
- Rubin, V. C. and Ford, Jr., W. K.: 1970, *ApJ* **159**, 379
- Sabbi, E., Gallagher, J. S., Tosi, M., Anderson, J., Nota, A., Grebel, E. K., Cignoni, M., Cole, A. A., Da Costa, G. S., Harbeck, D., Glatt, K., and Marconi, M.: 2009, *ArXiv e-prints*
- Sánchez-Salcedo, F. J., Reyes-Iturbide, J., and Hernandez, X.: 2006, *MNRAS* **370**, 1829
- Sanders, R. H.: 2001, *ArXiv Astrophysics e-prints*
- Sanders, R. H.: 2003, *MNRAS* **342**, 901
- Sarajedini, A.: 2007, in R. Guzmán (ed.), *Revista Mexicana de Astronomía y Astrofísica Conference Series*, Vol. 29 of *Revista Mexicana de Astronomía y Astrofísica Conference Series*, pp 48–50
- Sarajedini, A. and Yang, S.: 2010, in C. Sterken, N. Samus, & L. Szabados (ed.), *Variable Stars, the Galactic halo and Galaxy Formation, Proceedings of an international conference held in Zvenigorod, Russia, 12-16 October 2009. Published by Sternberg Astronomical Institute of Moscow University, Russia.*, pp 101–+
- Sawa, T. and Fujimoto, M.: 2005, *PASJ* **57**, 429
- Sawa, T., Fujimoto, M., and Kumai, Y.: 1999, in Y.-H. Chu, N. Suntzeff, J. Hesser, & D. Bohlender (ed.), *New Views of the Magellanic Clouds*, Vol. 190 of *IAU Symposium*, pp 499–+
- Shi, Y.: 2009, *ArXiv e-prints*
- Teuben, P.: 1995, in R. A. Shaw, H. E. Payne, & J. J. E. Hayes (ed.), *Astronomical Data Analysis Software and Systems IV*, Vol. 77 of *Astronomical Society of the Pacific Conference Series*, pp 398–+
- van den Bergh, S.: 1999, *ApJ* **517**, L97
- van den Bergh, S.: 2000, *PASP* **112**, 529
- van den Bergh, S.: 2003, *ArXiv Astrophysics e-prints*
- van der Marel, R. P., Alves, D. R., Hardy, E., and Suntzeff, N. B.: 2002, *AJ* **124**, 2639
- van der Marel, R. P. and Guhathakurta, P.: 2008, *ApJ* **678**, 187
- Volders, L. M. J. S.: 1959, *Bull. Astron. Inst. Netherlands* **14**, 323
- Young, C., Currie, M. J., Dickens, R. J., Luo, A., and Zhang, T.: 2008, *Chinese Journal of Astronomy and Astrophysics* **8**, 369
- Zwicky, F.: 1933, *Helvetica Physica Acta* **6**, 110

Appendices

Appendix A

Programmes

A.1 Overview

To perform my simulations, I have written several programmes, edited others or used third party programmes. All programmes, which I have used in my final simulations, have been developed by me. They are written in *Fortran90* and I have developed a parallelised version for some of them (*Cutter*, *NewHEXI* and *DeMonI*). Each of my programmes performs a single task of my simulations, some are only required once within a run while others many thousand times. The whole set of my programmes is controlled by a *Bash-Shell*-script. The following scheme provides a brief overview of the purpose of every individual programme and its role during a complete simulation run.

Mkinput: creates a set of initial conditions

RealDist: creates a file which will be used for comparison by the Genetic algorithm

begin a loop for all generations

begin a loop for all models

Mkmodel: creates a model due to the initial conditions

in the case of MOND: **Demoni**: integrates using deep-MOND and Hubble-expansion

in the case of Dark Matter: **Newhexi**: integrates using Newtonian gravity, Hubble-expansion, extended dark matter halos and dynamical friction

end loop

Cutter: extracts first and last snapshot from integrated models

only if it is the last generation **Output best**: finds best models and creates new clean initial conditions

else **GeneAI**: selects best models, creates new models by recombination, mutates them and produces new initial conditions

end loop

begin a loop for the best models

Mkmodel: see above

in the case of MOND: **Demoni**: see above

in the case of Dark Matter: **Newhexi**: see above

end loop

Of course, there are additional commands for tidying up, moving files, etc. in the *Shell*-script. This pseudo-script only illustrates the function of the programmes.

A.2 Mkinput

This is a very simple programme that creates a certain number of *initial condition files* which will be used by the programme *Mkmodel* to create a *model file* from them. *Mkinput* requires an input file itself which has to be titled *origin.dat*. This file contains parameters like the number of models that should be created, the number of massive particles and their masses, the number and arrangement of massless test particles. Furthermore there are restrictions on the orbit of the two main objects as well as on the velocities and positions of the other particles written in the file. *Mkinput* cannot create any set of models, because it has been designed only for those, which are within my working hypothesis (see sections 1.4 and 5.4). The output file contains the number of massive particles, the number of test particle clouds and particles in each of these clouds. In addition to that it encloses the filename for the *model files*, the masses of the particles and three parameters which describe the orbit of the two main particles. Moreover one will find the coordinates and velocities of the other massive particles as well as a dummy mass for the test bodies (which is required for the dynamical friction in another programme). Furthermore it contains the coordinates and velocities of the centre of the test particle clouds, their extension and velocity dispersion. The programme *Mkinput* is only used once per run but it provides essential information for other programmes. Although this programme is tightly specialised on my working hypothesis, it is flexible enough to create *initial condition files* for the Dark Matter and the MOND case, because one is able to edit the masses and the area in parameter space for the orbit of the two main particles.

A.3 Mkmodel

The programme *Mkmodel* converts an *initial condition file* into a *model file*. Therefore it needs an input file which should have exactly the same format like an output file of *Mkinput*. First it uses the three parameters to estimate the orbit of the dominant particles. This is done in the reference frame of the first particle. Using the property of the two body problem, namely that one can restrict all movements to a plane; the motion can be restricted to the x-y plane of the Cartesian coordinate system in this case. Afterwards the system is shifted to the centre of mass and the other massive particles are added. This is followed by another shift to the new centre of mass. In the next step the test particle clouds are created. There is always one test particle at the centre of the cloud with the given velocity of the cloud, but all others are randomly distributed around this central particle within a certain radius and within given boundaries a different velocity. This set of particles will be written by *Mkmodel* into a file using the *ASCII-Nemo* format for reasons of compatibility with the *NEMO*-package (Teuben, 1995). This format is quite simple: there is a header of three lines containing the number of particles n , the dimensions (usually three) and the initial time. This is followed by all n masses of the particles. Then there have to be written the positions of the particles with the x,y and z-coordinates in the same line. Finally the file contains the particles' velocities in the same format as the positions. The programme *Mkmodel* is used very often because it has to transform every *initial condition file* into a *model file*. Initial condition files can be created by *Mkinput* or the *GeneAl* programme and so there are usually several hundreds per generation. The programme *Mkmodel* is very important, because the *initial condition file* only contains parameters which are really necessary in the case of my working hypothesis. Though to be able to use a non-specialised integrator, one needs a format which is more flexible like that of the *model file*.

A.4 NewHEX I

The name *NewHEX I* is an abbreviation for NEWtonian Hubble EXpansion Integrator, which describes one of the main features of this programme. The programme is an integrator for stellar dynamics using Newtonian gravity (in contrast to Demoni (see the next section), which uses MOND) and it is also capable of simulating an extended dark matter halo with dynamical friction as well as a Hubble Expansion, which is included in the form of an additional force. *NewHEX I* requires three different input files to be able to work. The first file *para.dat* is a parameter file for the integration. It contains the name of the file which is filled with the initial conditions of the particles (a *model file*), the name of the output file, the length of the integration, the print step size, the softening length, the minimal mass and the offset time. The last parameters in this file indicate if the halo, the dynamical friction and the Hubble expansion are activated; the final parameters give the user a possibility to rescale the efficiency of the dynamical friction and the strength of the Hubble expansion. The terms in the equations of motion, which describe the dynamical friction or the Hubble expansion, are simply multiplied by a constant factor. At this point it should be noted that the programme uses n-body units. Another file which has to be labelled "halo.dat" is only required if an extended halo (with or without dynamical friction) enabled in the parameter file. The *halo.dat* file contains the radial extension of all halos of all massive bodies in the simulation. The last input file has to be written in the *ASCII-Nemo* format and contains the masses, the initial positions and the initial velocities of the particles of the integration. After all this files have been read in, the programme processes a loop for all test bodies (objects with a mass less than the minimal mass), which experience forces from all massive particles, the massive particles' halos and dynamical friction as well as from the Hubble expansion. The mutual gravitational forces are calculated using equation (A.1) if the object, which experiences the gravitation, is outside the halo of the attracting massive particle and in case it is inside the halo one uses equation (A.2).

$$\vec{a} = \frac{M}{r^3} \vec{r} \quad (\text{A.1})$$

$$\vec{a} = \frac{M}{r^2 r_H} \vec{r} \quad (\text{A.2})$$

One might have noticed that a singular isothermal halo with a radial mass profile of $M(r) = M \frac{r}{r_H}$ has been assumed. This type of halo is a good enough approximation for my simulations and it is also very simple in its implementation. The radius r_H is the extension of the halo, M its total mass, r the length (including softening) of the distance vector \vec{r} which connects two objects and \vec{a} the acceleration of the attracted particle. The acceleration caused by every massive particle on every object is summed up. For the dynamical friction one can choose between two different equations by setting the parameter which activates the dynamical friction either to *1* or to *2*. In case of *1* equation (2.21) is used and in case of *2* the less accurate but faster equation (2.17) is used by *NewHEX I*. It is obvious that in this formula massless test bodies are not affected by dynamical friction, but in my model those massless objects are dwarf galaxies with several million solar masses and those objects experience dynamical friction in reality. In case the object is "massless" the mass for the particle m in the formula is simply set to the minimal mass (which should be chosen to be a typical mass for the kind of objects the test body represents) and so the object is affected by dynamical friction too. At this point it should be noted that Newton's third law of motion (*actio est reactio*) is accounted

for massive particles. Finally the Hubble expansion is added. To do this it was necessary to find a force that creates an effect which corresponds to the observed Hubble law. I used equation (2.36) to simulate the Hubble expansion. I want to note that this formula requires a cosmological time. Therefore I introduced an offset time, which is the age of the universe at the beginning of the simulation. For most applications it is useful to calculate the length of the integration in such a way that it ends with today's age of the universe. This force is simply added to the acceleration of all particles and simulates the Hubble expansion quite well. For the very integration itself *NewHEX* uses a *Runge-Kutta* differential equation solver. This module is included using a library from the *Numerical Recipes* (Press et al., 1997), which I modified a little bit for my applications. Every print step the masses, positions and velocities are appended to a output file (*result file*) which uses the *ASCII-Nemo* format. *NewHEX* is a very flexible programme which has many applications beyond its purpose in this programme suite. It can be used for simple integrations of orbits as well as small cosmological simulations. There also exists a very fast parallelised version of this programme, which is very helpful because it shortens the integration time for simulations with many particles. During one run the programme *NewHEX* is used several thousand times to calculate the movement of all galaxies within the Local Group for many Gigayears.

A.5 DeMonI

DeMonI is the MONDian counterpart of *NewHEXI* and performs the integration in the MOND scenarios for the Local Group. The name of the programme is an abbreviation for DEep MONd Integrator. *DeMonI* is capable of calculating the motion of many massive and massless particles considering mutual deep-MONDian gravitational interaction and the Hubble expansion. Of course there are no Dark Matter halos and therefore no dynamical friction too. For this reason *DeMonI* requires only two input files. The first one, which is labelled *para.dat*, has to contain basic parameters needed for the integration: the name of the file which contains the initial conditions of the particles, the name of the output file, the length of the integration, the print step size, the MONDian acceleration constant a_0 , the softening parameter, the minimal mass, the offset time, the Hubble expansion on-off switch and the scaling parameter for the Hubble expansion. The second input file contains the masses, positions and velocities of all particles written in the *ASCII-Nemo* format. Only the deep-MOND limit is considered for the gravitation using equation (A.3).

$$\vec{a} = \frac{\sqrt{Ma_0}}{r^2} \vec{r} \quad (\text{A.3})$$

The assumption of deep MOND in the case of distance interactions between galaxies is valid, because even in our own galaxy the Newtonian area is only very few kiloparsec large and at these scales the treatment of a galaxy as a point particle breaks down anyway. Furthermore the softening length is set to be at the same scale. The Hubble expansion has been implemented in exactly the same way as in *NewHEXI*. For the integration the very same Runge-Kutta module as in the previous programme is used. The output file also uses the same format like *NewHEXI*. Despite many similarities there are also several important differences between *DeMonI* and *NewHEXI*. Of course the basic physics behind both integrators are quite different and because of the high complexity of MOND, *DeMonI* only uses an approximation, the deep-MOND limit. This is the reason for the fact that this integrator is not as flexible as *NewHEXI*, because the conditions for this approximation have to be fulfilled. One cannot simulate a single galaxy consisting of many particles with mutual gravitational interaction in *DeMonI*. Therefore the validity of *DeMonI* is restricted to the scales of galaxy groups and clusters. Because of the complex formula of the dynamical friction (no Dark Matter halo) do not have to be calculated, *DeMonI* is faster than *NewHEXI*, especially because there exists a parallelised version of *DeMonI* too. The programme is used many thousand times during one MOND-run and provides the other programmes with information about the evolution of an initial model. *DeMonI* is an essential part of the whole programme suite.

A.6 Cutter

There are only two snapshots needed from the whole integration: the first one and the last one. The programme *Cutter* has been written to extract exactly these two snapshots from the whole *result file*. Due to the fact that there are usually many *result files* which have to be split up, the programme *Cutter* is parallelized and it is able to split a whole sequence of result files extremely quickly. For input the programme needs several *result files* labelled *fmod*.dat* (where * represents a number counting from one) and a small parameter file called *c.dat*, which contains only two values: the number of *result files* to be processed and the number of time step in one of these files. The output of this programme are two *ASCII-Nemo* snapshot files labelled *mod*-0.dat* for the first snapshot and *mod*-F.dat* for the last snapshot. The programme *Cutter* simply reduces the data of the *result files* from the integrations and prepares it for the application of the programme *GeneAl*.

A.7 RealDist

This programme is able to create a "comparable" set of data out of the observational data from the Local Group. The title of this programme is an abbreviation for REAL DISTRIBUTION. *RealDist* requires a special input file and is able to create different types of output files. The input file has to have a three line header containing the modulus (0 for a *ASCII-Nemo* snapshot file; 1 for a normal *vgl-output file*; 2 for a *vgl-output file* that keeps the values for radial velocities from the input file), the number of galaxies in this file and the number of massive galaxies in this file. The next lines in the input file have to contain the masses of the massive galaxies. This is followed by lines for every model with six values: galactic longitude, galactic latitude, distance from sun, radial velocity with respect to sun, angle of transverse velocity, value of transverse velocity. The positions and velocities are transformed from galactic coordinates into Cartesian coordinates, except if the modulus is set to two. In this case only the positions are transformed by the programme. In the next step all positions are shifted to the centre of mass. It should be mentioned that during this whole process the position of the sun is always calculated with respect to the new coordinates for later use in the programme *GeneAl*. As already mentioned before, the programme is capable of creating different outputs. In case of mode 0 the output is a *ASCII-Nemo* snapshot file containing the masses, positions and velocities of all galaxies. In the other two cases the output has the format which is required by the programme *GeneAl*: the first line contains the number of massive galaxies and the second line the number of massless galaxies (test bodies). This is followed by lines containing the Cartesian positions and lines for the Cartesian (or in case of mode 2 : only radial velocity towards sun) velocities. The last set of positions and velocities in this file stands for the sun in the new shifted and transformed coordinate system. The programme *RealDist* is only executed once during a whole run. It processes the observational data and puts it into a for other programmes useful form.

A.8 GeneAl

The programme *GeneAl* is the very heart of this whole programme suite and therefore the most complex programme. The title *GeneAl* is an abbreviation for GENETic ALgorithm. This might be a little confusing because in fact the whole suite works as a genetic algorithm, but this programme performs the most essential parts of it. The purpose of this programme is to analysis all data, calculate the fitness function, find the best models, using them for recombination to create children, mutate them and finally produce the *initial condition files* for a whole new generation. The programme requires one parameter file called *in.dat* which contains the control parameters for the *GeneAl*. The list starts with some filenames like the name of the file which contains the observed distribution of galaxies, the filename of the already cut *result files*, the name of the old *initial condition files*, the name of the new ones and the name of the *protocol file*. This is followed by the number of models, the statistic weight of the positions and of the velocities of the massive particles and the statistic weight of the positions and of the velocities of the massless test particles. The number of parents for the next generation, the total number of mutations and an indicator if only the radial velocities are used in the fitness function are also in this parameter file. In addition to this file the *GeneAl* requires three times the number of models plus one more file to operate properly. The first number of model files are the *initial condition files* of all models to be evaluated. Then there has to be an *ASCII-Nemo* file of the initial time step of an integration and another one of the last time step for each model. The last file missing is the one which contains the observed data for comparison with the calculated models. The programme analyses one model at a time. First it moves and rotates the whole set of particles into a system where the first object is in the centre, the second on the x-axis and the third somewhere in the xy-plane. This is exactly the same system as the file produced by the programme *RealDist* uses. In the case of my simulations the first object is the Milky Way, the second the Andromeda Galaxy and the third M33. It calculates the fitness function f_{fit} (see equation (A.4)) of every model.

$$f_{\text{fit}} = g_{\text{mpos}} \sum_i^{n_{\text{m}}} (\Delta x_i)^2 + g_{\text{mvel}} \sum_i^{n_{\text{m}}} (\Delta v_i)^2 + g_{\text{tbpos}} \sum_i^{n_{\text{tb}}} (\Delta x_{\text{best},i})^2 + g_{\text{tbvel}} \sum_i^{n_{\text{tb}}} (\Delta v_{\text{best},i})^2 \quad (\text{A.4})$$

The variable g_{mpos} , g_{mvel} , g_{tbpos} and g_{tbvel} are the statistical weights which can be adjusted in the parameter file. n_{m} is the number of the massive particles, while n_{tb} is the number of test particles. The variables Δx_i represent the distances between the calculated positions and the real positions from the observation data and the variables Δv_i for the differences between the calculated velocity and the real velocity. If the parameters are set to radial velocities only then the Δv_i represent the differences between the measured radial velocity and the radial velocity with respect to the sun in the simulation. In the case of test particles the programme uses a small trick to enhance its efficiency. Instead of one single particle per each dwarf galaxy, a whole cloud of test particles is used. The programme tries to find the best test particles from all clouds for every observational data point. Only the values of the best are used in the fitness function and they will later become the centres of the new test particle clouds in the next generation. After the fitness functions for all models have been estimated the programme selects the best (those which have the lowest numerical value) and their models will become the parents of the next generation. These parents are going to have number of model minus number of parents' children which are created by recombination of their parents' parameters. A special feature of this genetic algorithm is that every child can have up the number of parents' parents, because when

giving birth to a child, a random generator picks up single parameters from all possible parents (all models, which survive the selection). In the next step a given number of mutations is applied on the children, but not on the parents because we do not want to lose the best model. These mutations are also randomly generated: First the random generator picks a child and then a parameter of this child which will be mutated. The mutations themselves are not simply replacing the parameters by any random generated numbers. The original values are manipulated wisely and they can only be changed by one order of magnitude. In most cases the variables are multiplied by a random number between 0.1 and 10 and if it is reasonable to do so there is also a 50% chance that the sign of the variable is changed. After this the programme checks if any centres of test particle clouds are the same within a model. This can happen if the best test particle is the same for more than one dwarf galaxy. It would not do any harm to the programme if it has been left at the same coordinates, but it would be a small waste of computation power. So the programme shifts the coordinates of the centre of the concerned test particle cloud to some random coordinates. The programme finishes with creating a new set of *initial condition files* for the next generation. The programme *GeneAl* is the actual heart of the whole programme suite and it is executed once per generation to perform the essential parts of a genetic algorithm: selection, recombination and mutation. Although the general concept is still the same as in evolution theory, some additional features have been added which cannot be found in nature. An example for this would be that in this programme a child can have more than two parents or that in the fitness function for test particles not all parameters (genes) are used but only the best of them (only one particle out of a test particle cloud).

A.9 Output Best

The programme *Output Best* is a modified version of the programme *GeneAl*, which helps tidying up the results after the last generation of a simulation run. The only differences are that the programme *Output Best* does not do any recombination or mutation. It only selects the best number of parents models and reduces the test particle clouds to only one particle in the centre. Finally *Output Best* creates a number of parents' *initial condition files* which will be the basis for the final result of a simulation run.

A.10 Other programmes and third-party programmes

I have developed many small programmes for creating test models, analysing them and some translation tools for the output and input of *N-MODY* and a third-party software which I did not use in the final simulations. There are also many other small programmes, which I used for minor tests during the development of the main software suite and which will not work now anymore because the other programme have significantly changed in their further development. An example for these programmes would be a small suite of programmes which creates a set of simple *model files* containing only two particles that cover a certain area of the parameter space and analyses the results after an orbit integration. This small suite has been used in section 5.3.

Although in the final version of the simulation does not include any third-party programmes, I used many of them on the way to get it finished. The first third-party programme, which has been used, was *N-MODY*. This is a modified Poisson solver which calculates n-body system with the full MOND formalism. But this programme has serious problems and does not work properly for my application. Furthermore I used the *NEMO*-package from Teuben (Teuben, 1995) for various applications. Especially, I want to mention the programmes *mkkd95* and *gyrfalcON*, which I used very often to create and calculate test models. Other tools and programmes from this package I regularly used during the development of my own software were *atos*, *stoa*, *mkking*, *glnemo* and some other small programmes to manipulate *NEMO*-snapshot files. I also used some other software like *gnuplot 4.2* and *Origin 5* to display data for analysis.

Appendix B

From the collisionless Boltzmann-equation to the Plummer-model

We are looking for a self-consistent description of collisionless stellar systems with gravitation. We assume that the potential of our system is smooth enough to apply the mean-field approximation. Furthermore let us treat the stars (or dark matter, ...) like some gas in thermodynamics. We find that the collisionless Boltzmann-equation (see equation (B.1)) provides a good description of this kind of systems. The variable f represents the distribution function, which definitely describes the evolution of the stellar system. The distribution function gives the probability to find a particle (star) in a phase-space volume-element. x_i are the position coordinates, v_i are the velocity coordinates, t the time parameter and Φ the potential of the system. One can also write the same equation in a simpler way (see equation (B.2)) if one goes into the system of a comoving observer, where w_i are six-dimensional phase-space coordinates.

$$\frac{\partial f}{\partial t} + \sum_{i=1}^3 \left(v_i \frac{\partial f}{\partial x_i} - \frac{\partial \Phi}{\partial x_i} \frac{\partial f}{\partial v_i} \right) = 0 \quad (\text{B.1})$$

$$\frac{\partial f}{\partial t} + \sum_{i=1}^6 \dot{w}_i \frac{\partial f}{\partial w_i} = 0 \quad (\text{B.2})$$

If $\partial f / \partial t = 0$ one has a stationary system and this case it is possible to use the Jeans-theorem, which states that every static solution of the Boltzmann-equation is an integral of motion I (see equation (B.3)) and that every function of integrals of motion provides a solution of the stationary Boltzmann-equation.

$$\frac{dI(\vec{r}(t), \vec{v}(t))}{dt} = 0 \quad (\text{B.3})$$

Let us consider a simple example. In case of a self-gravitating spherical symmetrical system stationary system one can derive equation (B.4).

$$\frac{1}{r^2} \frac{d}{dr} \left(r^2 \frac{d\Phi}{dr} \right) = 4\pi G \int f \left(\frac{1}{2} v^2 + \Phi, |\vec{r} \times \vec{v}| \right) d^3 \vec{v} \quad (\text{B.4})$$

By introducing a relative potential Ψ and relative energy ϵ and an isotropic velocity distribution we get a distribution function like in equation (B.5).

$$f(\epsilon) = \begin{cases} C\epsilon^{n-\frac{3}{2}} & \text{for } \epsilon > 0 \\ 0 & \text{for } \epsilon \leq 0 \end{cases} \quad (\text{B.5})$$

Now one can use this distribution function and equation (B.4) to derive the Lane-Emden equation (see equation (B.6)), where s is a dimensionless radius and ψ a dimensionless potential.

$$\frac{1}{s^2} \frac{d}{ds} \left(s^2 \frac{d\psi}{ds} \right) = \begin{cases} -\psi^n & \text{for } \psi > 0 \\ 0 & \text{for } \psi \leq 0 \end{cases} \quad (\text{B.6})$$

In case of $n = 5$ one gets the Plummer-model (see equations (B.7)) as a solution for the Lane-Emden equation.

$$\begin{aligned} \rho(r) &= \frac{3M}{4\pi r_0^2} \left[1 + \left(\frac{r}{r_0} \right)^2 \right]^{-\frac{5}{2}} \\ M(r) &= M \left(\frac{r}{r_0} \right)^3 \left[1 + \left(\frac{r}{r_0} \right)^2 \right]^{-\frac{3}{2}} \\ \Phi(r) &= \frac{-GM}{r_0 \sqrt{1 + \left(\frac{r}{r_0} \right)^2}} \end{aligned} \quad (\text{B.7})$$

Curriculum Vitae

Personal	
Name	Christoph Florian Dieter
Surname	Saulder
Date of Birth	23 th October 1984
Place of Birth	Wels, Austria
Education	
September 1991 - July 1995	elementary school Volksschule 9, Wels
September 1995 - June 2003	grammar school with focus on science Bundesgymnasium und Bundesrealgymnasium, Brucknerstrasse, Wels
21 th June 2003	Matura
3 th July 2001 - 12 th July 2001	summer school - course: bionics Sommerakademie für begabte Schülerinnen und Schüler, Bad Leonfelden
October 2004 - ongoing	diploma study in physics University of Vienna
October 2004 - August 2007	bachelor study in astronomy University of Vienna
30 th August 2007	bachelor (Bakk. rer. nat.) in astronomy with distinction topic of the bachelor thesis: Lie-Integrator
October 2007 - now	master study in astronomy University of Vienna
October 2007 - ongoing	bachelor study in mathematics University of Vienna
Languages	
German	native
English	fluent
French	good
Spanish	good
Russian	basics

Working experience	
September 2008 - Februar 2009	private tutor for mathematics Schülerhilfe, Wien
July 2006	janitor and gardener assistant Berufsschule Kremsmünster
June 2006	organisation assistant Vienna Seminar of Nobel Laureates
November 2005 - November 2009 about one week each year	organisation assistant, catering assistant Vienna Seminar on Particle Physics and Quantumfieldtheory
September 2005	interviewer department of social science, University of Vienna
September 2004	shop assistant at a trade fair Socher, Sattledt
August 2004	construction worker Floortec , Pichl bei Wels
July 2004	assembly line worker, quality inspector Trodat , Wels
September 2003 - April 2004	compulsory military service: soldier, clerk Austrian armed forces , Kirchdorf an der Krems
July 2003 - August 2003	promoter Wesser , Grünstadt and Worms